The effects of fluid flow geometry on the physics of flow

Anglia Ruskin University

Cambridge Chelmsford Peterborough

Dominic Onimowo, BEng (Hons), MSc

Department of Engineering and Built Environment

Anglia Ruskin University

This dissertation is submitted for the degree of

Doctor of Philosophy

Faculty of Science and Technology

December 2018

Dedication

This dissertation is dedicated to God almighty for taking me successfully through all my years of education. A deep feeling of gratitude and appreciation is expressed toward my parents, Engr. and Mrs. Dirisu Valentine Onimowo for taking on the great financial task of giving me an overseas education and my loving family and siblings for their continuous support and reassurance that I can succeed.

Declaration

I hereby declare that except where specific reference is made to the work of others, the contents of this dissertation are original and have not been submitted in whole or in part for consideration for any other degree or qualification in this, or any other University. This dissertation is a result of my own original work and does not include work done in collaboration, except where clearly stated in the text.

Dominic Onimowo

December 2018

Acknowledgement

All glory to the highest God for granting me the life and privilege to reach this level of academic pursuit and for this divine opportunity to graduate from this esteemed academic institution, Anglia Ruskin University. I would also like to express my utmost gratitude to my supervisor, Professor Hassan Shirvani for his consistent support, his constructive criticism, and for all his patience and the precious time he spent to go through my work, guide and direct me throughout my project. A very special thanks to Dr Ahad Ramezanpour, for sharing he's CFD knowledge on understanding of flow physics with me and advice during my research and Dr Javaid Butt for he's knowledge shared and support during this process. I am also grateful to the very proficient librarians who were ever ready and available to help whenever approached, my very lovely parents and siblings who have not only provided financial support but also moral and day to day advice.

Abstract

The effects of fluid flow geometry on the physics of fluid are of prime importance as optimisation of the geometry could lead to improved fluid flow for various engineering applications. One such area that has led to substantial research in the commercial and academic sectors is the oil industry. Coning is a phenomenon which occurs because of the difference in pressure drop between the heel and toe ends of the oil well leading to non-uniform pressure along the well-bore. This phenomenon is quite common with oil wells and causes water/gas breakthrough into the oil well leading to reduced oil recovery and increased separation costs. hence the need for different inflow control devices for oil extraction. These devices however, have shown limitations due to the mixing of oil with water and gas causing inefficient valve actuation and resulting in the oil pipeline to shut down. They require optimisation of the fluid flow geometry to ensure maximum turbulence and differential pressure can be generated leading to more oil recovery.

Autonomous Inflow Control Valve (AICV) is a commercially available control device that is widely used in oil wells. It is responsible for balancing the pressure drop while making use of a circular coil pipe between the laminar and turbulent flow elements. This research focussed on developing new geometry designs for the coil pipe without increasing the size or robustness of the design that can increase pressure drop and lead to turbulence of the incoming fluid to ensure separation of oil from water/gas. Eight different designs were developed, and numerical analysis was undertaken using ANSYS 19.2 under various boundary conditions. All the designs were analysed for pressure drop values using oil, water and gas as investigative fluids. The CFD (computational fluid dynamics) simulations were undertaken for laminar and turbulent flow regimes for all three fluids because as the AICV functions on these two regimes.

The results showed that one of the designs proposed in this work called ‘square swirl slinky coil pipe’ generated the maximum pressure drop for all three fluids. AICV makes use a circular coil pipe that can create a pressure drop of 3.18 Pa for water, 0.05 Pa for gas and 0.13 MPa for oil with laminar flow whereas the square swirl slinky coil pipe can create a pressure drop of 66.11 Pa for water, 0.8 Pa for gas and 2.98 MPa for oil with laminar flow. On the other hand, a circular coil pipe can create a pressure drop of 167 Pa for water, 2.41 Pa for gas and 6.6 MPa for oil with turbulent flow whereas the square swirl slinky coil pipe can create a pressure drop of 2,361 Pa for water, 33.54 Pa for gas and 93.23 MPa for oil with turbulent flow.

The new geometry has shown massive increases in the pressure drop that can help in a substantially large amount of oil extraction compared to a commercially available product. This work highlights the importance of optimising fluid flow geometry parameters that can affect the physics of flow to achieve optimum results for a specific application. This work has wider implications in other areas as well e.g., turbulence is a major factor in enhancing heat transfer which makes this square slinky coil pipe design an optimal choice for heat exchangers and thermal solar panels.

Table of Contents

Dedication ..... **ii**

Declaration ..... **iii**

Acknowledgement ..... **iv**

Abstract ..... **v**

Table of Contents ..... **vi**

Table of Figures ..... **vi**

Table of Tables ..... **ix**

Chapter 1 Introduction to fluid flow geometry optimisation ***1***

1.1 Background theory **3**

1.2 Gap in knowledge **7**

1.3 Aim and Objectives **7**

1.4 Methodology **8**

1.5 Thesis structure **10**

1.6 Publications **11**

Chapter 2 Literature review ***12***

2.1 Review of fluid flow through geometries **12**

2.2 Review on swirl flow **22**

2.2.1 Review of Computational Fluid Dynamics (CFD) regarding Swirl flow 27

2.3 Review on Inflow Control **31**

2.3.1 ICD Technology **32**

2.3.1.1 Nozzle-type ICDs 33

2.3.1.2 Helical-type ICDs 36

2.3.1.3 Slot-type ICDs 37

2.3.1.4 Orifice-type ICDs (FloReg™ and FluxRite™) 38

2.3.2 Autonomous Inflow Control Devices (AICD) **39**

2.3.2.1 Flapper-type AICD 40

2.3.2.2 Ball-type AICD 41

2.3.2.3 Swellable-type AICD 42

2.3.2.4 Disc-type AICD 43

2.3.2.5 Remote-type AICD 43

2.3.3 Inflow Control Valves (ICVs) **44**

2.3.3.1 Discrete-positions ICV (DP-ICV) 44

2.3.3.2 Variable-positions ICV (VP-ICV) 45

2.3.3.3 Control Line-free ICVs (CLF-ICV) 45

2.3.4 Autonomous-ICV (AICV) **45**

2.3.4.1 BECH constant flow control valve 45

2.3.4.2 Autonomous and Reversible Inflow Control Valve Review 47

2.4 Summary **50**

Chapter 3 Methodology ***51***

3.1 Introduction **51**

3.2 Computational Fluid Dynamics (CFD) methodology 51
3.2.1 Experimental, Analytical and Numerical methods 52
3.2.2 Finite Element Method (FEM), Finite Difference Method (FDM) and Finite Volume Method (FVM) 53
3.2.3 Continuity equation for the conservation of mass 54
3.2.4 Turbulence modelling 55
3.2.4.1 Large Eddy Simulation (LES) and Direct Numerical Simulation (DNS) 56
3.2.4.2 Reynolds averaged Naiver Stokes (RANS) approach 58
3.2.4.3 Wall Bounded turbulent flow near wall treatment 62
3.2.4.4 Numerical Schemes 69
3.2.4.5 Numerical Discretization 73
3.2.4.6 Pressure interpolation schemes 76

3.3. Modelling swirl flow 78
3.3.1 Swirl number, Swirl decay, Hydraulic diameter and wall shear stress 78

3.4 Summary 81

Chapter 4 New designs and numerical simulations 82

4.1 Introduction 82

4.2 Basic Model Assumptions 83

4.3 Laminar and Turbulent flow simulation set up 83

4.4 New designs and related numerical simulations 84
4.4.1 Straight pipe 85
4.4.1.1. Laminar and turbulent oil flow simulations 88
4.4.1.2. Laminar and turbulent water flow simulations 89
4.4.1.3. Laminar and turbulent gas flow simulations 90
4.4.2 Coil Pipe 93
4.4.2.1. Laminar and turbulent oil flow simulations 95
4.4.2.2. Laminar and turbulent water flow simulations 96
4.4.2.3. Laminar and turbulent gas flow simulations 97
4.4.3 Elliptical straight pipe 98
4.4.3.1. Laminar and turbulent oil flow simulations 99
4.4.3.2. Laminar and turbulent water flow simulations 100
4.4.3.3. Laminar and turbulent gas flow simulations 101
4.4.4 Straight Square Pipe 102
4.4.4.1. Laminar and turbulent oil flow simulations 103
4.4.4.2. Laminar and turbulent water flow simulations 104
4.4.4.3. Laminar and turbulent gas flow simulations 105
4.4.5 Square coil 106
4.4.5.1. Laminar and turbulent oil flow simulations 107
4.4.5.2. Laminar and turbulent water flow simulations 108
4.4.5.3. Laminar and turbulent gas flow simulations 109
4.4.6 Slinky Coil Pipe 110
4.4.6.1. Laminar and turbulent oil flow simulations 111
4.4.6.2. Laminar and turbulent water flow simulations 112
4.4.6.3. Laminar and turbulent gas flow simulations 112
4.4.7 Square slinky coil pipe 113
4.4.6.1. Laminar and turbulent oil flow simulations 113
4.4.6.2. Laminar and turbulent water flow simulations 114
4.4.6.3. Laminar and turbulent gas flow simulations 115
4.4.8 Square swirl coil pipe 115
4.4.8.1. Laminar and turbulent oil flow simulations 116
4.4.8.2. Velocity contour magnitude for oil flow 117
4.4.8.3. Laminar and turbulent water flow simulations 119
4.4.8.4. Velocity contour magnitude for water flow 120
4.4.8.5. Laminar and turbulent gas flow simulations 121
4.4.8.6. Velocity contour magnitude for gas flow 122

4.5. Summary of simulation results **124**
4.6. Design Rights related to this research **125**
Chapter 5 Conclusions and Recommendations ***126***
5.1 Conclusions **126**
5.2 Achievement of aim and objectives **127**
5.3 Novel contribution to knowledge **133**
5.4 Concluding Remarks **134**
References ***135***
Appendix A ***159***
Effect of the square swirl fluid flow on heat exchange 159
Appendix B ***164***
Effect of the square swirl fluid flow geometry on multiphase flow 164

Table of Figures

Figure 1.1: The Behaviour of Coloured Fluid Injected into the Flow in Laminar and Turbulent Flows in a Pip (Cengel & Cimbala, 2014, p.349) 4
Figure 1.2:Illustration of R/A Ratio (Shirayama & Kuwahara, 1987, p. 52) 6
Figure 1.3: Roadmap of the PhD research project 9
Figure 2.1:Types of swirl generation (Najafi et al., 2011) 22
Figure 2.2: Types of swirl and their classifications (Steenbergen and Voskamp, 1998). 23
Figure 2.3: Nozzle-Type ICDs (Shevchenko, 2013) 33
Figure 2.4:Reslink: ResFlowTM Nozzle-type ICD 35
Figure 2.5: Reslink: ResInjectTM Nozzle-type ICD 35
Figure 2.6: Flotech FloMatik-SubTM nozzle-type ICD 36
Figure 2.7: helical-channel type ICD (Shevchenko, 2013) 36
Figure 2.8: Slot-type ICD, Circular disc design 38
Figure 2.9: Slot-type ICD, Quadrant division design (source: Alkhelaiwi, 2013) 38
Figure 2.10: FloRegTM orifice-type ICD (Birchenko, 2010) 39
Figure 2.11:Oil Selector TM Autonomous water Valve 41
Figure 2.12: Oil Selector TM Autonomous Gas valve 42
Figure 2.13: Disc type AICD (Halvorsen, et al., 2012) 43
Figure 2.14:Two Bech flow control designs. The top one has a membrane while the bottom uses a piston. 46
Figure 2.15: Bech flow control valve prototype design 47
Figure 2.16: Autonomous reversible Inflow Control Valve (Inflow Control, 2016) 47
Figure 2.17: Laminar and turbulent flow restrictors in Series 49
Figure 3.1: Turbulence Models available to use in FLUENT (ANSYS, 2006) 56
Figure 3.2: near wall regions experienced in turbulent flows (ANSYS, 2011) 63
Figure 3.3: Overview of processes involved in the Pressure based segregated algorithm solution methods (ANSYS, 2011) 72
Figure 3.4: Overview of processes involved in the Pressure based coupled algorithm solution methods (ANSYS, 2011) 73
Figure 4.1: Straight pipe geometry 86
Figure 4.2: mesh grid generated for straight pipe 87
Figure 4.3: Laminar (left) and turbulent (right) oil flow - Contours of static pressure 88
Figure 4.4: Laminar (left) and turbulent (right) water flow - Contours of static pressure 89
Figure 4.5: Laminar (left) and turbulent (right) gas flow simulations - Contours of static pressure 90
Figure 4.6: increase in pressure drop values with increase in pipe length 91
Figure 4.7: Graph comparing CFD and Analytical pressure drop values 93
Figure 4.8: Coil pipe geometry 95
Figure 4.9: Laminar (left) and turbulent (right) oil flow - Contours of static pressure 96
Figure 4.10: Laminar (left) and turbulent (right) water flow - Contours of static pressure 97
Figure 4.11: Laminar (left) and turbulent (right) gas flow - Contours of static pressure 98
Figure 4.12: Elliptical Straight pipe geometry 99
Figure 4.13: Laminar (left) and turbulent (right) oil flow - Contours of static pressure 100

Figure 4.14: Laminar (left) and turbulent (right) water flow - Contours of static pressure 101
Figure 4.15: Laminar (left) and turbulent (right) gas flow - Contours of static pressure 102
Figure 4.16: Square pipe geometry 103
Figure 4.17: Laminar (left) and turbulent (right) oil flow - Contours of static pressure 104
Figure 4.18: Laminar (left) and turbulent (right) water flow - Contours of static pressure 105
Figure 4.19: Laminar (left) and turbulent (right) gas flow - Contours of static pressure 106
Figure 4.20: Square coil geometry 107
Figure 4.21: Laminar (left) and turbulent (right) oil flow - Contours of static pressure 108
Figure 4.22: Laminar (left) and turbulent (right) water flow - Contours of static pressure 109
Figure 4.23: Laminar (left) and turbulent (right) gas flow - Contours of static pressure 110
Figure 4.24: Optimised slinky coil geometry 111
Figure 4.25: Laminar (left) and turbulent (right) oil flow - Contours of static pressure 111
Figure 4.26: Laminar (left) and turbulent (right) water flow - Contours of static pressure 112
Figure 4.27: Laminar (left) and turbulent (right) gas flow - Contours of static pressure 113
Figure 4.28: Square slinky coil pipe 113
Figure 4.29: Laminar (left) and turbulent (right) oil flow - Contours of static pressure 114
Figure 4.30: Laminar (left) and turbulent (right) water flow - Contours of static pressure 114
Figure 4.31: Laminar (left) and turbulent (right) gas flow - Contours of static pressure 115
Figure 4.32: Optimised square swirl coil geometry 116
Figure 4.33: Laminar (left) and turbulent (right) oil flow - Contours of static pressure 117
Figure 4.34: Laminar (left) and turbulent (right) oil flow - Contours of velocity magnitude 118
Figure 4.35: Vectors of velocity magnitude showing turbulence and recirculation zones observed 119
Figure 4.36: Laminar (left) and turbulent (right) water flow - Contours of static pressure 120
Figure 4.37: Laminar (left) and turbulent (right) water flow - Contours of velocity magnitude 120
Figure 4.38: Vectors of velocity magnitude showing turbulence and recirculation zones observed 121
Figure 4.39: Laminar (left) and turbulent (right) gas flow - Contours of static pressure 122
Figure 4.40: laminar and turbulent gas flow (Square swirl slinky pipe) - Contours of velocity magnitude 123
Figure 4.41: Vectors of velocity magnitude showing turbulence and recirculation zones observed 123

Figure 4.42: Comparison of the effect of coil pipe currently in use to developed square swirl slinky pipe geometry design on pressure drop 125
Figure 5.1: effect of flow geometry on the physics of flow regarding pressure drop in the laminar flow regime..... 129
Figure 5.2: the effect of the optimised fluid flow geometry enhancing oil recovery (LFE) 130
Figure 5.3: effect of flow geometry on the physics of flow regarding pressure drop in the turbulent flow regime..... 131
Figure 5.4: the effect of the optimised fluid flow geometry enhancing oil recovery (TFE) 132
Figure 5.5: Graph showing K factor values for various fluid flow geometry cases 133

Table of Tables

Table 4-1: Table of Fluid properties for numerical simulation 84
Table 4-2Table of values (pipe length, mesh elements, CFD, analytical pressure drop and correlation: 92
Table 4-3: Summary of laminar flow pressure drop values attained for each fluid flow geometry case 124
Table 4-4: Summary of turbulent flow pressure drop values attained for each fluid flow geometry case 124
Table 5-1 Correlated Laminar flow pressure drop values 128
Table 5-2: Correlated turbulent flow pressure drop values 128
Table 5-3: K factor values 132

Chapter 1 Introduction to fluid flow geometry optimisation

Fluid flow can be classified as either an external flow or an internal flow Cengel & Cimbala (2014). The importance of fluid flow transport in daily operations cannot be over emphasised as the application of flow in a pipe is very diverse. Flow can happen in an assortment of natural, mechanical and building procedures, for example, very simply hot and cold water in the home after coming through extensive piping networks is distributed through pipes, the oil industry thrives on transportation of oil and gas over hundreds of miles of pipelines, arteries and veins are our bodes own pipes, engine cooling is achieved by fluid flow through radiator pipes, hydronic space heating and solar water heating systems transfer their thermal energy in through fluids circulated by pipes. Other applications of fluid flow are contaminant clean up Mercer and Cohen, 1990; Mulligan et al., 2001, liquid detachment in power modules (He et al., 2000; Srinivasan, 2006), improved oil recuperation (Lake, 1989), and carbon dioxide stockpiling in land permeable media (Marini, 2006). The analysis of fluid flow and how the fluid flow geometry affects the physics of flow very important in engineering due to the rigorous engineering applications and its implications.

The effects of fluid flow geometry on the physics of fluid will be considered during this thesis in through the study of the Autonomous Inflow Control Valve (AICV) which is used to enhance oil recovery. The influx of water and or gas into the wellbore is a problem which diminishes oil recovery, increases separation costs and drastically reduces well production life. The current solution to this problem is the use of an Autonomous Inflow Control Valve (AICV) developed through the European Union's Seventh Framework Programme (EU FP7) project called Reversible Inflow Control Valve (REVIVAL). The current Autonomous Inflow Control Valve AICV works based on different viscosity of oil, water, and gas. The hostility of the oil recovery

environment in terms of high temperature and pressure makes the case for the use of mechanical actuation in the AICV. The actuation of a piston which controls the working of the AICV is based upon the pressure drop between laminar and turbulent flow elements hence as will be seen in the thesis, the fluid flow geometry which leads up to these elements is very important and its effect on the physics of flow will be optimised.

A considerable collection of writing, including exploratory, explanatory and numerical investigations, demonstrates that exact measurement and understanding of the material science of such streams is of overwhelming significance to plan and control these procedures ideally and securely (Blunt, 2017). The broad term “flow” can be used to address a large variety of flow patterns and regimes involving flow of two or more phases; in this work, as a specific class of flow through varying geometry, the focus is on immiscible liquid flow at the micro-scale in geometry and its effect on physics of the fluid. In this type of flow, the flow regime are distinct interfaces which can also form contact with the conduit surface. The variety of possible topological configurations for the interfaces, different degree of affinity for fluids to cover the affected geometries which form inherent complexity of the flow path which makes the prediction of the flow behaviour a very challenging task.

In general, fluid must be conveyed from one location to another using conduits hence, aspects of the physics of flow in conduits with relevant simulations will be discussed. Fluid properties such as the effect of one or more phase present during fluid flow in the conduit, friction, fluid flow in the laminar or turbulent flow regimes, dissipation or transfer of energy will be tackled in terms of fundamental physics and empirical approaches. In order to gain further understanding into the physics of fluid flow, flow through the conduits such as straight tubes have been the subject of various studies over a long period of time. Placing streams of ink into water flowing in pipes was one of the fundamental ways Reynolds used to carry out his original experiments. Fundamental flow equations and their exact solutions exist for only a few flow

problems such as for axial laminar flow through a cylindrical pipe in the steady state. The Naiver-stokes equation which is effectively an illustration of the conservation of both mass and momentum for fluid flow is used to analyse fluid flow in conduits by fusing viscous stresses in order to generate a friction force term with its basis on both physics and empirical results. The physics of fluid flow is made up of elements which include the forces, motion and energy transformations. These elements help to gain understanding into the effects of fluid flow geometry on the physics of flow. The existing level of understanding in this area and some of its background knowledge will be reviewed in this thesis.

1.1 Background theory

Fluid flow can be classified as either an external flow or an internal flow Cengel & Cimbala (2014), This classification solely based on whether the fluid flows through a conduit or over a surface. This thesis will only focus on internal fluid flow with the pipe geometry filled entirely with fluid and the flow driven by the differential pressure (Gwinnutt, 2018). Therefore, all the discussed theories of fluid flow and how its conduit geometry affects the flow physics below are about the characteristics of internal fluid flow. The best way to distinguish the flow regime according to Cengel & Cimbala (2014), is injection and observation of dye in the middle of a flow stream. In a steady flow stream with low velocity, there is a straight- and smooth-line pattern exhibited by the injected dye however when the velocity increases, there is a sudden change in pattern. The dye will become zigzag swiftly and unsystematically in very high velocities. It can be deduced from this illustration that the laminar flow regime is characterised by the dye which displays steady and smooth lines while random patters are categorized as turbulent flow. Osborne Reynolds, a British engineer conducted the experiments involving injecting dye the fluid flow stream. He discovered that the laminar flow regime is specified as smooth streamlines with highly ordered motion and the turbulent flow regime is identified by velocity fluctuations with

highly disordered motion. The picture of the dye injection experiment can be found in Figure 1.1.

When the effects of momentum due to high Reynolds numbers dominate the viscous forces, the flow is said to be turbulent (Jurih, 2007). Randomly fluctuating velocity fields at many distinct length and time scales and random motion of fluid masses in three dimensions are major characteristics of turbulent flow. These fluctuations in velocity field are exhibited as regions of swirl motion or eddies (Wilcox, 2004). Turbulent flow which is almost always present during free surface flow in nature. The flow is irregular, random and chaotic. According to Launder and Spalding (1972), a spectrum of different sized eddies are contained in the flow; with the largest eddies being of the order of the fluid flow geometry. Since turbulent flow is dissipative, smaller eddies which are governed by viscous forces are dissipated into internal energy. Kinetic energy is transferred to the small eddies from the larger eddies and those obtain their energy from even larger eddies etcetera. The mean flow supplies energy to the largest of the eddies. The cascade process describes this transfer of energy from the largest turbulent eddies to the smallest.

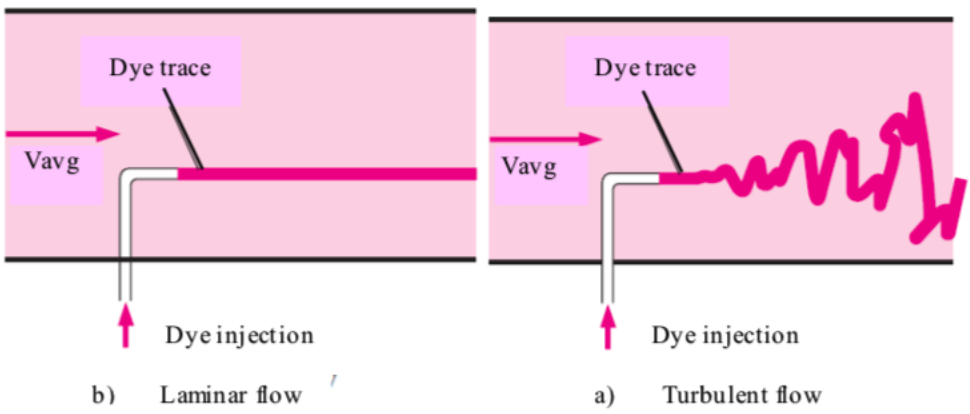

Figure 1.1: The Behaviour of Coloured Fluid Injected into the Flow in Laminar and Turbulent Flows in a Pip (Cengel & Cimbala, 2014, p.349)

The different behaviours of laminar and turbulent flow are depicted in Figure 1.1. A great mixture of fluid is exhibited in the turbulent flow regime due to prompt fluctuations. This phenomenon supports an increase in transfer of momentum between fluid particles. According to Cengel & Cimbala, (2014), the momentum transfer also results in an increase in frictional forces on the pipe wall which maxes out at fully turbulent flow. This is because at fully turbulent, the momentum between fluid particles becomes very high which leads to the large friction force on the pipe wall.

Reynolds number which describes the ratio of inertial and viscous forces of the fluid is a non-dimensional number used to determine the flow regime; whether laminar, transitional or turbulent of a fluid flowing through a pipe. Low Reynolds number leads to laminar flow regimes as the flow is dominated by viscous forces. Reynolds number is defined as

$$Re = \frac{Inertia\ forces}{Viscous\ forces} = \frac{\rho VD}{\mu} \quad (1.1)$$

Where V is the velocity, D is the pipe geometry diameter, μ is the viscosity and ρ is the density

Mostly, in the empirical condition, the flow regime inside the circular pipe can be defined as laminar flow with $Re \lesssim 2300$; transitional flow with $2300 \lesssim Re \lesssim 4000$; and turbulent flow with $Re \gtrsim 4000$ (Cengel & Cimbala, 2014). This thesis does not consider transitional flow and deals with laminar and turbulent flows.

Flow in a pipe is affected by parameters such as pipe wall roughness or friction factor, pipe diameter, pipe length and viscosity and straightness of the pipe. All the above-mentioned variables can be accounted for in the Hagan-Poiseuille equation

$$\Delta P = \frac{128\mu LQ}{\pi d^4} \quad (1.2)$$

Where ΔP is the drop-in pressure, L is the pipe geometry length, μ is the dynamic viscosity, Q refers to the volumetric flow rate, d is the pipe geometry diameter and π is a mathematical constant.

Fully developed flow in a curved pipe and its effects have been reviewed in previous studies. A solution to depicting how fluid behaved in the central core which experienced a prompter flow than the average flow because of centrifugal forces was discovered by Dean during his investigations of flow in a curved pipe. According to Spedding, et al., (2004), slow moving fluid at the wall region moves towards the centre of the pipe where there a lower pressure. Hence the ratio of inertia forces to viscous forces acting on a fluid flowing in a curved pipe under the effects of centrifugal forces can be represented by a non-dimensional Dean number (De) given by (Shirayama & Kuwahara, 1987): Thus, to give a non-dimensional number from mathematical expression for the ratio of the viscous force acting on a fluid which is flowing in a curved pipe to the centrifugal force, Dean Number (De) is given:

$$De = Re\sqrt{\frac{R}{A}} \qquad (1.3)$$

Where Re is the Reynolds number, R is the radius of the cross section, and A is the outside radius of the curve. The ratio of R/A is shown in Figure 2.

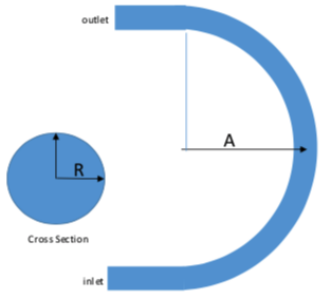

Figure 1.2:Illustration of R/A Ratio (Shirayama & Kuwahara, 1987, p. 52)

1.2 Gap in knowledge

Oil recovery is a multi-billion-dollar industry that will continue to grow with every passing day. The reasons for its growth are endless but it mostly comes down to the profitability that is associated with this operation. To achieve maximum oil recovery, several inflow control devices have been developed and used in oil wells. However, due to water/gas breakthrough, it is extremely difficult to extract all the oil from a well. Premature breakthrough can make oil recovery very expensive that could lead to substantial losses. The control devices for oil extraction have evolved over the years starting from ICDs (Inflow Control Devices) to AICDs (Autonomous Inflow Control Devices), then ICVs (Inflow Control Valves) and finally AICVs (Autonomous Inflow Control Valves). They all work on the principle of pressure drop that can help in maximising oil extraction. Despite advances in the study of fluid flow geometries, a clear gap in knowledge exists when it comes to the study of optimum fluid flow geometries that affect the physics of flow in terms of pressure drop. For oil extraction control devices, fluid properties such as density, viscosity, effect of one or more phase present during fluid flow in the pipes, friction, fluid flow in the laminar or turbulent flow regimes, dissipation or transfer of energy etc., play a crucial role in determining their optimal performance. This research work aims to propose new designs for the AICV that can lead to enhanced pressure drop and can compete with the performance of the existing circular coil pipe used for AICV.

1.3 Aim and Objectives

The aim of this research is to design a fluid flow geometry capable of achieving optimal pressure drop for oil recovery. The objectives of this work are listed below in a logical order:

1. To undertake literature review of fluid flow parameters and their effect on the physics of flow
2. To identify geometry parameters for AICV that can avoid premature water and or gas breakthrough
3. To propose new designs for the AICV that can lead to optimum pressure drop
4. To compare the CFD results of the circular coil pipe of the AICV with the newly proposed designs
5. To optimise the design with the best results compared to the circular coil pipe of the AICV
6. To compare the simulation results of the optimal design with analytical values

1.4 Methodology

Qualitative, quantitative and mixed methods are the three major approaches for research. According to Connelly (2009), research methods should follow research questions in a way that the best chance to obtain useful answers is offered (Connelly, 2009). A mixed method approach is used for this research as it involves the analysis of both quantitative (numerical/measurable data) and qualitative (understanding of underlying reasons) data. The data is collected sequentially starting from theoretical knowledge (laws, principles, models, concepts, etc.) and then moves towards empirical knowledge (acquiring data through numerical simulations, observations, facts etc.). The collected data is then integrated to make a complete model of research that could either be inductive or deductive. This research first formulated a theory and then tested it, therefore, it falls under the deductive approach as like other engineering related researches. Inductive approach is the opposite of deductive and is more suitable to social sciences and humanities. The aim and objectives of the research (Section 1.3) were formulated first to develop a road map for the research (Fig. 1.3).

Figure 1.3: Roadmap of the PhD research project

1.5 Thesis structure

The thesis is divided into six chapters. A summary of the contents of each chapter are outlined below.

Chapter 1: Introduction

This chapter introduces us to the topic and area of research. It covers a general overview of fluid flow in geometries, the physics and background theory, laminar and turbulent flows, the problem statement, gap in knowledge, aim and objectives, hypothesis and a breakdown of the thesis and the research to be undertaken in each chapter.

Chapter 2: Literature review

This chapter gives us an in-depth review through review of published work and various resources on flow through various geometries in section 2.1, heat transfer in turbulent flow in section in 2.2, swirl flow in section 2.3, inflow control in section 2.4 and solar water heating in section 2.5.

Chapter 3: Methodology

This chapter focuses introduces the background of CFD, its codes and elements, applications of CFD to enhanced flow, swirl flow and the equations that govern the flow in section 3.3 and pressure drops in the conduits simulated and heat transfer are covered in this chapter.

Chapter 4: Numerical cases and simulations

This chapter presents the fluid flow model geometries as constructed in ANSYS Fluent's pre-processor programme ANSYS design Modeller from sections 4.2 to 4.4. The chapter further investigates how suitable the CFD package is to model the flow

scenarios, the mesh independency test, length independency tests, ideal pitches for the swirl pipe geometry and general optimization of the numerical cases.

Chapter 5: Results and Discussions

This chapter presents the Computational Fluid Dynamics Simulation work done, the results obtained. The chapter also analyses the results achieved

Chapter 6: Conclusions and Recommendations

This chapter draws conclusions on simulations run and results analysed and suggest some recommendations and future work.

1.6 Publications

The following is a list of publications that are available at the time of thesis defence.

Published Peer-Reviewed Journal Papers

Butt, J., **Onimowo, D**., Gohrabian, M., Sharma, T. and Shirvani, H. (2018). A desktop 3D printer with dual extruders to produce customised electronic circuitry. Frontiers of Mechanical Engineering, 13(4), pp.528-534.

Chapter 2 Literature review

Geometry optimisation is a crucial element for enhanced fluid flow capable of providing different applications. Natural oil is a fluid that has been investigated rigorously as its extraction could lead to billions in profits. Drilling into the oil reservoir and installation of pipe lines for oil extraction are considered to be highly lucrative businesses. To improve oil extraction through these pipes, control devices have been put into operation since the early 1990s. This chapter will provide literature review of such devices and the effect of different fluid flow regimes i.e., laminar and turbulent. The use of numerical analysis with Computational Fluid Dynamics (CFD) has been discussed. The focus has been on the control devices i.e., ICDs (Inflow Control Devices), AICDs (Autonomous Inflow Control Devices), ICVs (Inflow Control Valves) and finally AICVs (Autonomous Inflow Control Valves). They all work on the principle of pressure drop that can help in maximising oil extraction from oil wells. The discussion involves the effect of fluid flow with numerical and analytical studies through straight and curved pipe geometries. The only true autonomous valve is the AICV that regulates the pressure drop to allow for crude oil to be extracted without the mixing of water/gas.

2.1 Review of fluid flow through geometries

Many research analyses have been carried out on internal flow and how the flow is affected by the fluid flow geometry over the years. A study which found out that the energy conservation equation can be used for a steady incompressible fluid flowing through a smooth pipe, was carried out and used by Taylor (1984) to model airflow through sampling pipes. This energy conservation equation is applicable to either laminar or turbulent flow.

The laminar flow of an incompressible fluid in the pipe inlet was investigated by Hornbeck (1964) with a numerical solution. Using finite difference meshing procedures in which pressure and velocity at various positions in the pipe were calculated from upstream values obtained at that point, the numerical solution was attained. Hornbeck deduced that he could use numerical techniques to provide a close approximation to the equations of fluid flow. The results obtained from his research were significantly different in terms of velocity profiles and development lengths in comparison to previous research due to a no flat core assumption. In the previous research by Campbell and Slattery (Campbell & Slattery, n.d. cited in Hornbeck, 1964, p.224), in almost the entirety of the entrance region, a flat central core was assumed to be installed in the centre of the pipe (Radius (R) =0) until R = 0.9. The velocity derived from numerical solution increased faster than the velocity at the centreline (R = 0) due to this flat core assumption. The previous work also saw a more rapid increase in velocity at R = 0.6. at R = 0.9, the results were similar. This agrees as the velocity in this region is not affected by the flat core.

At different low and moderate Reynolds numbers (Re) between 0 to 500, laminar flow of a homogenous viscous liquid in a pipe was studied by Friedmann et al., (1968) and compared to previous research. Using the finite difference equations, they calculated the distribution of velocity and velocity profiles numerically. The letter u and v were used to denote the velocity and the axial velocity component. Axial coordinates and radial coordinates are connoted by x and r respectively. The velocity distribution curve was in agreement with previous work by Nikuradse's experiment (Prandtl & Thetjens, 1957, p. 27, cited in Friedmann et al, 1968, p.431) for the downstream region ($2x/Re \leq 0.07$) for Reynolds number Re = 200 and 500. When the values of x became larger the distribution curve fit deteriorated. At the location, x = 0 at the inlet of the pipe, a "kink effect" was detected in the velocity profile. Other studies on flow in a straight channel also detect this effect as demonstrated by Brandtl and Gillis (Brandtl and

Gillis, 1964 cited in Friedmann et al., 1968, p.432) and by Wang and Longwell (Wang and Lognwell, 1964 cited in Friedmann et al., 1968, p.432).

The distinctive flow parameters of natural gas, its velocity and pressure distribution inside the straight pipes which had elliptical and circular cross sections were studied by Cade et al. (2010). A three-dimensional mathematical model was used to study the fluid flow and the results were acquired by using CFX-3D CFD. The ratio of L_1 and L_2, where L_1 was the radius of the cross-section in the horizontal axis, and L_2 was the radius of the cross-section in the vertical axis were used to define characteristic parameters for the setup of the elliptical and circular cross section pipes. An elliptical pipe with dimensions L_1 = 0.1 m and L_2 = 0.3 m and a circular pipe with dimensions $L_1 = L_2$ = 0.173205 m and were studied. 0.1 m/s was used as the inlet velocity boundary condition for all pipes. A pressure drop of about 0.014347 Pa occurred in the circular pipe while in the elliptical pipe, the pressure drop was about 0.021516 Pa. the pressure drop in the elliptical pipe is 50% higher than in the circular pipe at equivalent mass flow rates. It was also discovered that the elliptical pipe experienced 50% higher volumetric flow rate than the circular pipe in other analysis run with on two pipes with dimensions; $L_1 = L_2$ = 0.1 m, a pressure drop of 0.032060 Pa and a second pipe was elliptical pipe with dimensions L_1 = 0.1 m and L_2 = 0.15 m with a pressure drop of 0.025226 Pa. it could therefore be concluded that the fluid flow geometry affected the physics of flow in terms of the velocity of natural gas. A longer hydrodynamic entrance length was required with a higher the aspect ratio (L_2/L_1) inorder to achieve fully developed flow.

Analysis of the Navier-Stokes equations of laminar and incompressible flow in a curved pipe using finite difference procedure of numerical solution was carried out by Shirayama & Kuwahara (1987). The pressure equations were solved using the consecutive over relaxation method while the Euler implicit scheme studied the time

integration for this study. The third order upwind scheme was used to approximate the non-linear terms while central difference approximation was use for the spatial derivative terms. The simulation was run using Japanese super computers such as Fujitsu VP 200, VP 400, and NEC SX/2. A circular pipe with straight pipes at the inlet and outlet formed the computational domain. The circular pipes had radius of 0.05, 0.143, and 0.148 and a varied Dean number from 183 to 3847. Two symmetric recirculating regions were observed in flows with low-Dean- Numbers. The separation of cross- sectional flow occurs due to secondary motions with an increase in Dean Numbers. An unsteady flow field occurred because of separation of the main flow in high Dean number flows while recirculation occurred when the flow is subject to the viscous fluid element's response to the instability between the acceleration of centripetal forces and the pressure gradient of the cross section encouraged by lateral curvature of the main flow. Some occurrences of recirculation due to the main flow separation were still noted.

To improve the available techniques to mathematically model the performance of aspirated smoke detection systems, Cole (1999) investigated the disturbances to pipe flow regimes by jet induction. A significant area of uncertainty with regards to the friction factor was brought up by the study. Cole suggested that it may not be true to assume the flow regime was fully developed. The division of energy losses in pipe fitting into three components, namely; entry loss, exit loss and friction losses by Cole (1999) was in unison with previous and similar research carried out by Taylor (1984). To determine when turbulent motion starts to develop in the wake region of the flow; using Reynolds numbers of 200 to 400, Bloor (1964) investigated the flow around a circular cylinder. He observed that large-scale three- dimensional structures triggered the transition of flow in the wake region.

Mullin and Peixinho (2006), Sahu *et al* (2009), Willis *et al* (2008) performed several studies on the patterns of flow in pipes. The accuracy of numerical modelling of the laminar equation to determine the friction factor of pipe was tackled by Saho *et al* (2009). At an entrance length of 2.7068m, the friction factor was found to be 0.0151. A laser-Doppler velocimeter was used to study transitional pipe flow with regards to the effect of varying the Reynolds number from 1500 to 4000 on the velocity fluctuations by Banfi *et al* (1981). The study showed that in the transition region at a Reynolds number of about 2800, the velocity fluctuations were at maximum. Results from experimental and numerical investigations of both non–Newtonian fluids at transition to turbulence were compared by Rudman *et al* (2002). Flow features like turbulent puffs and slugs observed in Newtonian transitional flows were picked up in experimental results. Turbulence suppression drag reduction and delayed transition as observed experimentally were also detected Numerically however, there were some quantitative discrepancies with the experimental results. Yogini (2010) used the large eddy simulation (LES) and RANS Shear-Stress Transport (SST) approaches to carry out a numerical simulation of flow past a circular cylinder for Reynolds 1000 and 3900. The results he extrapolated from his numerical analysis agreed with the experimental data of Zdravkovich (1997). The analytical results obtained when Bhandari D. and Singh S. (2012) analysed fully developed turbulent flow in a pipe agreed with those obtained they used computational fluid dynamics. The hypothesis that 'turbulent stresses are linearly proportional to mean strain rates' as suggested by the idea of an eddy viscosity in addition to molecular viscosity was introduced by Boussinesq (1877) is still the cornerstone of most turbulence models.

The idea of a mixing length for determining the eddy viscosity was introduced by Prandtl (1925). Taylor (1935) introduced formal statistical methods involving correlations, Fourier transforms and power spectra tools for the analysis of homogeneous isotropic turbulence and was the first researcher to utilize a more

advanced level of mathematical rigor. Some of the most important and most often quoted results of turbulence theory often referred to as the “K41 theory”, are found in three papers published by Kolmogorov (1941). Two specific testable results, the $\frac{2}{3}$ law which leads directly to the inertial range of the energy spectrum the $K^{\frac{-5}{3}}$ decay rate and the $\frac{4}{5}$ law for results of turbulence at high Reynolds numbers. Kolmogorov scale is an alternative name for dissipation scales. These scales were predicted based on dimensional analysis as part of the K41 theory. The ω eddy viscosity which is dependent on turbulent kinetic energy was theorised by Prandtl (1945).

In the late 1950s, mathematical methods from quantum field theory were used as part of new techniques to analyse turbulence as seen in the work of Kraichnan (1958). A deterministic solution to a simple model of the Navier-Stokes equations was presented by Lorenz (1963). The most important advances of the 1970s and 80s were the computational techniques as viewed from present day turbulence investigations. Large-eddy simulation (LES) as proposed by Deardorff (1970) was the first of these closely followed by Orszag and Patterson (1972) with the first direct numerical simulation (DNS). Launder and Spalding (1972) heralded the introduction of a wide range of Reynolds-averaged Navier– Stokes (RANS) approaches.

The dynamic models of Germano *et al* (1991) and Piomelli (1993) for construction of the required subgrid-scale models are some of the new approaches being explored. Launder and Spalding (1972) have done the most in-depth work on two-equation models hence, Launder’s $k - \varepsilon$ model is the most widely used two-equation model. After some improvements were made to the $k - \varepsilon$, it was called the standard $k - \varepsilon$ by Launder and Sharma (1974). Kolmogorov (1942) proposed the first two-equation $k - \omega$ model. Various improvements to the model by Saffman (1970), Wilcox and Alber (1972), Saffman and Wilcox (1974), Wilcox and Traci (1976), Wilcox and Rubesin

(1980) and Wilcox (1998), Speziale e*t al* (1990), Menter (1992) and Peng *et al* (1997) have been made to the $k - \omega$ model. Where integrating through the viscous sub layer and effects of adverse pressure gradient prediction is required, the $k - \omega$ model sees its advantages over the $k - \varepsilon$ model.

The analyses of laminar flow have been approached with different views by several researchers. The analysis of laminar flow in porous circular pipe by perturbation theory, in which flow parameters such as axial and radial velocity profile, skin friction, axial pressure and mass flow were considered, was conducted by Soundalgekar et al (1993). They discovered that with an increase in pressure gradient comes a decrease in skin friction while with an increase in pressure drop you also obtain an increase of mass flow. After studying laminar forced convection in a heated pipe subjected to a reciprocating flow, a numerical solution was generated by Zhao et al (1995). The four major heat transfer parameters associated with this problem, which are; the kinetic Reynolds number, $R\omega$, the oscillation amplitude, A_o, the length to diameter ratio (L/D), and the Prandtl number of the fluid were included in the findings. As deduced from the results, when the kinetic Reynolds number, R_ω, and oscillation amplitude, $A_{o\ increase}$, the average heat transfer rate increases. The reverse occurs with length to diameter ratio (L/D). The pressure drop in a flowing fluid through a channel with a porous wall is a function of wall permeability, channel dimension, axial position, and fluid properties (Karode., 2001).

In the study of fluid mechanics, flow through the annular region is an important form of flow. In oil industries, the behaviour of fluid flow through the annular region has its great application hence its behaviour cannot be overstated. Therefore, with the help of Computational Fluid Dynamics (CFD), the effect the fluid flow geometry on the flow and losses encountered with this kind of flow will help in the effective design, parameters such as; the profiles of pressure drop, entrance length, axial and

tangential velocities, and the flow path prediction have been thoroughly investigated. According to Pereira1et al (2010), these variables are usually considered relevant for an understanding of well drilling mudflow and the particles transported by it.

Laminar flow of water over an ice layer which is subjected to slip condition is used to analyse mass and heat transfer. A para- metric mathematical model is used to simulate the coupled heat and mass transfer events occurring in moving boundary, problem associated with a quasi-steady state steady flow process (Raoufpanah, 2005) is used to analyse this problem. The simple algorithm is used to also numerically analyse vapour flow in a concentric annular heat pipe. The fluid flow and the heat transfer in the annular vapour space are simulated using the Navier-stoke equations while the finite volume approach is used to solve the governing equations. Nouri-Borujerdi and M. Layeghi, (2004) tell us that when compared to previous research works the results were in strong agreement in accuracy. Using a drift flux model, Nouri-Borujerdi et al (2010) carried out an analysis that predicts the critical mass flow rate, pressure, vapor quality, and void fraction in a capillary tube under critical condition. Some generalized correlation for predicting the flow properties as a function of the flow parameters and the capillary tube sizes under various critical conditions were developed by using the dimensional analysis by Buckingham's π theory. An inlet pressure in the ranges of $0.8 \leq P_{inlet} \leq 1.5$ MPa, the sub cooling temperature in the range of $0 \leq \Delta T_{sub} \leq 10$℃, the tube diameter is in the range of $0.5 \leq D \leq 1.5$mm and tube length is in the range of $1 \leq L \leq 2$m for water, ammonia, refrigerants R-12, R-22 and R- 134 as working fluids are some of the parameters used in this research. This study is of a great importance in the design of refrigeration system

Another important area of fluid flow investigation is the behaviour of gas flowing in pipes. Compressible flow in gas pipeline was numerically modelled and subjected to

wall friction and heat transfer. The effects of heat on the pressure drop, temperature, and the mach number were also investigated using the result obtained from this study on a natural gas pipeline under different thermal condition. These are caused by the friction and the heat exchange changes Nouri-Borujerdi et al (2007). Fluids flow through smooth circular micro-channels with different diameter was studied using Numerical analysis air with slip boundary conditions and water with no slip boundary conditions were the two fluids considered. The finite volume approach was used to solve a combination of the momentum and energy equations. The dissipation term in the energy equation was considered due to the small dimensions of the micro-channel. The results show that with the air as flowing fluid the pressure gradient is nonlinear along the micro-channel, while considering water as the flowing fluid and considering adiabatic boundary condition, the smaller the micro-channel the higher the velocity of flow, and an increase in the flow temperature would be observed, and the temperature increase is a linear function of the axial position (Nouri and A. Nabovati, 2008).

Micro-channels with a partial semi-circular profile have also been used to analyse laminar flow. This work investigated fully developed laminar flow as a function of the circularity index, κ, which is the ratio of the radii along the curved surface to the radii along the flat surfaces of the partial semi-circular profile. A correction factor, K, to the Hagen-Poisuille could be determined, and was related to the circularity index. It was observed that, the level of wall shear stress, when normalized by the pressure drop per unit length, increased approximately linearly with increase in the circularity index, K (Federspie and I. Valenti, 2012).

In the study carried out by Yang et al (1993), the finite difference numerical method is used to solve the full Navier-stokes for the modelled problem for fully developed flow in a curved pipe with arbitrary curvature ratio (the ratio of the pipe radius to the

pipe curvature), but in the study also put heat transfer into consideration by heating the pipes. The curvature ratio was varied in ranges from 0.1 to 0.9, while both the Reynolds Pradtl number were varied from 1 to 2000, and 0.7 to 300 respectively as opposed to previous studies which considered the curvature ratio in the ranges less than 0.3. A good correlation with the curvature ratio parameters, the Dean number (De) and the prandtl number and the friction ratio and the Nusselt number ratio was seen from the results.

Brebbia et al. 1984 cited in (Sarbu and A. Iosif, 2009) tells us about another important approach to reduce the quantity of data necessary to solve the problems, which is very effective for the analysis of heat flux in the flowing fluid is boundary element method (BEM), which has a better advantage compared to finite difference or finite element method due to the fact that instead of full domain discretization, only the boundary is discretized into elements and internal point position can be freely defined. Dual reciprocity boundary element method (DRBEM) was used to analyse under constant heat flux boundary condition the laminar heat convection problem between two coaxial cylinders. This kind of numerical approach to fluid flow and heat transfer between two coaxial cylinders under different number of boundary elements has given a strong accuracy compared to other numerical tools (Sarbu and A. Iosif, 2009).

Heat transfer in fluid flow has also been considered by focusing on the effect of fins which contributes to the rate of heat transfer. For both laminar and turbulent flow, internal fins were investigated as a function of number of fins present and as a function of the height of the fins in this study. The rsults as discussed by ucel and N. Dinler, 2006 show that for laminar flow it was discovered that the mean Nusselt number decreases and the friction factor increases as the number of fins increases, while for turbulent flow, both the mean Nusselt and friction factor increase but, for

increase in the height of the fins led to increase in friction factor for all Reynolds numbers selected.

Cade et al, (2010), conducted a research study on fluid flow in another important form of pipe configuration, that is, elliptic cylindrical pipe detracting from most of the research works which have concentrated much on fluid flow in circular pipes. The fluid flow in elliptic cylindrical was investigated in the hydrodynamics entrance region in this study. The results derived from various flow parameters used are reliable and can be used to describe the behaviour of laminar flow in an elliptic cylindrical pipe.

2.2 Review on swirl flow

In a pipe flow, when both vortex and axial motions are combined with helical streamlines, the flow is said to be a swirl flow (Baker and Sayre, 1974). Where the swirl flow contains a tangential component of velocity, there is bound to be an increase in the velocity oscillations (Fokker, 2006, Algifri et al., 1988). According to Gupta et al, (1984), swirl flow can be majorly applied in furnaces, gas turbines and cyclones with the aim of enhancing heat transfer, better mixing, and better separation and so on. There are three general methods used to induce swirl flow;

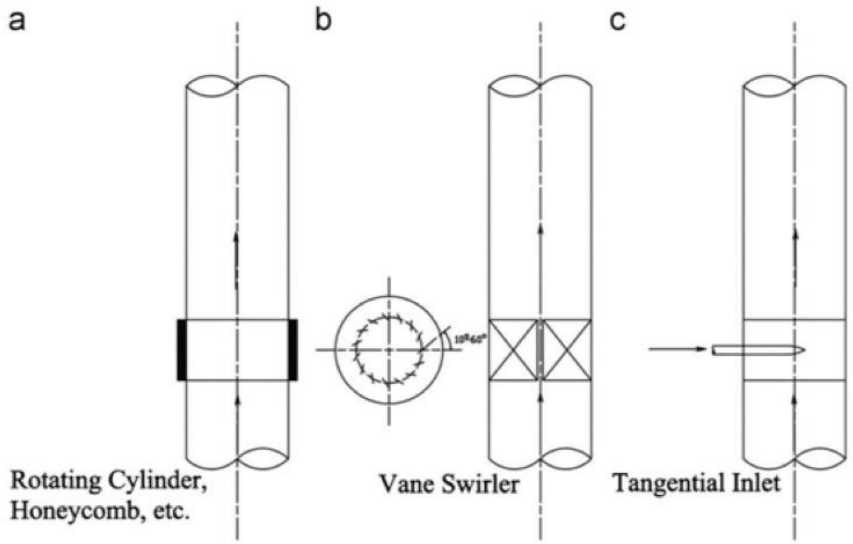

Figure 2.1:Types of swirl generation (Najafi et al., 2011)

From the image above, in a, the swirl flow is generated when the fluid flows through the rotational section and acquires a tangential momentum. Where fixed blades are mounted in the pipe at a specific angle as shown in b, and the fluid is introduced into the pipe, the angle at which the blades of the vane sits acts as an efficient constraint for determining the intensity of the swirl flow field. When the flow acquires a rotational momentum after being introduced into the conduit via a tangential inlet as shown in c, it also forms a swirl flow (Gouzhen, 2016). These are swirl generators which impart the flow with swirl when it goes through them and downstream of the generators, the flow has tangential velocity component known as the swirl velocity component. Kitoh (1991), suggests that most methods of swirl generation are correlated with the radial distribution of tangential velocities. According to the radial distribution of tangential velocities, there are three different types of swirl (Steenbergen and Voskamp, 1998).

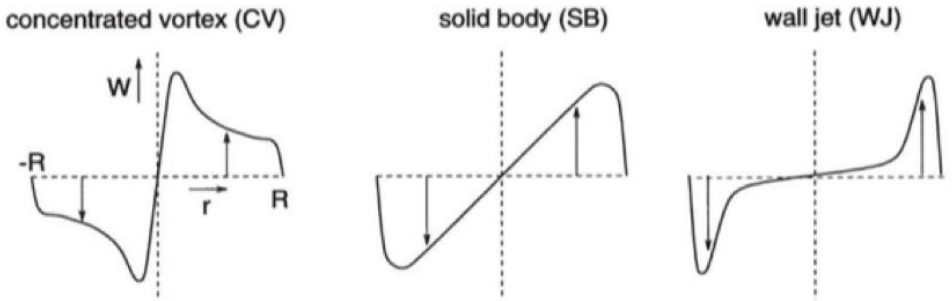

Figure 2.2: Types of swirl and their classifications (Steenbergen and Voskamp, 1998).

The first type as shown in figure 2is the concentrated vortex (CV) type of swirl in which the rotation occurs close to the pipe centre, solid body swirl types are characterised by almost uniform rotation while the wall jet (WJ) types see the concentration of angular momentum near the pipe wall (Steenbergen and Voskamp, 1998).

Non-circular cross section swirl inducing pipes which generate swirl when the flow passes through them including spiral ribs or fins located within the pipe (Robinson, 1921, Yuille, 1927, Wolfe, 1967, Charles et al., 1971, Schriek et al., 1974), pipes with

rifles installed inside (Howard, 1939) and tubes with spiral grooves (Spanner, 1940) have also been studied in addition to the already stated three methods. Reduction in deposition of particles in pipes, heat exchanger augmentation, reduction in wear and tear of pipes. Power consumption efficiency and particle conveyance enhancement are some of the applications of swirl inducing conduits. Direct particle impact from flowing particles could give rise to damage and wear of the pipes which contain insertions or ribs and also create problems of cleaning and or fouling when used in food or beverage industries (Gouzhen, 2016). Swirl induction in helically shaped pipes can be tracked back to 1993 when there was an idea suggested by jones to solve the issue of low velocity particles settling in the pipe by giving a helical profile to promote suspension (Jones, 1997). Raylor (1998), Ganeshalingham (2002), Tonkin (2004), Ariyaratne (2005) and Fokeer (2006) also went on to investigate Jones idea. In this thesis, the pipes investigation which induce swirl do not make use of ribs, fins or vanes within them. The physics of flow in the fluid which creates swirl is however induced by the fluid flow geometrical shape of the swirl pipe through which the fluid flows.

In 1998, Raylor carried out an experimental investigation which has its basis on the improving the efficiency of marine boilers using swirl pipes. He however just focused on sing the swirl flow generated to reduce wear and enhance the flow of fluid through a bend (Raylor, 1998). Various pipes shapes and their swirl induced flow fields were examined by Raylor using commercial CFD software fluent. In a geodesic pipe as suggested by Raylor, the swirl produced, and pressure drop created increased when the pitch to diameter ratio reduces. The simulation results were tested using a mixture of water and plastic beads in an experimental rig. It was concluded from he's tests and simulation that the swirly flow pipe when compared to a standard pipe, increased the drop-in pressure along the pipe length. There was less pressure drop across the pipe bend due to swirl flow induced by the swirly-flo pipe in comparison to the non-swirl induced flow of water and plastic beads. The problem of wear in the pipe bend

could be solved as there was a more uniform distribution of particles throughout the bend due to the swirl induced flow before the bend (Gouzhen, 2016). The distance the rib travels axially as it rotates through a 360-degree angle, is known as the pitch. A defining basis Raylor used to define the pitch of his swirl inducing pipe. A very important parameter which defines the properties of a swirl inducing pipe is the pitch to diameter ratio (P: D) (Singh and Charles, 1976).

In 2002, using results obtained from Particle Image Velocimetry (PIV), Electrical Resistance Tomography (ERT) and, measurements of pressure, Ganeshalingham validated the CFD code used in the swirly-Flo pipe study carried out by Raylor (Ganeshalingam, 2002). From the study of the radial distribution of tangential velocities experiences after the device induces swirl flow, it was found that the results were in accordance to the wall jet swirl type as classified by Steenbergen and Voskamp (1998) based on the tangential velocities' radial distribution. For flows with a higher Reynolds number, it was also discovered that the decay of swirl downstream of the swirl inducing devices was faster as inferred form CFD results. Further optimisation of the swirl pipe using computational fluid dynamics which was aimed at solid mixture flows was carried out by Ganeshalingam. After testing various cross sections which included squares, triangles, pentagons and hexagons, he found out that the corss section with 4 lobes has the most effective swirl generation as compared to the others. A pitch to diameter ratio of 8 for a 400mm length of pipe was recommended by Ganeshalingam.

The application of the swirl pipe when pumping an array of fluid and or fluid particle mixtures through various pipe configurations was investigated by Tonkin in 2004. Using fluid mixtures such as coal and water, sand and water or magnetite and water slurries, each varying in particle size, the effect of induced swirl from the swirl pipe was studied experimentally. There was greater improvement noticed in the mixtures

which were denser slurries and has higher concentrations from the results and also more rapid swirl decay was experienced in the slurries with denser particles (Tonkin, 2004). The application of swirl induced into non-Newtonian which are also considered as shear thinning fluids was also researched into by Tonkin. The research made use of a fluid flow independent of time and with a stable rheology which would not be affected by pumping time. The fluid chosen was carboxymethyl cellulose (CMC) (Guozhen, 2016). The test involved measuring the axial and tangential velocity which occurred in the water and CMC mixture downstream of the swirl inducing pipe using Particle Image Velocimetry (PIV). The results of the experiment showed that the increase in tangential velocity was negligible in higher viscous fluid in the laminar flow regime while there was generation of a significant velocity in the tangential direction when water in the turbulent flow regime was pumped through the pipe.

Further optimisation of the swirl inducing pipe using computational fluid dynamics to simulate single phase flow and validating the results with experimental pressure drop measurements, was carried out by Ariyaratne, who decided to add some extra pipe length in front of and behind the swirl inducing section. He called this the transition pipe length (Ariyaratne, 2005). The gradual transition of the flow from the entry length before the swirl inducing pipe to the exit length after the swirl has been induced was found to reduce the loss in pressure and also reduce swirl decay. The optimum setting for this configuration was seen to be a beta (β) type transition with an n=0.5 multiplier for the geometries tested. There is a gradual change in shape from circular to 4 lobed as shown in the figure below, the areas and cross section are kept constant, the pitch to diameter ratio is still 8 and each lobe rotates by 90 degrees for each 100 mm length of pipe section (Guozhen, 2016). As recommended by Ariyaratne, the swirl inducing pipe should be integrated with an entry and exit length as it showed to increase the efficiency of swirl and decrease the pressure losses which occurred due to a sudden change in flow geometry and hence decrease the energy costs. After carrying out slurry testing, it was also discovered that as opposed to the solid particles dragging

along the base of the pipe, the induced swirl created room for better particle dissemination thus reducing erosion which occurred locally and enabling better operation at low velocities without blockages.

A lean phase of particulate suspension in air along a horizontal pipe section was used to test a three-lobed helix pipe using high speed photography, particle Image velocity (PIV), laser Doppler Anemometry and computational fluid dynamics for the application of geometrically induced swirl and its effect on the air flow behaviour (Fokeer, 2006). The air only flow and lean pneumatic flow are imparted with jet type swirl which has both velocity and momentum which changes from axial to tangential closer to the wall. The results showed that downstream of the swirl pipe, the swirl decayed proportionally and inversely to the flow's Reynolds number. The increase in pressure drop was seen to increase when there is an increase in particles to a swirl flow and to be proportional to the increase in the Reynolds number.

2.2.1 Review of Computational Fluid Dynamics (CFD) regarding Swirl flow

Kitoh (1991) tells us about the turbulence of swirl flow which is caused by the anisotropy in stress and the dissipation tensor which leads to a high anisotropic eddy viscosity. Turbulence is an important factor when modelling swirl flow because the flow can be characterised by the fluctuation in space and time of both velocity and pressure (Bhaskaran and Collins, 2003). Using the Reynolds-averaged Navier Stokes (RANS) equations and assuming the standard K-ε model for turbulence and its variations which include the k–ε model, realizable k–ε model and the Renormalization Group (RNG), a host of researchers have made an effort to scrutinize swirl flow and its properties. The time averaged flow equations of the Reynolds stresses are as a result of the Navier stokes equations being time average in the Reynolds-averaged Navier Stokes (RANS) method. Classical turbulence models such as the K-ε models are used to model the Reynolds stresses (H.K.Versteeg and W.Malalasekera, 2010). Two transport equations which include the turbulent kinetic energy, k and the rate of

dissipation ε are solved by the standard k- ε model. The results achieved are then used to solve the Reynolds averaged Navier-Stokes equations by solving for the turbulent viscosity, μ_t (ANSYS, 2011).

The applicability of the k-ε model regarding flow swirl along a twisted tape which was used to create swirl flow and increase the surface transfer coefficient, was examined by Launder and Spalding (1974). Because the turbulent viscosity of the field of fluid flow strain might have become very anisotropic, there wasn't sufficient agreement with the results. It was also debated that due to the anisotropic nature of swirl flow and its eddy viscosity components, the k-ε model and its higher order Reynolds stress model derivative modifications would be incapable of axial and tangential velocity profile prediction (Kobayashi and Yoda, 1987). Nejad et al (1989) also reported the inability pf the k-ε model to accurately solve the velocity field in swirl effected flows. The inability of the k-ε models to accurately solve swirl flow and predict its effects such as the axial and mean velocity which are rotationally dependent and the swirl velocity, which is relative to the rotating pipe, with conventional near wall treatment was emphasised by Speziale et al (2000). He however also stated that when a more sophisticated near wall treatment which predicts non-zero $\tau_{r\theta}$ Reynolds shear stress is applied to a model, the tradition two model equations could be used to forecast the behaviour and properties of swirl. This can only be applied to flows with high Reynolds numbers.

In 1998, it was proved that the K-ε model could be used to describe weak swirl flow by Bali. Using a propeller type swirl generator, the tangential velocity component is imparted into the air flow to create a pneumatic swirling flow. Good agreements were found between both numerical and experimental distributions of axial and tangential velocities (Gouzhen, 2016). Ganeshalingham (2002) also examined weak swirling flows which were caused using the swirly flow pipe using the standard k-ε model. After solving computationally and comparing results obtained from the standard k-ε model, the realizable k-ε model, RNG k-ε model and the Reynolds stress Model

(RSM), Ganeshalingham concluded that the results obtained from the realizable k-ε model, RNG k-ε model and the Reynolds stress Model (RSM), displayed substantial improvement as opposed to the standard k-ε model where streamlined curvature and rotations are key features of the flow. The substantial improvement Ganeshalingham talks about is not substantial enough when the extra computational time is considered.

Ariyaratne (2005) and Fokeer (2006) also drew similar conclusions from their studies. Due to the large number of experiments he had to study, Ariyaratne (2005) used the standard k-ε model for his initial work. Similarly, the standard k-ε model was used to derive a starting point solution by Fokeer (2006) before aiming to improve results by using the Reynolds Stress Model. ANSYS (2011) details some of the limitations of the standard k-ε model as follows;

- When all Reynolds stresses are of the same order i.e. isotropic eddy viscosity, the standard k-ε model is valid. This goes to say that the standard k-ε model is not accurate where the eddy viscosity is not isotropic.
- Its application is limited to flows with high Reynolds number.
- The constants used in the k and ε transport equations are obtained from measurements thereby making the model semi-empirical.
- Wall function is used to accomplish near wall treatment.

The standard k-ε model has its robustness, economy and realistic precision of its results which can be applied to a wide range of flows in the turbulent regime as some of its advantages in industrial flow numerical analysis.

The swirl decay rate trend and the factors which affect the rate of decay for turbulent swirl flows were examined by Najafi et al (2011). A rotating honeycomb which produces solid body rotation is placed at the inlet of a pipe and is used to generate the swirling flow. Some of the turbulent flows studied were considered to have an anisotropic viscosity as they often had swirl numbers as high as 0.6 (Kitoh, 1991).

This formed the basis for Najafi et al's use of the Reynolds Stress Model (RSM) which according to (Najafi et al., 2005, Spall and Ashby, 2010), was the most reliable turbulence model. After validating the results obtained with experimental data and mathematical relations, the results were seen to conform. Solving the transport equations for Reynolds stresses in conjunction with the dissipation rate equations close the Reynolds-averaged Navier Stokes equations. This means that in the case of 3 dimensional flows, seven addition transport equations would be necessary (ANSYS, 2011). H.K.Versteeg and W.Malalasekera (2010) help us to identify the pros and cons of using the Reynolds Stress Model.

Pros:

- It is one of the most common of the classical turbulence models
- The only conditions required are the initial or boundary conditions
- For many complex flows which include wall jets, asymmetric channel and non-circular ducts and curved flows, the Reynolds Stress Model can be used to provide very accurate results of mean flow properties and Reynolds stresses.

Cons:

- Seven additional partial differentiation equations need to be solved when using this model hence it required extra computational requirements and costs.
- The Reynolds Stress Model has not been as extensively validated as the k-ε model.
- When it comes to flows which involve axisymmetric jets and unconfined recirculating flows, due to similar problems, the Reynolds Stress Model performs almost as poorly as the k-ε model.

The use of the RNG k-ε model, realizable k-ε model, or Reynolds stress model which are some of the more advanced models is strongly recommended by ANSYS

FLUENT (ANSYS, 2011) for solving the significant amount of swirl occurring in turbulent flows. The swirl number is used to determine the strength of a swirl flow and this also governs the choice of model to be used. The realizable k-ε model and the RNG k-ε model provide improved results for swirl flows with moderate strength ($S < 0.5$) as opposed to the standard k-ε model. Once the swirl number is stronger and ranges between ($S > 0.5$), the Reynolds stress model (RSM) is highly recommended (Gouzhen, 2016).

Large eddy simulations are becoming more and more popular for solving industrial simulations due to the increase computational power over the years. The Reynolds averaged Navier-Stokes (RANS) equations methods is however still the preferred method in the industry. According to H.K.Versteeg and W.Malalasekera, (2010) , the fact that the large eddy simulation methods directly resolves the large turbulent structures and models solely the influence of sub grid scales on the eddies which have been resolved, makes it more superior than the RANS method. If the resolution of the large-scale eddies is very important or when there is the need for flow variation or turbulent fluctuations, the LES has a chance for improved accuracy. Subsonic turbulent flow between the swirl generator blades was simulated using the large Eddy Simulation method by Conway et al. (2000). The LES captured the time dependent structures which are associated with the wake of the blades and the time dependent vortices which occur due to the surface curvature of the blades.

2.3 Review on Inflow Control

All current inflow control devices or valves are all based on restriction principles which create a pressure drop. A difference in pressure between the inlet and outlet ports of a device must exist for flow to pass through it. The pressure differential, also denoted as pressure drop or ΔP is the difference between the pressure that goes into the device and the pressure that comes out in pounds per square inch, Psi or kilo Pascal,

KPa. This pressure drop is greatly influenced by how much resistance the device poses to flow. Due to the length of the horizontal well, there are three different pressure drops that govern the fluid flow in the well.

1. The drawdown pressure, which controls the flow capacity in the reservoir and other parameters such as permeability and fluid viscosity as stated in the radial flow equation.
2. The pressure differential experienced along the horizontal tubing which is a function of the cumulative flow through the production conduit causes coning at the heel of the reservoir. High capacity wells experience laminar flow which is viscosity dependent at the toe. When an increase in flow occurs towards the heel, the flow tends to become density dependent which is turbulent flow. The plot of the flow rate and the pressure differential is non-linear and experiences variations with various degrees of depletion.
3. The Inflow control device also generates its own pressure drop and this value is very important

The flow in the horizontal well can simply be shown as:

$\Delta P \sim \mu Q$ for Laminar flow and

$\Delta P \sim \rho Q^2$ for Turbulent flow

Where: ρ = fluid density, μ = fluid viscosity, Q = fluid flow rate

2.3.1 ICD Technology

Inflow Control device (ICD) technology also known as passive flow control devices owing to their torpid flow control nature, were initially developed in the early 1990s to tackle the problem of water and/or gas breakthrough of copious horizontal wells. The device was initially designed to equalize flux (rate of flow per unit length) along the length of the horizontal well in its entirety and makes use of choke mechanisms to choke flux in the heel region (Krasnov et al., 2012) They are installed at regular

intervals in order to crease a pressure differential. This ideology was since assuming a level of choke which is proportional to the rate of flow, the ICD should inevitably produce a more uniform flow profile. The pressure differential through the Inflow Control device is subject to change depending on the nature of fluid flowing through it and the choke mechanism parameters. It must however be noted that the choke mechanism cannot be adjusted any further once the Inflow control device has been fitted in the wellbore. Once coning which leads to water and/or gas breakthrough occurs in the oil well, ICDs do not possess the capability to alter or stop the inflow of the undesirable fluid at the point of influx (AlKhelaiwi, 2013). A more appropriate term used to describe ICDs would be proactive ICD and this is because once they are installed in the early days of the well's life cycle, they are only able to influence and control the wells inflow profile prior to water and/or gas breakthrough. The effect of this is simple, the flow is now influenced by both Darcy and choke. However, during depletion the change in pressure may lead to uneven flow. Bernoulli's equation, which is valid for all tubular flow with restrictions, controls the flow at the nozzle. Designs have progressed from ICDs to AICDs to ICVs and then AICVs. All mentioned designs are therefore governed by this law, Bernoulli's equation.

2.3.1.1 Nozzle-type ICDs

Nozzle-type ICDs

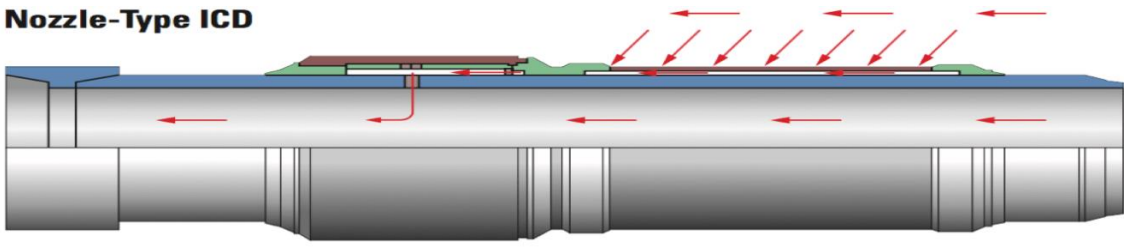

Figure 2.3: Nozzle-Type ICDs (Shevchenko, 2013)

These are self-regulating inflow control devices which are usually designed using a ratio of the pressure drop at the inlet of the device as is governed by the Bernoulli equation to the average drawdown pressure of the formation which is governed by

Darcy's equation. When this ratio is close to unity, the device can be said to be autonomous. Some types of the nozzle type ICD are ResFlow™, ResInject™, FloMatik-Sub™ and FloRight™ produced by Reslink which a subsidiary of Schlumberger and Flotech which is a Tendeka subsidiary. The nozzle-type inflow control devices are used completion components as well. This means that even with the variations in permeability of the wellbore, every joint where an Inflow control device is located behave independently of the local heterogeneity and fluid type which changes with time. The former occurs due to compaction and well subsidence while the latter occurs as a result of second phase fluid influx into the wellbore.

The pressure drops caused by the nozzle type ICD is based on the rate of flow of the formation fluids as they pass through the restricting orifices either into a housing outside the base pipe or within the base pipe itself. According to Bernoulli's principle, the pressure drop through an orifice increases as the square of the fluid flow velocity, the fluid flow velocity also increases as the orifice diameter increases. Fluid such as water and gas have a lower viscosity than oil, hence when they flow into the wellbore through high-permeability interval streaks at higher velocities because they are more mobile, there is an increase in backpressure at the point of ingress. This prevents water or gas from reaching the wellbore before or with oil reserves in less permeable areas of the formation. Designed based on the ratios stated above previously, are simple and effective in horizontal wells with relatively high production indexes and minimum restriction of flow. To improve flow in the wellbore and ensure uniformity, there must be uniform distribution of nozzle type inflow control devices of the same number and size along the well from toe to heel and this helps to counter the heel toe effect (Shevchenko, 2013). These kind of ICDs are sensitive to the density and the square of the velocity of the fluid passing through the ICD.

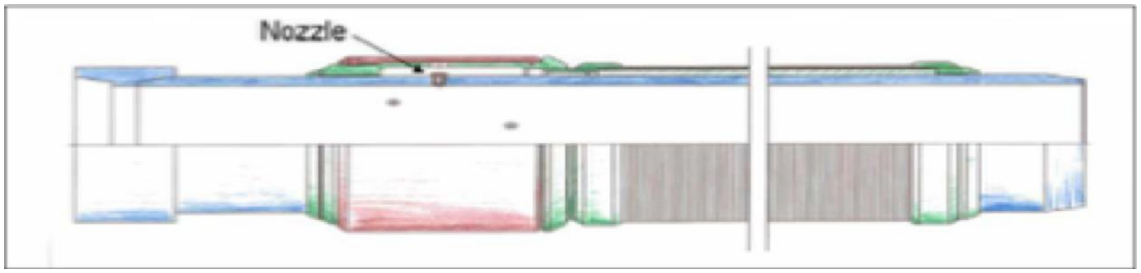

Figure 2.4:Reslink: ResFlowTM Nozzle-type ICD

The Reslink ICDs for well production, ResFlow™ shown in figure 2.4 above is different form the ones intended for well injection, ResInject™ shown in figure 2.6 below. In the production ICD, the nozzles are grooved into the base pipe while they are embedded in a jacket around the base pipe in injection design.

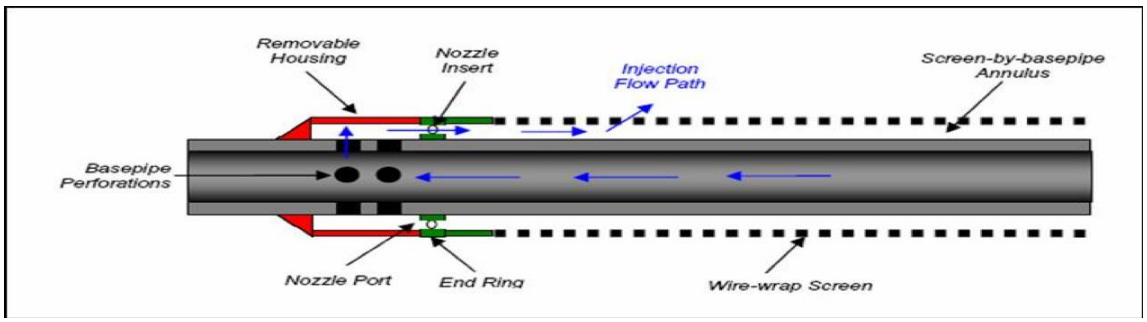

Figure 2.5: Reslink: ResInjectTM Nozzle-type ICD

There is also a difference between the Flotech FloMatik™ and the FloRight™ design. The design of the FloMatik™ aligns its application to a consolidated formation because it enables flow to go directly into the nozzle without a screen or filter. On the other hand, the FloRight™ possesses a stand-alone screen before the chamber and then check valves within each nozzle to prevent back flow.

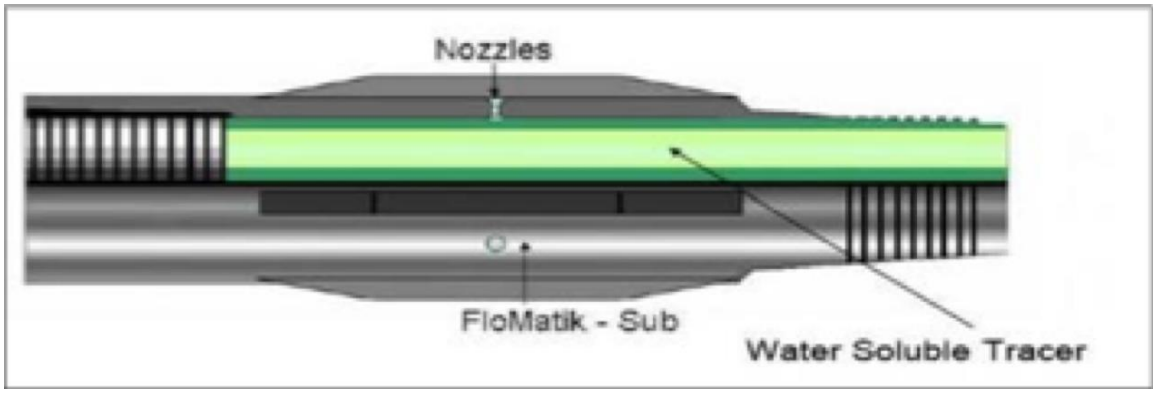

Figure 2.6: Flotech FloMatik-SubTM nozzle-type ICD

2.3.1.2 Helical-type ICDs

These are inflow control devices developed by baker oil tools (Production Equalizer^{TM}) and they are based on helical channels which have a set length and diameter. The differential pressure caused by the friction the fluid experiences against the surface of the channel when flowing through it is dependent on properties of the fluid and the rate at which it flows through the channel. This characteristic means that the device is viscosity dependent and this may result in inefficient operation because there can be breakthrough streaks in regions of the wellbore where production oil has a lower viscosity due to entrained water and gas. The pressure drop is distributed along a longer channel path when passing through these ICDs due to the fluid will changing direction. This kind of ICD is supposed to have enough length, typically 120 inches to create enough pressure drop (Torbergsen, 2010).

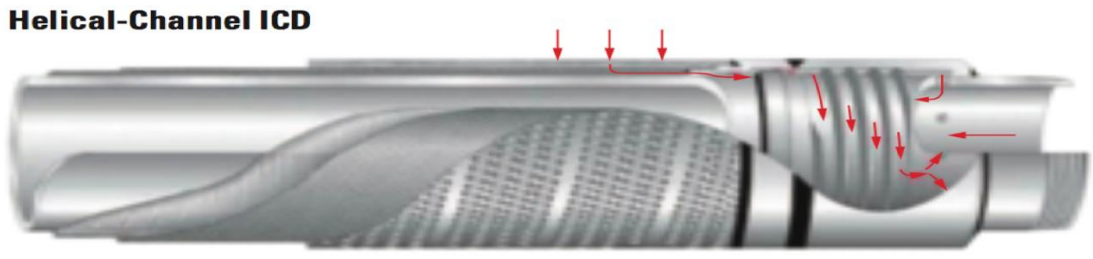

Figure 2.7: helical-channel type ICD (Shevchenko, 2013)

The ICD operation is based on the Poiseuille's Law, . As the fluid flows through the

ICD, the drop-in pressure is proportional to the fluid viscosity and velocity as shown.

$$\Delta P = \frac{128\mu LQ}{\pi d^4} \quad (2.1)$$

Labyrinth Channel-Type ICDs

The labyrinth channel type ICD is also a type of channel inflow control device. It uses a labyrinth channel to produce a flow resistance. Formation fluids flow through a screen and then into the device chamber where it is met by the labyrinth channel. The length and diameter of the channel is specially designed to generate the required pressure drop at a specified rate of flow. The pressure differential created by this device in a perfectly horizontal well is dependent on the viscosity and flow rate of the fluids rather than their densities. The advantage of this dependence is that the device has a low change of experiencing erosion however, where the oil and water flow forms an emulsion mixture, the fluid viscosity changes and the pressure drop is affected.

The pressure drop in both channel type ICD devices occurs over a greater distance when compared to the slot, nozzle and orifice-type inflow control devices due to their design. This means that the fluid viscosity plays a greater role and when the fluid type, phase, pressure or temperature changes or an emulsion is formed due to break through the device is ineffective.

2.3.1.3 Slot-type ICDs

The Slot-type ICD (Hybrid Equalizer™) is a modified version of the helical channel the inflow control device which was developed by Baker Oil tools to minimise the dependence of the pressure differential of channel type ICDs on fluid viscosity. The slot type ICD exhibits multi choke flow characteristics also generates pressure drops within the same range as the helical channel type. The Slot type ICD was produced in two designs:

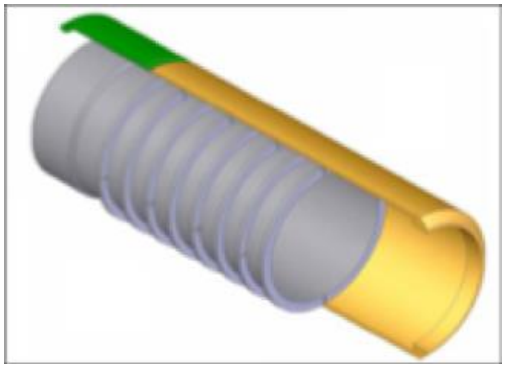

Figure 2.8: Slot-type ICD, Circular disc design

A circular disc design, in which the number of stages or discs installed in the ICD chamber determines the pressure drop across the entire device. Each disc or stage contains two slots of a pre-determined size. This causes a pressure to drop to occur at the specified flow rates.

Figure 2.9: Slot-type ICD, Quadrant division design (source: Alkhelaiwi, 2013)

The second design has 4 quadrant divisions in the chamber, each of these divisions a designed to impose a specific pressure differential at a specific flow rate. When a pressure differential is required, the number of stages within each quadrant can be varied. This means that an increase in number of stages gives rise to an increase in pressure drop. This design is thought to be the least dependent on fluid viscosity.

2.3.1.4 Orifice-type ICDs (FloReg^{TM} and FluxRite^{TM})

These devices mode of operation is like that of a nozzle type inflow control device. They are manufactured by both weatherford (FloReg^{TM}) and Schlumberger

(FluxRite^{TM}) the orifices which are inserted into a jacket around a base pipe or an annular chamber on a standard oilfield tubular on the device are of a known diameter, hence back pressure can be generated by adjusting the number of the orifices and therefore their flow characteristics. Reservoir fluid flows through a sand screen and into a flow chamber after which, it moves through parallel tubes in the production string. This device is also reliant on friction to create a pressure differential which is dependent on the tube length and internal diameter. Both orifice ICD types have the same orifice sizes however, to achieve the desired pressure differential, the number of open orifices can easily be reduced by plugging or unplugging orifices on the well site.

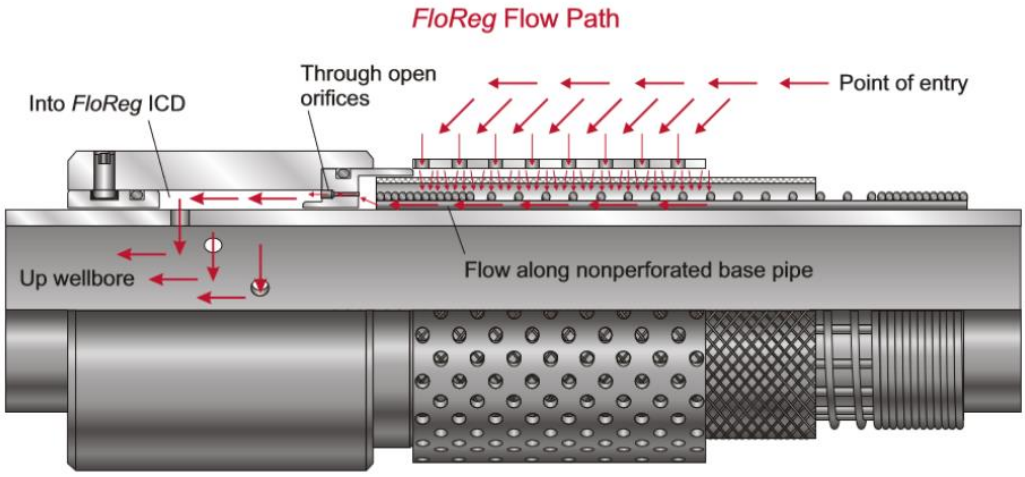

Figure 2.10: FloRegTM orifice-type ICD (Birchenko, 2010)

2.3.2 Autonomous Inflow Control Devices (AICD)

The year 2010 saw the start of AICD development. Five designs have come up so far. An AICD combines the passive section of an ICD with an active section. Buoyancy is a concept used in three of these valves to design the active sections which open and shut. In the fourth design, the opening and shitting of the valve is controlled by an osmosis-based swelling material. The final design used a hydro cyclone mechanism to control the influx of water and gas into the wellbore based on viscosity changes.

The autonomous Inflow Control Devices are classes into two:

1. Those triggered by the presence of water, these AICDs assist the well outflow performance by using the restriction principle to prevent inflow of water into the well until it ceases to flow. They also exert large pressure differentials which could potentially reduce the productivity of the well.

2. Those triggered by the presence of gas. These devices work by limiting the amount of free gas that flows through the wellbore, but this may affect the use of the well for gas production soon.

2.3.2.1 Flapper-type AICD

This device is used as a means of controlling flow from the channel ICD chamber to the inner section of the case. When the density of the production fluid is equal to the oil density, the flapper is designed to remain open. The reverse is the case when the fluid density decreases due to influx of gas, the flapper closes. The design makes use of a counterweight opposite the flapper and the rate at which the flapper closes can be controlled by changing the mass of the counterweight. As the completion runs in the wellbore, the flapper is orientated using a gravity ring. The rubber seal placed behind the gravity ring expands slowly when it comes in contact with formation fluids. This completely seals the device in place when it lands in its finial position.

A bypass orifice is incorporated into the valve design to allow for continuous back pressure build up in order to ensure oil production continues from the other screen joints. This orifice allows for slow gas bleed off enabling the device to reopen when the gas cone regresses ensuring maximum oil production. Orientating the AICD flapper to 180^{O} from the gas sensitive device enables it control water production or both water and gas control. The flapper is lifted to the shut position by the denser fluid which stops the influx of water.

2.3.2.2 Ball-type AICD

Easywell solutions, a Halliburton subsidiary provides the ball-type AICD also known as the Oil Selector™. The operation of the ball type AICD is like that of the flapper type in the sense that they are both dependent on fluid density which they use to create buoyancy which activates the valve. The difference between the two designs is that the shut off active nozzles that control the flow from the AICD chamber to the inner section of the casing in the ball-type AICD are made from metal balls. To create a specific pressure, drop, the nozzles can be adjusted to create a restriction or be large enough to allow flow and create slight restriction.

During oil production, the balls lay at the bottom of the device in a water control AICD. As the water cut increases, the density of the fluid produced increases and this causes the balls to rise to the top and shut the valves one at a time. Figure 2.12 below shows the water autonomous valve for an oil Selector ™. We see the balls at the bottom of the device and then how they start to rise when there is an influx of water.

Figure 2.11:Oil Selector TM Autonomous water Valve

When it comes to gas control, oil floating balls are used. This enables them to float in the oil phase due to their density. When there in an influx of gas, the density of the fluid reduces and this in turn causes the balls to slowly sink to the bottom and plug the nozzles thereby preventing gas breakthrough. In order to maintain high production rates, the valve is designed with by-pass valves which allow up to 20 per cent of the total flow area. This is used to ensure the pressure differential across the

completion is maintained and the balls are held in their shut-in position whenever fluid is flowing. The device is only rest to its open position by shutting-in the well. Figure 2.13 below shows an example of the valve.

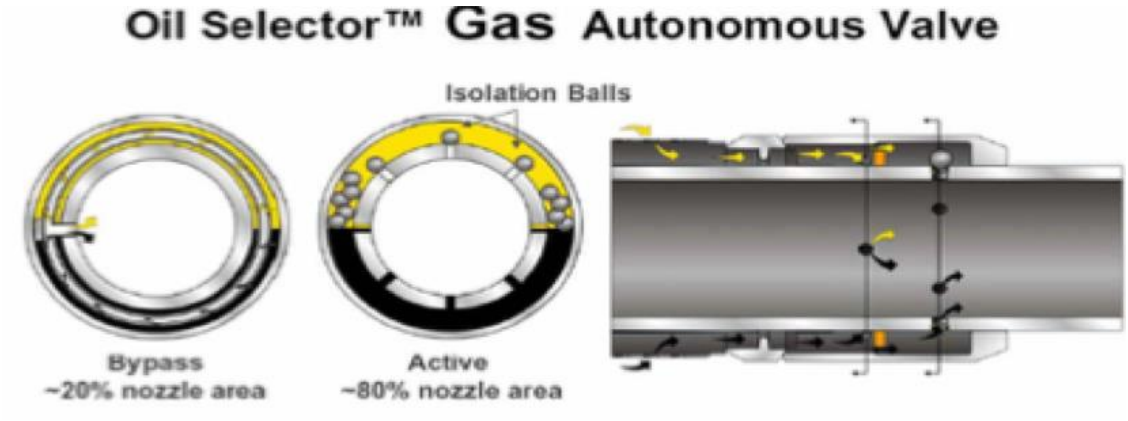

Figure 2.12: Oil Selector TM Autonomous Gas valve

2.3.2.3 Swellable-type AICD

Statoil has developed the Swellable-type AICD to curb the influx of water into the well bore. It makes use of the principle of thermodynamic adsorption or osmosis. The device senses the change in properties of the flowing fluid depending on the swellable material. When there is an inflow of water, the swellable membrane expands and forces an inner plate which contains spiral flow paths to firstly reduce the flow area which in turn restricts the fluids flow path. Where a specific pressure differential is required, the spiral fluid flow path can be designed to equalize the influx along the wellbore. Where efficient water flow restriction is required, multiple devices must be installed in a screen joint.

2.3.2.4 Disc-type AICD

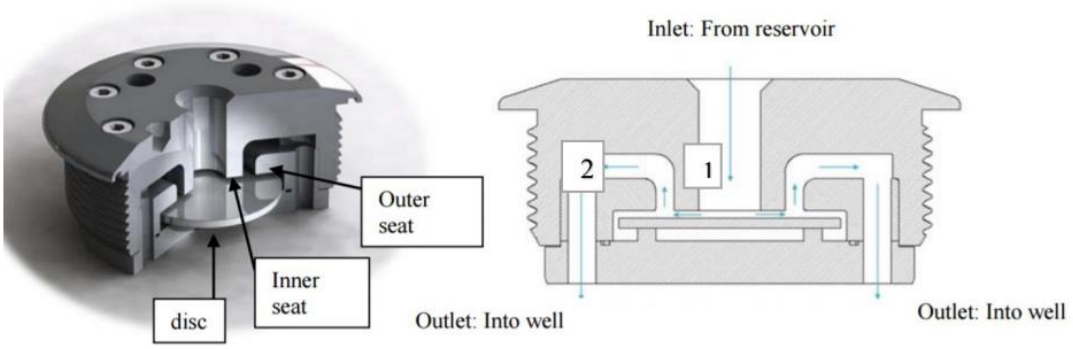

Figure 2.13: Disc type AICD (Halvorsen, et al., 2012)

The disc type AICD as shown in figure 2.14, was also introduced by Statoil is used to control gas inflow. The fluid flow area is reduced by a spring which imposes a specific pressure on a movable disc based on the fluid properties. The disc is maintained in the open position as the liquid flows through the device. The valve shuts off influx of gas when there is excess back pressure on the disc. The desired flow restriction is achieved by using a particular number of devices in the screen joint. In this device, the pressure differential is imposed by controlling the flow opening area of the device. This helps equalize the inflow of gas into the horizontal wellbore.

2.3.2.5 Remote-type AICD

The AICD device and its specific sleeve are controlled by Radio Frequency Identification, RFID. It is provided by petro well and consists of an RFID frequency detector and reader, a hydraulic pump, sleeve and power source. The opening and closing of the sleeve to prevent influx of unwanted fluids is controlled by a small chip which is programmed with instructions and then sent into the well to pass through the RFID reader. The instructions sent down are decoded by the reader and then an action is initiated. A downhole power source or battery is used to power the hydraulic pump which controls the sleeve installed on the inner side of the base pipe. Once an ingress of water or gas is detected, the sleeve can be actuated by the operator. This

sleeve isolates the path of flow between the ICD chamber and the inner section of the production tube. Remote control of the device has a greater advantage; however, the device does not respond automatically to the inflow of unwanted fluids. The device is also limited as it requires electric power for both signal receiver and sleeve actuation and the battery operation of the hydraulic pump limits the operational life to a 2-year maximum. The solution to this is a downhole power generator.

2.3.3 Inflow Control Valves (ICVs)

Inflow control valves are active flow control devices which offer a proactive and reactive control of flow. Well dynamics, baker oil tools, Weatherford and Schlumberger have provided this technology since the 1990s. Inflow control valve control can either be remote, wireless or entirely autonomous. Those that are controlled remotely using hydraulic or electrohydraulic actuation make use of either control lines or just send wireless signals from the surface. The other ICVs which are wirelessly actuated make use of radio frequency identification technology to convey information back and forth between the surface and the inflow control valve. ICVs which have preset actions and either programmed before or after installation. These preset actions are programmed into the module directly linked to the actuation system of the ICV.

2.3.3.1 Discrete-positions ICV (DP-ICV)

The device, Discrete-positions ICV is electric, hydraulic or electro-hydraulically actuated. It can have between 2 and 12 openings which are selected to permit efficient control of fluid breakthrough, ranging from fully open to fully closed. For best results when controlling gas breakthrough, most of the openings are relatively small with only 2 or 3 large ones while to control water breakthrough, the openings are even spaced between open and closed positions.

2.3.3.2 Variable-positions ICV (VP-ICV)

This valve has a limited application as compare to the Discrete-positions ICV because it is less reliable and much more expensive. It is controlled using electrical actuation and can have any desired size opening.

2.3.3.3 Control Line-free ICVs (CLF-ICV)

Control line-free ICVs are developed by Petrowell. They required a battery powered hydraulic pump to actuate the valve to either open or closed based on the instruction conveyed through a tiny electronic chip which contains instructions for the ICV known as an RFID. The chips are sent down through the RFID reader which interprets the instruction and then starts ICV actuation. This valve is better than the Discrete-positions ICV and the variable Positions ICV because they require control lines of the value N + 1 (where n is the number of ICVs). This therefore limits ICV installation on the mother bore to a value of six.

2.3.4 Autonomous-ICV (AICV)

This device, Autonomous-ICV is developed by Saudi Aramco, Schlumberger and Halliburton-well dynamics to curb both water and gas breakthrough. It uses Electrode Array Resistivity (ERA) sensors which detect and monitor the approaching water or gas front, for phase identification. Only one control line is required per well to power the ICVs hence there is more room to install more inflow control valves in a multi branched well. It has also overcome the short range for signal travel and power transmission that other systems which are free from control lines experience.

2.3.4.1 BECH constant flow control valve

This flow control valve attempts to overcome the lack in the other designs. It provides flow at a constant rate despite the state of pressures in the wellbore. This means that the flow rate in the wellbore remains constant, preventing water breakthrough until the well completes its life cycle. This is a constant flow controller. There are two

different designs for the Bech constant flow control valve however they since they both aim for constant flow control; they both possess a flow adjustment mechanism. This can either be a screw, needle or obtaining the desired rate of flow by plugging several nozzles. This is known as a flow set point. The flow goes into a chamber which due to the floe set point or restrictions, has a lower pressure. Then a compensation part which is usually a spring-loaded membrane or piston which is connected to a needle is controlled by the varying pressure from the reservoir to the production tubing. The movement of the piston is in accordance with the pressure such that it ensures constant flow through the nozzle and into the production tubing.

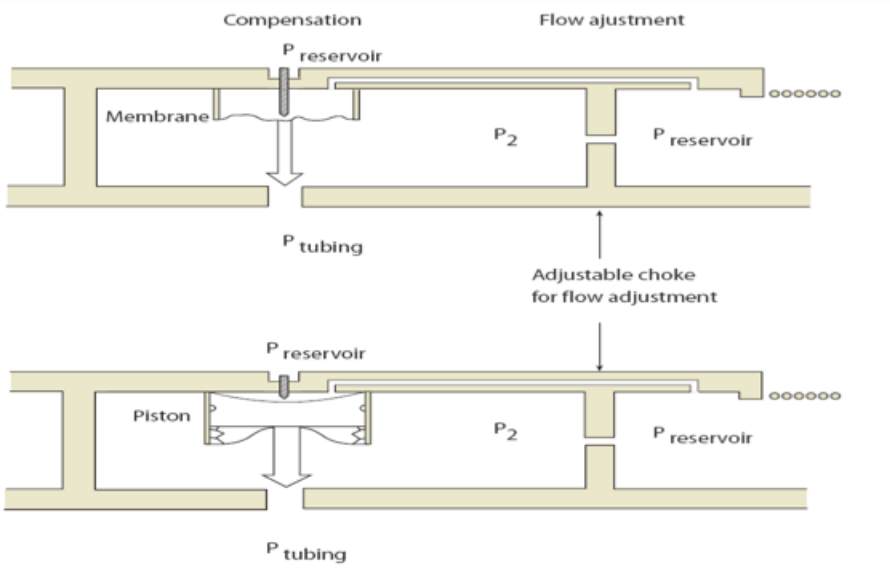

Figure 2.14:Two Bech flow control designs. The top one has a membrane while the bottom uses a piston.

The design above which uses just a membrane must have a spring to mimic the piston design. The valve is only fluid density sensitive and not fluid viscosity sensitive because from research, over the life cycle of a well, density is fairly constant while viscosity varies. Figure 2.16 below shows a prototype Bech flow control valve. The entire piston is oil filled and enclosed with two seals to avoid impurities going into the device.

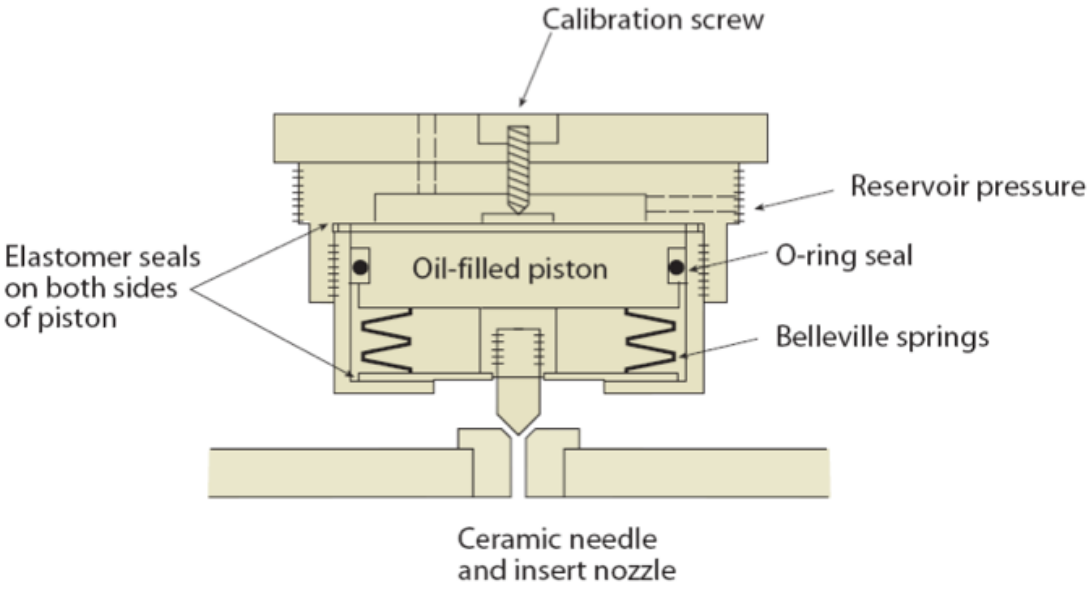

Figure 2.15: Bech flow control valve prototype design

2.3.4.2 Autonomous and Reversible Inflow Control Valve Review

It separates flow based on the difference in pressure drop in a laminar flow restrictor as compared to a turbulent low restrictor. The pressure drop is dependent on the fluid properties and is proportional to the flow rate, V, fluid density, ρ and length of the well, L.

Figure 2.16: Autonomous reversible Inflow Control Valve (Inflow Control, 2016)

In the AICV, two flow paths exist, the pilot flow path and the main flow path. Most of the fluid flowing through the AICV goes through the main flow path and the pilot path only sees about 1% of the total flow. Both paths end up at the outlet. A pressure sensitive piston is placed in the pilot path which shuts off liquid flowing into the main flow path. There are also laminar and turbulent flow elements in the pilot flow path. The viscosity of the fluid controls the pressure drop in the laminar flow element.

Where there is high viscosity, the pressure drops created across the laminar flow element is high. This means that the net force which is the difference between the force (F1 = P1 x A1) the fluid exerts on the piston and the force (F2 = P2 x A2) acting upwards is positive hence the valve is open. Where the viscosity is low, the pressure drops created across the laminar element is low and the pressure in the chamber is high is high. In this case, the force F2 is greater than F1 hence and the net force is negative hence the valve closes. Where: P1 is the inlet pressure, P2 is the outlet pressure A1 is the area of the top surface of the piston and A2 is the area of the bottom surface of the piston. The inlet pressure, P1 is always greater than the outlet pressure, P2. The ratio A1:A2, is a design parameter whose optimum ratio is dependent on the properties of oil, water and gas.

The components of the AICV are the locking ring, Filter, AICV inlet, Piston, Bushing, Bellow, Housing, Laminar Flow Element, Turbulent Flow Element, Base pipe, Sand screen, Inner sleeve and End cap. This case study will focus on the Laminar and turbulent flow elements, the geometry leading up to both elements and how the fluid flow geometry will affect the physics of flow.

The laminar flow element is designed based on its application. It generates a pressure differential which is dependent linearly on the volumetric flow rate through the flow element and the flow viscosity according to Hagen-Poiseuille Law (LFE - LAMINAR FLOW ELEMENTS, 2015). It operates by flow division into several orifices or small diameters. This reduces the Reynolds number drastically and this ensures that laminar flow is maintained. Laminar flow elements are stable and repeatable as they

do not have any moving parts. The pressure drops created by the Laminar Floe Element is shown by the below equation:

$$\Delta P = \frac{32\mu VL}{D^2} \qquad (2.1)$$

Where: ΔP = differential pressure, μ = Viscosity, V = velocity, L = Length of pipe, D = diameter of pipe

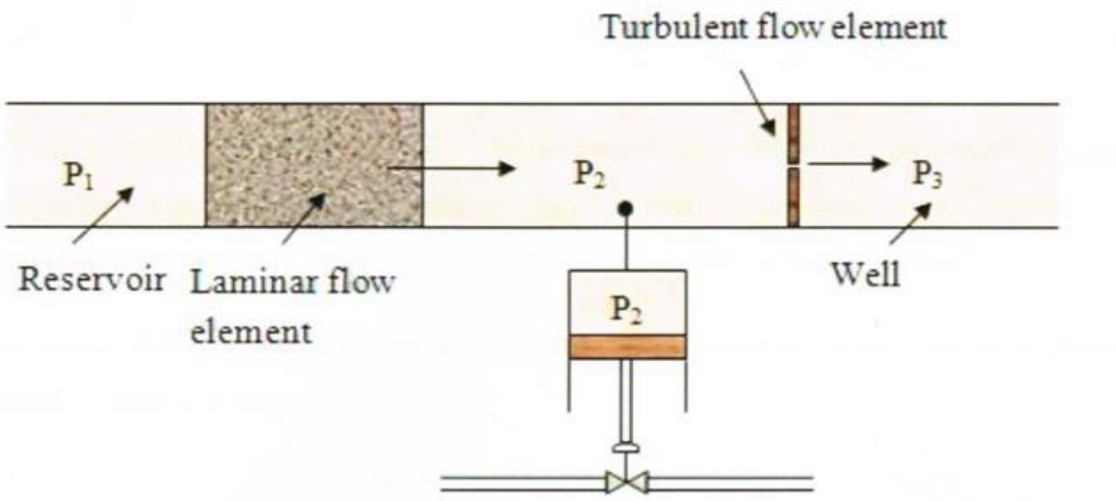

Figure 2.17: Laminar and turbulent flow restrictors in Series

Due to higher flow rate per unit area through the orifice, when the fluid leaves the laminar flow element, there is a higher rate of flow through the turbulent element which results in turbulent flow. The pressure differential in the chamber changes with reference to the fluid properties such as:

- flow rate,
- density of the fluid,
- Inlet or outlet orifice sizes.

The drop-in pressure for this section is depicted by the equation:

$$\Delta P = K \frac{1}{2} \rho V^2 \qquad (2.2)$$

Where: ΔP = differential pressure, K = Geometrical constant, ρ = density, V = velocity

The AICV design has been mastered to the various states and oil types found in an oil reservoir. These include; Gas, Ultra-Light Oil, Light Oil, medium oil, Heavy oil and

Extra heavy oil (Wolfram, 2016). The initial problem faced by oil producing wells was the by production of Gas hence the valve was designed with intent to shut off gas production. However, in a gas producing well, where water production is an issue which will eventually lead to low recovery rates and or early shut down of the well, the use of Monoethylene Glycol (MEG) injection which involves the control of hydrates in subsea flow lines was a previous solution. The value derived from a producing well has been seen to be immense when water production is delayed or even stopped in its entirety and due to the reversibility of the autonomous inflow control valve, it is possible to have oil shut off instead and allow for sole gas production where the well is a gas producing one.

2.4 Summary

The chapter provides an in-depth discussion of the literature regarding different control devices used in oil pipes for its extraction. All the devices work on different fluid flow geometries that range from nozzle and flapper to helical and ball type as well as slot type to orifice. The aim of these different devices is to regulate the pressure drop along the length of the oil pipe to achieve a uniform flow profile leading to maximum extraction.

Chapter 3 Methodology

3.1 Introduction

Numerical analysis is a crucial element for a vast majority of engineering applications as it helps in virtually analysing the problem before physical implementation. This chapter presents the processes, concepts and theories that accentuate the methods and approaches used to collect data during this research. The techniques used in this research are based on theoretical approaches as they are characterised by physical phenomena and the principles of fluid flow. Correlation between the mathematical models in existence and numerical (CFD) and experimental work has also been presented.

3.2 Computational Fluid Dynamics (CFD) methodology

The process whereby computer-based simulations are used to scrutinize systems which involve flow, heat transfer or other phenomena associated with the previously mentioned, is known as Computational Fluid Dynamics, CFD. It is used for a wide range of industrial and non-industrial applications hence making it a very influential technique (H.K.Versteeg and W.Malalasekera, 2010). The ability to study systems where it is not possible to carry out experiments in a controlled environment, reduce the cost and time of creating new designs are some of the unique advantages CFD has over experimental investigations. The thesis employs the use of CFD in order to determine the effectiveness and usefulness of the geometrical cases to be modelled as it is very cost effective. The governing equations which represent mathematical statements of the conservation laws of physics are applied by the fundamental laws which govern fluid flow mechanics, laminar and turbulent included (H.K.Versteeg and W.Malalasekera, 2010, Bhaskaran and Collins, 2003). Some of these fundamental laws are; the fluid mass is conserved, according to newton's second law, the sum of forces acting on a fluid particle is equal to the rate at which the momentum changes

and the first law of thermodynamics which dictates that the summation of the rate fop heat addiction to and the work done on a fluid particle must be equal to the rate of change of energy. The continuity equation, the momentum equation and the energy equation, are jointly referred to as the Navier-Stokes Equations and are the three fundamental principles in their partial differentiation form. In this thesis, the momentum and continuity equations are used as the flow is isothermal.

3.2.1 Experimental, Analytical and Numerical methods

Experimental methods are usually a reliable way of predicting phenomenon that occur by gathering information and colleting measurements. It is a common way of gathering information on scaled equipment and transferring this to full-scale real-life applications (Dibyajyoti, 2017). This method is advantageous as the actual model can be used for experimental analysis, when the results obtained are accurate, they can be used to understand the phenomenon being tested or solved for and it gives the opportunity to derive statistics for future work. Its disadvantages lie in the fact that the actual prices of test equipment's can sometimes be on the high end and using this method is time consuming and rigorous experiments have to be carried out to find out little changes. Analytical methods make use of mathematical models which are usually a set of differential equations to deduce a solution to the problem. It is also therefore known as the mathematical model. Its advantage is that it uses pre-defined differential equations while on the other hand, where too many assumptions and or simplifications are made, the validity of the solution is limited, and this puts this method at a great disadvantage. Numerical methods make use of computational power to determine the behaviour of physical properties on a model by using a set of defined differential equations. Physical properties from experimental data and pre-defined set of equations are used to understand the behaviours and effects. The problem or model is broken down into discrete parts and each part is solved according

to the predefined set of equations. The numerical methods of discretization are divided into three categories (Dibyajyoti, 2017)

.

3.2.2 Finite Element Method (FEM), Finite Difference Method (FDM) and Finite Volume Method (FVM)

The finite element method is a computational method that divides a Computer Aided Design model into simple geometrical shapes which are very small but finite sized. When these elements are grouped together, they make up a finite element mesh (Machine Design, 2016). The year 1960 saw this method surface for analysis especially for structural dynamics problems. It is a beneficial method when compared to the finite difference method as it can handle complex geometries and use arbitraries on irregular shapes because it functions based on the weight residual method. The finite difference method is said to be the simplest method used to arrive at the discrete forms of differential equations. It can be used for very efficient solutions as it is typically defined on a regular grid. The derivatives are derived using the Taylor series in this method which is also the simplest way to apply differential equation to uniform grids therefore, it is highly unusual for it to be used for irregular CAD geometries but rather for regularly shaped rectangular or block shaped models (Peiró and Sherwin, 2005).

The finite volume method has one similarity to the finite element method; this is the fact that they both divide the CAD model into simple geometrical shapes which are very small but finite sized. That being the only similarity, the finite volume method is very different from the finite element method. The first major difference is the concepts of elements in the finite element method which are referred to as cells in the finite volume method (Machine Design, 2016). This method is solely based on laws of conservations, stating that what goes into one cell on one side must leave the same cell on the other side. Based on this theory, a variety of flux conservation equations

which define certain parameters over the cells are formulated. The finite volume method has been seen to be very effective in solving fluid flow problems. The finite volume method is the numerical method of choice for this research as the research is focused on mesh generation, fluid flow and its properties.

3.2.3 Continuity equation for the conservation of mass

The continuity equation for conservation of mass is used to ensure that the mass of fluid flowing into a control volume is equal to the amount flowing out of it and to ensure that the mass of fluid flow within the control volume is balanced. In Cartesian form for incompressible flows, the continuity equation is given by;

$$\frac{\partial \rho}{\partial t} + \nabla . \left(\rho \vec{V}\right) = 0 \qquad (3.1)$$

$\frac{\partial \rho}{\partial t}$ Represents the rate at which the mass changes with regards to time in an infinitesimal control volume, while the mass convection through the control volume is denoted by $\nabla . \left(\rho \vec{V}\right)$. To ensure that the total force due to surface stresses and body forces which act in aligned direction with a chosen coordinate axis, are equal to the rate at which the momentum of fluid particles in a fluid flow change, Newton's second law of motion is applied thereby obtaining the equation from viscous stresses as detailed below;

$$\frac{\partial (\rho \vec{V})}{\partial t} + \rho \, (\overrightarrow{V} . \nabla) \, \vec{V} = \rho \vec{f} + (-\nabla p + \nabla . \tau_{ij}) \qquad (3.2)$$

The rate at which momentum changes with time is represented by $\frac{\partial (\rho \vec{V})}{\partial t}$, the advection of momentum is described by $\rho \, (\overrightarrow{V} . \nabla) \, \vec{V}$, the body forces including gravitational and buoyant are represented by $\rho \vec{f}$ and the forces due to pressure and stress gradients on the fluid are represented by $(-\nabla p + \nabla . \tau_{ij})$. It is not possible to generate a solution to most engineering problems because these partial differential equations cannot be resolved analytically. Therefore, through flow equation discretisation by approximate modelling which solves for turbulent motion statistical

characteristics, it is possible to generate numerical solutions. During numerical simulations, CFD strategy is to create a grid to replace the flow domain. Each flow variable is then solved at each of these grid points (Bhaskaran and Collins, 2003). The flow problem can be resolved through numerical simulation by using various iterative or direct solving methods or techniques once all boundary or initial conditions which relate to the specific problem at hand have been specified (Shaw, 1992).

3.2.4 Turbulence modelling

Above certain Reynolds numbers in engineering practice, instability can be noticed in all flows. The Reynolds number can be defined for pipe flows as $Re = \frac{UD\rho}{\mu}$ where u is velocity, ρ is the density, and μ represents the viscosity. The flow is said to be turbulent at higher Reynolds numbers while at lower Reynolds numbers it is laminar flow. During turbulent flow, there are continuous fluctuations of pressure and velocity with time because of the chaotic and randomised motion experienced. A combination of vortex and axial motion are experienced during turbulent swirl flow and there is always an increase in velocity fluctuations die to the tangential velocity component which accompanies swirl flow (Fokeer, 2006, Algifri et al., 1988). Length and time scales which interact complexly and dynamically, range widely due to the presence of eddies in the flow. The development of a vast number of numerical methods which are grouped into three categories has been made possible to the important role turbulence plays in the engineering industry (H.K.Versteeg and W.Malalasekera, 2010). The three categories are as follows;

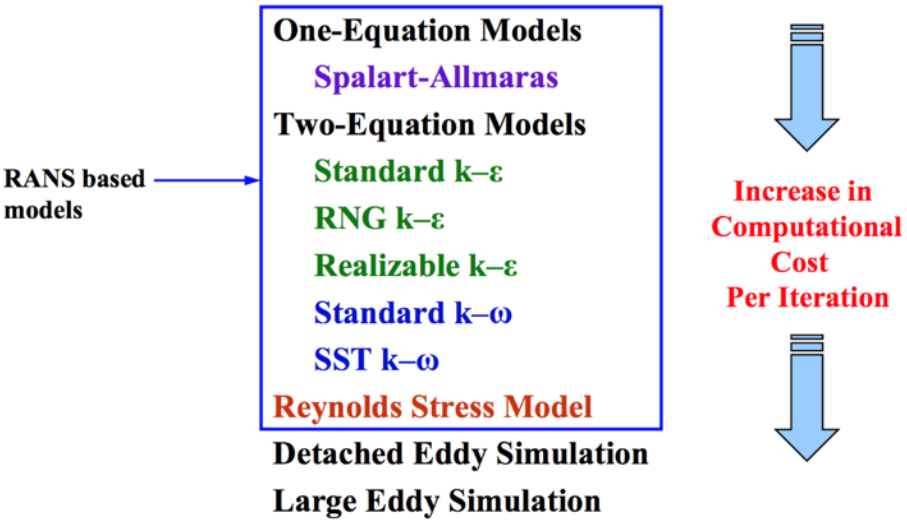

Figure 3.1: Turbulence Models available to use in FLUENT (ANSYS, 2006)

The Navier stokes equations are time averaged prior to the numerical methods being applied using this method. Due to the interactions between various turbulent fluctuations, extra terms such as the time averaged Reynolds stresses appear in the flow equations. The standard k-ε turbulence model, its variations and the Reynolds stress model are some of the most common of the classical turbulence models used to resolve the Reynolds stresses (Gouzhen, 2016). The effects turbulence has on mean flow and mean flow itself are predicted using this method. Over the last few years, this method of numerical simulation has been used widely in the industry as the resources it requires to solve and produce accurate results are not overbearing. When it comes to modelling of turbulent flows in steady state, RANS turbulence models are the only way to do that. It is also the most widely used method in the industry due to the high interest in time averaged values, its simple post processing and shorter time for simulation as compared to other methods (Gouzhen, 2016).

3.2.4.1 Large Eddy Simulation (LES) and Direct Numerical Simulation (DNS)

The behaviours of large eddies are tracked in this intermediate large eddy simulation method of resolving turbulence. The larger eddies are passed through filtered spaces while the smaller eddies are rejected during simulations run using this method. A smaller sub grid scale model is used to resolve the eddies which are smaller than the mesh size while the larger scale eddies are resolved in a portion of the domain. Somewhere between the RANS and DNS, Direct numerical Simulation methods, LES can be found. The resources required to carry out computational numerical simulations and storage of calculation results are very demanding due to the fact the LES method solves unsteady flow equations due to its unsteady nature. When unsteady results data is required of when the resolution of large eddies is very important, the accuracy of the LES method could potentially be improved. Long run times and large volumes of data are generated from the higher resolution mesh grids and the small-time steps required to run an unsteady simulation thereby making this method very cost intensive computationally. All turbulent fluctuations in velocity and the mean flows are calculated using this method of simulation. By using spatial grids which are sufficiently fine and sufficiently small enough fluctuations which can resolve fast periods of fluctuations according to the Kolmogorov length scales. This method is not used industrially as it is very expensive in terms of the computational resources required. Direct Numerical Simulation can be used to solve the Navier stokes equations theoretically, however, due to the volume of the computational domain required and the practicality of obtaining a sufficiently refined mesh resolution, it is not ideal to use the DNS methods for practical engineering. The Reynold Averages Navier Stokes equation method will be used in this thesis due to the cost intensity, computational requirements of the DNS and LES methods and the Reynolds numbers being dealt with doe not require any of those two methods either.

3.2.4.2 Reynolds averaged Naiver Stokes (RANS) approach

It is not a requirement to resolve the turbulent fluctuations experienced in most engineering processes. This is because the satisfaction of the time averaged properties of the flow such as the mean velocities, mean pressures and mean stress is achieved for most problems. This therefore means that the RANS approach will maintain its hierarchy and continue to be used in resolving a vast majority of turbulent flow problems in the near future (H.K.Versteeg and W.Malalasekera, 2010). The Reynolds decomposition or the Reynolds averaged approach is used to solve the effects fluctuations have on the mean flow. For the unsteadiness experienced during the flow to be averaged properly, when compared to the typical timescale in which the turbulent fluctuations occur, the Navier stokes equations are averaged over a large enough time. The mean fluctuation components are used to replace the flow variables such as u which includes *u, v* and *w* and the pressure at a instant, *p* in the Navier Stokes equations.

$$\boldsymbol{u} = \boldsymbol{U} + \boldsymbol{u}' \qquad u = U + u' \qquad v = V + v' \qquad w = W + w' \qquad p = P + p'$$

The time average of the steady component u is represented by U, the fluctuations or perturbations of which their averages equal zero are shown by u'. When the governing rules for the fluctuating time averaging properties, are substituted by the Reynolds decomposition equations for mass and momentum conservation, we then obtain the Reynolds averaged Navier stokes equation for incompressible flow as shown (H.K.Versteeg and W.Malalasekera, 2010);

$$\frac{\partial(u_i)}{\partial t} + \frac{\partial}{\partial x_j}\left(u_i u_j\right) = -\frac{1}{\rho}\frac{\partial p}{\partial x_i} + \frac{\partial}{\partial x_j}\left[v\left(\frac{\partial u_i}{\partial x_j} + \frac{\partial u_j}{\partial x_i}\right)\right] - \overline{u_i' u_j'} \qquad (3.3)$$

New terms such as the Reynolds stresses, $-\overline{u_i' u_j'}$ have been introduced due to the time averaging. Many different turbulence models such as the standard k-ε turbulence models and its variations such as the RNG k-ε model and Realizable k-ε model which are used widely around the world for engineering simulations have been used for modelling to solve the non-linear stress terms in the RANS equations.

The Reynolds stress and mean rate of deformation being the same in all directions when using the isotropic eddy viscosity assumption, is the basis for solving the Reynolds stress tensor in the k-ε model. Two transport equations, namely; the turbulent kinetic energy, k and the rate at which it is dissipated, ε are both part of the two-model equation solved in the K-ε model family. In order to completely solve the RANS equations, the above transport equations are then used to calculate the turbulent viscosity, μ_t. solving the transport equations for Reynolds stresses and the equations for dissipation rate toobtainher, the Reynolds Stress model, RSM solves the RANS by obtainting rid of the isotropic viscosity assumption (Gouzhen, 2016**).** Launder and Spalding (1972) suggested that the determination of both turbulence length and time scales using two distinct transport equations could be possible with the aid of a two-equation turbulence model known as the standard k-ε model. The derivation of the model is based on considerations which are phenomenological and empirical hence making it a semi-empirical model. The kinetic energy k, and the dissipation rate ε which are used to define the scale of velocity, v and the representative length of the large-scale turbulence length, l are the two-model equation that make up the standard k-ε model.

$$v = k^{\frac{1}{2}} \qquad (3.4)$$

$$l = \frac{k^{\frac{3}{2}}}{\varepsilon} \qquad (3.5)$$

The eddy viscosity can be specified as shown below when dimensional analysis is applied with the dimensional constant, C_μ .

$$\mu_t = C\rho vl = \rho C_\mu \frac{k^2}{\varepsilon} \qquad (3.6)$$

When the rate at which k or ε is destroyed is subtracted from the sum of the k or ε transport by diffusion and the rate at which k or ε are produced, equals the sum of the rate of change of k or ε and the transport by convection of k or ε we have the following transport equations for k and ε respectively in formula for the standard k- ε model.

$$\frac{d(\rho k)}{\partial t} + u_i \frac{\partial(\rho u_j k)}{\partial x_j} = \frac{\partial}{\partial x_j}\left(\frac{\mu_t}{\sigma_k}\frac{\partial k}{\partial x_j}\right) + \mu_t \frac{\partial u_i}{\partial x_j}\left(\frac{\partial u_i}{\partial x_j} + \frac{\partial u_j}{\partial x_i}\right) - \rho\varepsilon \quad (3.7)$$

And

$$\frac{d(\rho k)}{\partial t} + u_i \frac{\partial(\rho u_j \varepsilon)}{\partial x_j} = \frac{\partial}{\partial x_j}\left(\frac{\mu_t}{\sigma_\varepsilon}\frac{\partial \varepsilon}{\partial x_j}\right) + C_{\varepsilon 1}\frac{\varepsilon}{k}\mu_t \frac{\partial u_i}{\partial x_j}\left(\frac{\partial u_i}{\partial x_j} + \frac{\partial u_j}{\partial x_i}\right) - \rho C_{\varepsilon 2}\frac{\varepsilon^2}{k} \quad (3.8)$$

There is always a close relation between the production and destruction of turbulent kinetic energy. The production and destruction of ε in its model equation is assumed to be proportional to the production and destruction of in the k model equation hence, where k is largely produced, the dissipation of ε is also large. The transference of energy from mean flow to turbulence which is compensated by the way the mean velocity interrelates with the Reynolds stresses, gives rise to the innate production of turbulence. Due to the viscous properties of the flow, the dissipation of energy through heat is represented by the destruction term.

There are five adjustable constants namely; μ_t, σ_k, σ_ε, $C_{\varepsilon 1}$ and $C_{\varepsilon 2}$ which are used in the k- ε model, can be found in the equations discussed above and are obtained from all-inclusive data fitting for an immense range of turbulent flows (Gouzhen, 2016).

μ_t = 0.09 σ_k = 1.00 σ_ε = 1.30 $C_{\varepsilon 1}$ = 1.44 $C_{\varepsilon 2}$= 1.92

The standard k-ε model is very popular in industrial applications due to its robust nature, economy and wide range of accuracy in turbulent flows. However, when it comes to flows which have separated boundary layers, flows with swirl, rotating flows over surfaces which are curved causing sudden changes to the mean strain rate, the model is not very efficient. The assumption that the turbulent viscosity is isotropic when using the k- ε model has its basis on the Boussinesq hypothesis. Numerical simulation of strong swirling flows which have eddy viscosities could also be a source of inefficiency from the k-ε model as the geometry affects the anisotropy (Gouzhen, 2016).

There are two variations soft the standard k-ε model namely; the Realizable k-ε model the RNG k- ε Model. A mathematical technique known as the renormalization group

(RNG) method, is used to derive the instantaneous Navier Stokes equations used in the RNG turbulence model. There are certain refinements such as the additional terms and functions for the k and ε transport equations, used to derive results analytically with constants which differ from the standard k-ε model. Some of the refinements made to the standard k-ε to create the RNG model are as follows (ANSYS, 2011);

- When used in rapidly strained flows, the additional term in the ε transport equation, causes and improvement in accuracy of the RNG k-ε model.
- The accuracy of the RNG model is enhanced for swirling flows as the effect of turbulence is catered for.
- User specified constant values are used in the standard k-ε model while for turbulent prandtl numbers, analytical formulas are used in the RNG theory.
- The effects of a low Reynolds number flow is accounted for by the differential formula for effective viscosity which is derived analytically in the RNG model whereas, the standard k-ε model is more of a model which is applicable to high Reynolds numbers.

In comparison to the standard k-ε model, for a wider range of flows, the RNG k-ε model has more accuracy and reliability.

There are two very distinct ways the realizable k-ε model stands apart from the standard k-ε model (Shih et al, 1995).

- An alternative formulation for the turbulent viscosity is used in the realizable k-ε model.
- An exact equation for the transport of the fluctuation of the mean square vorticity is used to generate a modified transport equation for the dissipation rate ε.

Certain mathematical constraints on the Reynolds stresses which are consistent with the physics of turbulent flows make the model realizable. Neither the RNG k-ε model nor the standard k-ε models are realizable.

Where the fluid flow features strong streamline curvature, vortices and rotation, there is substantial improvement shown when using the realizable k-ε model and the RNG k-ε model as compared to the standard k-ε model. The situations where the realizable k-ε model performs better than the RNG model are not yet definite as the model is still relatively new. After using separated and complex flows to carry out several validations, the realizable k-ε model has proved to be the most efficient fop all the k-ε models (ANSYS, 2011).

The boussinesq hypothesis of isotropic eddy viscosity is not used in the Reynolds stress model. The Reynolds stresses transport equation as well as the equation for the dissipation rate, are solved in order to close the Reynolds averaged Navier stokes equations. When solving 3 Dimensional flows, seven additional transport equations are needed when using the Reynolds Stress model. The transport of the Reynolds stresses is depicted by the transport equation below (Speziale et al., 1991);There is a higher chance of obtaining more accurate results for complex flows when using the RSM model because the model makes use of additional seven equations, it caters for the effects streamline curvature has on flow, swirl rotation and the swift changes in strain rate as compared to the one equation and two equation models (ANSYS, 2011).

3.2.4.3 Wall Bounded turbulent flow near wall treatment

The existence of wall affects turbulent flow ominously. All three components of the fluid velocity on a solid surface are deemed to be equal to the individual components of velocity at the surface and this is because a non-slip boundary condition is assumed in computational fluid dynamics (Lauga et al., 2005). The velocity ranges

from zero at the walls to the mean flow velocity at the core and this leads to a very steep velocity gradient being formed as the mean velocity has to be zero close to the wall. This phenomenon creates an area which can be referred to as the near wall region. In accurate modelling and flow prediction in the near wall region will be a problem when using the k- ε models and the RSM as they are intended for turbulent flow in the core region. There are two regions which make up the turbulent boundary layer adjacent to the solid surface (H.K.Versteeg and W.Malalasekera, 2010, ANSYS, 2011).

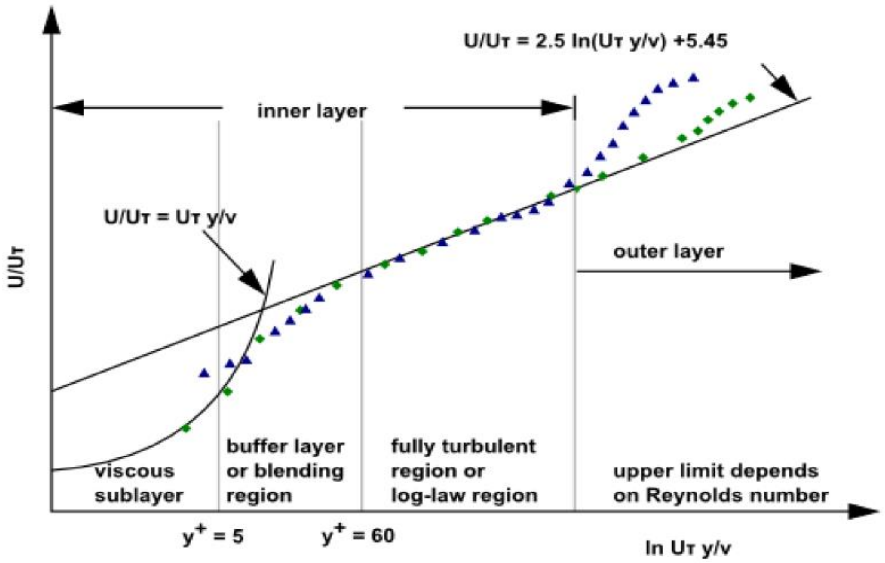

Figure 3.2: near wall regions experienced in turbulent flows (ANSYS, 2011)

- **The inner region:** in this region, the shear stress is practically constant and equal to the wall shear stress, τ_w and makes up between 10 to 20 percent of the wall layer's total thickness. The inner region also has three layers which in order of growing distance from the wall are as follows;
    - The region adjacent to the wall surface where viscous forces are dominant referred to as the linear or viscous sublayer. In this layer the wall has a dampening effect on the turbulence thereby making the flow in this innermost layer almost laminar.

- When the viscous and turbulent forces start to become of equivalent magnitude, the region is then referred to as the buffer layer.
- The external flow and the boundary layer flow merge in the fully turbulent region otherwise known as the log-law layer. Turbulence plays a key part is this region.

- **The law of the wake layer or out region:** this region is far from the wall, mostly free from direct effects of viscous forces and is dominated by the core inertia forces.

Special wall modelling procedures and increased mesh quality are needed to predict the behaviour of flow more accurately and to resolve the velocity gradient. Fully turbulent flows can be resolved mostly with the turbulence models we have discussed above. However, in some regions close to the solid wall, the viscous effects dominate the turbulent effects because the Reynolds number in that local area is so small. To solve wall bounded flows, we must therefore make certain adjustments. Treating the boundary conditions present at the solid walls will go a long way to determine how successful a turbulence model will be in predicting the flow (Chen and Patel, 1988).
The wall function method and the near wall modelling method are two of the approaches used to model the flow in near wall regions (ANSYS, 2011). The viscous sublayer and buffer layer in the inner region which are affected by viscosity are not solved when the wall function method is used. The regions affected by viscosity between the wall and the fully turbulent flow regions are bridged by using wall functions which are semi-empirical formulas. This ensures that the presence of the wall does not require the turbulence models to be modified due to the use of wall functions (Gouzhen, 2016). The turbulence model is modified with a mesh which goes all the way to the wall including the viscous sublayer and this enables the regions affected by viscosity to be resolved using the method known as near wall modelling.

There are several wall function approaches which could be adapted in ANSYS FLUENT dependent in the turbulence model chosen;

- The Standard Wall Functions
- Non – Equilibrium Wall Functions
- Scalable Wall Functions

The standard wall functions which is available when using the K-ε models and Reynolds Stress models, is most widely used in industrial flows based on research done by launder and Spalding (1974). For mean velocities, in standard wall functions the law of the wall is as follows;

$$U^* = \frac{1}{k}\ln(Ey^+) \quad (3.9)$$

The dimensionless velocity is represented as

$$U^* \equiv \frac{U_p C_\mu^{\frac{1}{4}} k_p^{\frac{1}{2}}}{\frac{\tau_w}{\rho}} \quad (3.10)$$

And the dimensionless distance from the wall is shown as

$$y^+ \equiv \frac{\rho C_\mu^{\frac{1}{4}} k_p^{\frac{1}{2}} y_p}{\mu} \quad (3.11)$$

Where k = von Kármán constant (0.4187), E = empirical constant (9.793), C_μ = constant (=0.09), U_p = mean velocity of the fluid at the near-wall node P, k_P = turbulence kinetic energy at the near-wall node P, y_P = distance from point P to the wall, μ = dynamic viscosity of the fluid, τ_W = wall shear stress. The laminar stress-strain relationship written as $U^* = y^+$ is applied by FLUENT when the mesh at the wall-adjacent cells is $y^+ < 11.225$. When $y^+ > 11.225$, the log law is used. The wall functions are used to solve solution variables which include temperature, mean velocity, concentration of species, k and ε for the wall boundary conditions. Broad ranges of wall bounded flows can be resolved using the standard wall functions however, when the ideal conditions assumed for derivation for the flow conditions, the standard wall functions tend to be less effective. The universality of the standard wall

functions is mostly limited by the assumptions of constant shear and local equilibrium. This means that the quality and accuracy of the results are debatable when the flow is subject to strong non-equilibrium forces and severe pressure gradients affect the flows nearest to the wall. Potential improvement can be achieved when non-equilibrium wall functions are used.

The non-equilibrium wall function is a two-layer based model which is available to use in K- ε models and Reynolds Stress transport models as an improvement to the standard wall functions (Kim and Choudhury, 1995). There are two notable elements when using the non-equilibrium wall function;

- There is high sensitivity to the effects of pressure gradient on the flow from the Launder and Spalding's log law for mean velocities.
- In the neighbouring cells of the wall, the turbulent kinetic energy $(\overline{G_k}, \bar{\varepsilon})$ budobtain is computed with the two-layer based concept.

In standard wall functions the law of the wall for mean temperature or species mass fraction is still same. While to cater for the pressure gradient, the log law for mean velocity is as follows;

$$\frac{\tilde{U}C_\mu^{\frac{1}{4}}k^{\frac{1}{2}}}{\frac{\tau_w}{\rho}} = \frac{1}{k}\ln\left(E\frac{\rho C_\mu^{\frac{1}{4}}k^{\frac{1}{2}}y}{\mu}\right) \qquad (3.12)$$

Where

$$\tilde{U} = U - \frac{1}{2}\frac{dp}{dx}\left[\frac{y_v}{\rho k\sqrt{k}}\ln\left(\frac{y}{y_v}\right) + \frac{y - y_v}{\rho k\sqrt{k}} + \frac{y^2{}_v}{\mu}\right] \qquad (3.13)$$

When computing the turbulent kinetic energy at the cells adjacent the wall, a two-layer concept is applied to solve the k equation at the cells neighbouring the wall when using the non-equilibrium wall function.it is assumed that a viscous sublayer and fully turbulent layer make up the neighbouring cells to the wall. The proportions of viscous sublayer to fully turbulent layer varies from cell to cells in highly non-equilibrium flows and this is a major determinant of the turbulent kinetic energy . The effect pressure gradients have on the distortion of velocity profiles is accounted for by the non-

equilibrium wall functions. Hence is it not accurate to assume that the rate at which turbulent kinetic energy is produced is equal to the rate at which is it destroyed in such scenarios. This therefore means that the non-equilibrium effects which the standard wall functions do not account for are taken care of by the non-equilibrium wall functions. Where complex flows characterised by separation, reattachment, impingement and rapid pressure gradients and rapid changes affect the mean flow, the non-equilibrium wall functions are recommended due to their ability to account for these effects the pressure gradient has on the mean flow.

Where the mesh grid refinement is below $y^+ < 11$, the depreciation of the standard wall functions is avoided by using the scalable wall functions. Therefore, when grids of uninformed enhancement are used, consistent results are obtained with the wall functions however, the results obtained when using standard wall functions are identical where the grids are coarser than $y^+ > 11$. The compulsory usage of the standard wall function approach in combination with log law, is a purpose of the scalable wall function. Introducing the limiter in the y^+ calculation ensures this. $\bar{y}^+$ is used in the scalable wall functions to replace the y^+ used in standard wall function formulas.

A majority of high Reynolds wall bounded flows can be reasonable predicted using the standard wall functions. The effects of pressure gradient on the flow is catered for by the non-equilibrium wall functions thus increasing the applicability of the wall function approach. When the flow conditions move off too much from the model conditions which underlie the wall functions as will be discussed below, the above discussed wall functions become less effective.

- Prevalent low Reynolds number or near wall effects such as flow through a small gap, highly viscous, low velocity fluid flow
- Massive transpiration such as blowing or suction through the wall
- Boundary layer separations caused by severe pressure gradients

- Flow near rotating disks, buoyancy driven flows all under strong body forces
- Highly 3-dimensional flow such as the Ekman spiral flow and strongly skewed 3D boundary layers near the wall region

If any of these above mention properties exist in the flow that is being modelled, the near wall modelling approach combined with adequate mesh grid generation in the near wall region should be used (ANSYS FLUENT Theory guide, 2011).

A refined mesh grid which goes all the way to the wall and a modified turbulence model is used to resolve the regions affected by viscosity including the viscous sublayer in the near wall modelling approach (ANSYS, 2011). There are identical elements between the traditional two-layer zone model and the enhanced wall treatment where the first near wall node is placed at about $y^+ \approx 1$ and the near wall mesh is refined enough to resolve the viscous sublayer. The near wall modelling method which overcomes the issues which arise from near wall modelling, combines the two-layer method with enhanced wall functions and is known as the Enhanced wall treatment method. Except for the Quadratic Reynolds Stress Model, the enhanced wall treatment method is available with all ε-equation models and ω-equation models (ANSYS, 2011). The specification of both ε and turbulent viscosity in near wall cells is done by the two-layer model which is an essential part of the enhanced wall treatment. The division of the whole domain into the region affected by viscosity and the fully turbulent region is how this approach works. The wall distance and turbulent Reynolds number, Re_y are used to determine the segregation between these two regions.

The k-ε model or the RSM model is adopted for fully turbulent regions where $\mathrm{Re}_y > 200$, while the one equation model employed by Wolfshtein is used in regions affected by viscosity where $\mathrm{Re}_y < 200$ (Wolfshtein, 1969). The enhanced wall treatment allows for the effects of pressure gradients or variable properties to be

taken into account with the modification of the fully turbulent law. For large and small values of y^+, an accurate asymptotic behaviour is guaranteed and where the y^+ is within the wall buffer region ($3 < y^+ < 10$), this approach ensures a fair representation of the velocity profiles (Fokeer, 2006). ANSYS (2011) recommends the usage of the enhanced wall treatment function with all models for which it is available as the most consistent wall heat transfer predictions and wall shear stress values are obtained with least sensitivity to y^+ values. However, for swirling flows which are come upon in devices such as cyclone separators and swirl combustors, the secondary issue is near wall turbulence because the turbulence model in the core region often determines the accuracy of the turbulence model. Non-equilibrium wall functions can often increase the accuracy of results obtained in flows where the wall activity is part of the swirl generation process as the mean velocity is sensitive to the pressure gradients (ANSYS FLUENT user guide, 2011).

3.2.4.4 Numerical Schemes

A control-volume based technique is used to solve scalars such as turbulence and chemical species, the integral equations which govern the conservation of mass, momentum and energy (when apposite). The control volume-based technique consists of;

- Using a computational mesh grid to divide the whole domain into discrete control volumes.
- Algebraic equations for discrete dependent variables such as velocities, pressure, temperature and conserved scalars are constructed for the integration of governing equations in individual control volumes.
- Updated values for the dependent variables are achieved by linear discretization of the linear equations and solution of the resultant linear equations.

The pressure-based solver and density-based solver are the two numerical methods which ANSYS FLUENT offers for solving fluid flow numerically. Traditionally, the incompressible and mildly compressible flows have been solved by the pressure-based solver. High speed compressible flows were originally solved by the density-based approach. It is now possible for a range of flows ranging from highly incompressible to highly compressible to use both methods. The density-based formation gives a higher accuracy for high speed compressible flows in comparison to the pressure-based solver. In ANSYS FLUENT, the segregated algorithm and the coupled algorithm exist within the pressure-based solver. The governing equations are segregated from one another and solved sequentially when using the segregated algorithm while the momentum equations and pressure-based continuity equations are solved in a coupled manner when using the coupled algorithm. The coupled algorithm requires a lot more memory in comparison to the segregated algorithm, but it also offers an improvement in convergence speed which surpasses the segregated algorithm.

In ANSYS FLUENT, the equations which govern momentum, continuity, species transport and where appropriate, energy are solved simultaneously when using the density-based solver as a set of vector equations. Where there are additional scalars such as turbulence or radiation quantities, their governing equations are also solved sequentially. The density-based solver is also subdivided into two formulations namely, the implicit and explicit. The way the couple equations are linearized is the differentiating factor of the implicit and explicit density-based formulations. In some cases, certain flow features may be resolved better, and a faster solution may be reached with the use of one formulation instead of the other although ANSYS (2011), tells us that for a expansive range of flows, both the pressure based and density based solvers can be applied. There are generally more physical models available to

use with the pressure-based solver in comparison to the density-based solver. Some solutions techniques which are only possessed by the pressure-based solver are advantageous in this thesis to resolve and calculate swirl or rotating flows. Therefore, as Ariyaratne (2005) and Fokeer (2006) implemented, the pressure-based solver will be used in this thesis to analyse incompressible fluids. The projection method described by Chorin (1968), is the general umbrella under which the algorithm employed by the pressure-based solver lies. Deriving an equation in such a way as to ensure the continuity is satisfied with the velocity field corrected by pressure, from the continuity and momentum equations is a way by which the mass conservation constraint is achieved. The entire set of governing equations are repeatedly solved in iterations until the solution converges. This is done due to the non-linearity of the governing equation and their coupled nature. The option of segregated algorithm or coupled algorithm solving is made available by ANSYS FLUENT. In this thesis, the coupled algorithm is used as it solved all governing equation is a coupled manner and the issue of memory consumption is tackled via length or size independency tests.

The individual equations which govern the solutions variables such as, u, v, w, p, T, k and ε are solved sequentially in the segregated algorithm. While being solved, each individual governing equation is separated or decoupled from other equations. The discretised equations are only stored in memory one at a time when using the segregated algorithm but due to the equations being solved in a decoupled manner, there is relatively slow convergence of the solution.

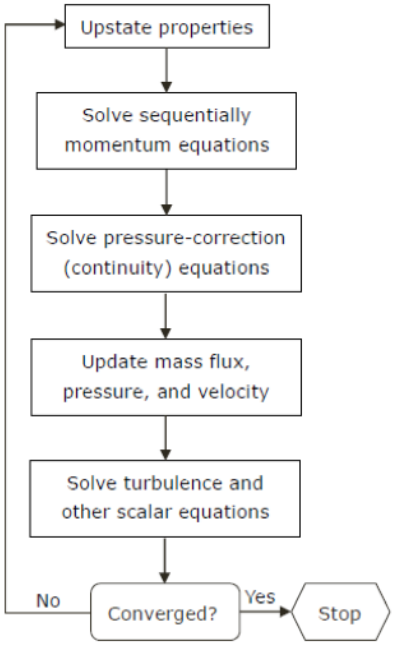

Figure 3.3: Overview of processes involved in the Pressure based segregated algorithm solution methods (ANSYS, 2011)

The momentum equations and pressure-based continuity equations are coupled to obtain in a system of equations and solved using the pressure based coupled algorithm. The coupled systems of equations are solved in a single step which replaces steps 2 and 3 from the pressure based segregated algorithm while in similar fashion with the segregated algorithm, the rest of the scalar equations are solved in a decoupled manner. The rate of convergence is significantly improved in comparison to the segregated algorithm because the equations of momentum and continuity are solved in a coupled manner.

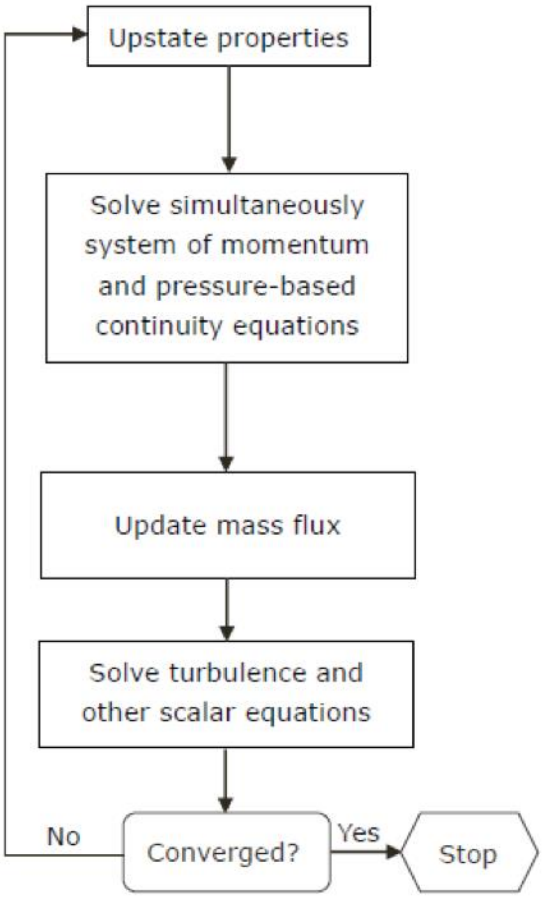

Figure 3.4: Overview of processes involved in the Pressure based coupled algorithm solution methods (ANSYS, 2011)

3.2.4.5 Numerical Discretization

The surfaces, boundaries and computational domains are discretised before they can be solved numerically. This discretization process can be done via either the Finite-Difference Method (FDM), Finite-Volume Method (FVM) or Finite-Element Method (FEM) (Versteeg and Malalasekera, 1995). The Finite-Volume Method (FVM) can be used with either structured or unstructured meshes, conservation is meticulously imposed and can relay directly to physical quantities such as mass fluxes. These facts and the fact that in terms of CFD code development, it is relatively easier, contribute to making it the most used in CFD packages such as ANSYS FLUENT.

ANSYS FLUENT operates through the conversion of a general scalar transport equation to an algebraic equation which can be solved numerically using a control volume-based technique. According to H.K.Versteeg and W.Malalasekera, (2010) the numerical algorithms used in the FVM method consists of the following;

- The governing equations of fluid flow over all the finite control volumes of the domain are integrated.
- A system of algebraic equations which are for convenience purposes written in a matrix form are discretized resulting in integral equations.
- Using iterations, the algebraic equations are solved, and solutions obtained.

An unknown scaler variable, ϕ as well as unknown values found in the neighbouring cells are some of the values contained in a discretised scalar transport equation which due to the convection term present in the equations, they are usually non-linear in nature. Additional nonlinearities arise from other phenomena such as chemical reactions and turbulence. According to Bhaskaran and Collins, (2003), iterating a guess value until it agrees with the solution to a specified tolerable level, is the tactic adopted to make the nonlinear equations linear. The discretised transport equation is written as $a_p\emptyset = \sum a_{nb}\,\emptyset_{nb} + b$ in its linear form (Gouzhen, 2016). The neighbouring cells are represented by the subscript nb, the linearized coefficients for $\emptyset_{nb}$ and $\emptyset$ are represented by a_{nb} and a_p respectively. Except for boundary cells, the number of faces encompassing a cell is usually equal to the number of neighbours each cell has but this again is dependent on the topology of the mesh. Each cell in the mesh grid can have a similar equation and these build up to form a sparsely coefficient matric of algebraic equations. A point implicit of Gauss-Seidel linear equation solver as well as an algebraic multigrid method (AMG) is used to solve these liner systems of equations in ANSYS FLUENT.

The computational domain is divided into control volumes made up of a finite number of elements by either a regular or irregular nodal arrangement otherwise known as a mesh or grid in the Finite Volume method. To allow for the velocity of the fluid to be specified arithmetically at every point in space and time, the flow constraints are resolved around these nodes. The values for convection terms have to be interpolated from the values at the cell centres as by default, the discrete values such as pressure, velocity and turbulence are stored by ANSYS FLENT at the cell centres. Where the value relative to the normal direction of the velocity at the face is obtained from the cell quantities upstream or upwind is referred to as Upwinding or an Upwind Scheme (Gouzhen, 2016).

The first-order upwind scheme, second-order upwind scheme, power law scheme, QUICK scheme and third Order MUSCL scheme are the upwind advection schemes for momentum, kinetic energy, dissipation rate and Reynolds stresses offered by ANSYS FLUENT. Assuming that the average cell value and hold throughout the whole cell is represented by the values present at centre of the cell for any field variable is the way the values at cells faces are obtained when using the first-order upwind scheme. This means that the value calculated at the centre of an upstream cell is equal to the value measure at the face when using the first-order upwind scheme (Gouzhen, 2016). The Taylor series expansion of cell centred solution about the centroid of the cell is used to achieve higher order accuracy quantities at the cell face in the second-order upwind scheme. The value of the displacement vector from the upstream centroid to the face centroid multiplied by the gradients in the upstream cells and summed with the cell centre value gives us the face value. Assuming a convectional diffusion equation which one to one dimensional, a variable is interpolated to obtain the face value when using the power law scheme. A weighted average of the second order-upwind scheme and variable interpolation forms the basis for the Quadratic Upstream Interpolation for Convection Kinetics (QUICK) Scheme. The unique Monotone Upstream-Centred Schemes for Conservation Laws

(MUSCL) was combined with the second-order upwind and a central scheme for differencing thereby giving rise to the third Order MUSCL scheme (Gouzhen, 2016). When the flow is aligned with the mesh, numerical diffusion is naturally low and according to ANSYS FLUENT (2006), a better convergence without any loss of accuracy can be achieved while using the first-order scheme. Numerical discretisation error can however be increase by the first-order convective discretisation when the flow is not aligned with the mesh. Results for complex flows are generally more accurate when using the second-order upwind scheme (Gouzhen, 2016). In conclusion, using the right mesh, the first-order upwind discretization will yield better convergence than the second order upwind however with more complexity in flows and mesh irregularities such as triangular or tetrahedral meshes, the first-order upwind could be less accurate. With regards to swirl or rotating flows, better accuracy in results may be achieved by using the QUICK and third order MUSCL discretization schemes. There is no significant enhancement in accuracy when using the QUICK and third order MUSCL discretization schemes, so the second-order scheme is generally adequate enough. The accuracy of the power law scheme tends to be in the same range as the first-order upwind scheme.

3.2.4.6 Pressure interpolation schemes

Pressure interpolation schemes are adopted and used to compute the pressure values form cell values. The standard, second-order, body-force-weighted, linear and PREssure Staggering Option, PRESTO! Schemes are available to use under the pressure-based solver in ANSYS FLUENT. When the variations in pressure between cell centres is smooth, the standard scheme is efficient. Large jumps in gradients in the momentum source terms between control volumes and high gradients at cell faces makes it difficult to interpolate using the standard scheme. Flows under the influence of strong swirls, large body forces and flows through geometries with curvatures, are also difficult for the standard scheme to solve. The second order

accurate convection terms are used to reconstruct the face pressure in the same manner in the second order scheme. Although this scheme shows considerable improvement over the standard and linear schemes, if this scheme is used at the beginning of a calculation or with a bad mesh, it may encounter some problems. The use of Volume of Fluid (VOF), mixture model for multiphase flow and porous mediums cannot be solved using the second order scheme. Assuming that there is a constant normal gradient of the difference between pressure and body forces, the face pressure is calculated using the body-weighted scheme. Where the body forces such as buoyancy and axisymmetric swirl calculations are deductive from momentum equations. The average of the pressure values in adjacent cells is used to compute the pressure at the face when using the linear scheme. The staggered face pressure is computed using a discrete continuity balance for a staggered control volume in the PRESTO! Scheme (Gouzhen, 2016). In conclusion, PRESTO! Is suggested for flows which are influenced by high speed rotation, porous media, and domains with strongly curved geometries, high swirl numbers and natural convection with high Rayleigh numbers while for flows with large body forces, using the body-force0weigthed scheme is advised.

The continuity equation is usually not satisfied by the resulting face flux because an estimated pressure field is normally used to solve the momentum equations. To ensure that the face flux satisfies the momentum equation, a combination of continuity and momentum equations are used to arrive at a pressure or corrected value of pressure. This is achieved by using a pressure velocity coupling algorithm. Semi-Implicit Method for Pressure Linked Equations (SIMPLE), Semi-Implicit Method for Pressure Linked Equations-Consistent (SIMPLEC) and Pressure-Implicit with Splitting of Operators (PISO) are three types of segregated algorithms available in ANSYS FLUENT when using a pressure-based segregated solver (Gouzhen, 2016). The pressure field is obtained by enforcing conservation of mass through the relationship between the velocity and pressure corrections in the SIMPLE algorithm.

A discrete equation for the correction of pressure in the cell is obtained by substituting the flux correction equation is into the discrete continuity equation. A different expression for the correction of the face flux is used in the SIMPLEC method and this differentiated it from the SIMPLE algorithm. Approximation of the relation between pressure and velocity correction at a higher degree forms the basis for the Pressure-Implicit with Splitting of Operators, PISO. It considers neighbouring cell correction and skewness correction and after the solving of the pressure correction equation and this allows for the momentum balance to be satisfied by new velocities and corresponding fluxes thereby increasing calculating efficiency. SIMPLE or SIMPLEC methods are used in general for calculations done in the steady state while for transient calculations or steady state or transient calculations with meshes of high skewness, PISO is recommended (Gouzhen, 2016). Discretization of the governing equations must be done in both space and time when dealing with unsteady flows. As in the case of steady state equations, the time dependent equations are spatially discretised in the same way while splitting the time in the continuous flow into discrete time steps adopts temporal discretization to achieve time discretization.

3.3. Modelling swirl flow

The terms and equations used to study swirl flows will be discussed in this section.

3.3.1 Swirl number, Swirl decay, Hydraulic diameter and wall shear stress

The swirl number, S which is also sometimes known as the swirl intensity, is often used to quantify the strength of swirl a flow has in a pipe as there is no standard for that. The value obtained by multiplying the hydraulic radius with the ratio of the axial momentum flux to the angular momentum flux is known as the swirl intensity (Li and Tomita, 1994, Steenbergen and Voskamp, 1998, Rocklage-Marliani., 2003).

$$s = \frac{\int_0^R uwr^2.dr}{R\int_0^R u^2 r.dr} \qquad (3.14)$$

S = swirl intensity w = tangential velocity, m/s, r = radius at point where tangential velocity is calculated, m, u = axial velocity, m/s, R = pipe radius, m

The transport of angular momentum to the pipe wall causes the swirl effect to decay as the flow moves downstream. The law governing the decay of swirl has been studied by various researchers in order to determine the distance the swirl will last in the flow (Steenbergen and Voskamp, 1998, Li and Tomita, 1994, Halsey, 1987, Reader-Harris, 1994). Most of the studies showed that the intensity of swirl was in agreement with exponential decay functions however, there was no united agreement with all the results on the rates of decay.

$$S = S_0 e^{-\beta \frac{x}{D}} \qquad (3.15)$$

S_0 = initial swirl intensity

β = swirl decay rate parameter = α*f'

x = distance along pipe, m

D = pipe diameter, m

f' = Moody friction factor

α = empirical coefficient

Nesbitt (2000) defines the hydraulic diameter as the area the fluid is in contact with for partially filled pipes, non-cylindrical pipes and open channels. In fully cylindrical pipes, the hydraulic diameter is the same as the pipe diameter.

$$d_h = \frac{4A}{P} \qquad (3.16)$$

d_h = hydraulic diameter, m, P = wetted perimeter, m, A = area, m^2

There is a shear stress imposed on a boundary by any real fluid flowing along a solid boundary. The speed of the fluid at the boundary is zero where a no slip condition is assumed however the speed of flow at the boundary equals the speed of the fluid at a certain height above the boundary (Gouzhen, 2016). The boundary layer is the

defining region between these two points. Where the viscosity of a fluid flowing in the laminar regime is kept constant, the shear stress is proportional to the strain rate for all Newtonian fluids. When the flow starts to lose velocity, the boundary layer starts to be affected by the shear rate (Day, 2004, Timoshenko and Stephen, 1983). For a Newtonian fluid, at point y on the surface element parallel to a flat plate, the shear stress is given by;

$$\tau_W(y) = \mu \frac{\partial u}{\partial y} \qquad (3.17)$$

Where: μ = dynamic viscosity of the fluid, u = velocity of the fluid along the boundary, y = height above the boundary. The pressure loss experienced in a cylindrical pipe due to wall shear stress is shown by (Sleigh and Goodwill, 2008).

$$\Delta P = \frac{\tau_w 4L}{d} \qquad (3.18)$$

Therefore,

$$\tau_w = \frac{\Delta P d}{4L} \qquad (3.19)$$

ΔP = pressure loss due to friction in pipe

d = pipe diameter

L = length of pipe corresponding to pressure loss

Sleigh and Goodwill (2008) tell us that here is a positive relation between the velocity of flow and the drop in pressure in laminar regime flow as $\Delta P \propto u$, and in turbulent flow as $\Delta P \propto u^{1.7 \text{ to } 2.0}$, the flow rate is proportional to the wall shear stress when measured on a mean value basis for fluid flow in a closed processing system with cylindrical pipes (PathogenCombat, 2011). The Reynolds number of the flow and the ratio of wall roughness to the diameter of the pipe determine the friction factor (Douglas et al, 2006). It was concluded that the intensity of the swirl flow is drastically reduced due to the presence of tangential wall shear stress (Steenbergen and Voskamp, 1998, Kitoh, 1991). An equation was derived by Kitoh (1991) for incompressible, stationary and axially symmetric flow by treating the Reynolds averaged angular momentum equation for the expression of tangential wall shear

stress. As described later by Steenbergen and Voskamp (1998) and Najafi et al. (2011.

3.4 Summary

This chapter covered the basics of computational fluid dynamics, laminar/turbulent modelling theories, swirl theories and modelling of swirl, the models used, solvers and factors, pros and cons to be considered when attempting to run a CFD simulation using ANSYS. These will form the basis for the simulations carried out for this research work on the different fluid flow geometries presented in Chapter 4.

Chapter 4 New designs and numerical simulations

4.1 Introduction

This chapter introduces the different fluid flow geometries that have been proposed for the AICV to regulate pressure drop that will lead to maximum oil recovery. There are 8 designs in total that have been proposed, analyzed and discussed (Section 4.4). They include a coil pipe, a straight pipe, an elliptical straight pipe, a straight square pipe, a square swirl coil pipe, a slinky coil pipe, a square version of the slinky coil pipe and a swirl variation of the slinky coil pipe. These geometries have been designed based on existing literature and underpinning research into different geometries. The flow through different geometries in this research work has been simulated using ANSYS FLUENT academic code 19.2. Modelling fluid flow, heat transfer and chemical reactions in geometries ranging from simple to complex is achievable using this computational analysis (ANSYS, 2013). ANSYS FLUENT is used to analyze the behavior of fluid flow in a geometry in real life scenarios before prototyping or production. The fluid flow geometry is isolated into little cells or grids to shape volume by utilizing the program ANSYS modeler, meshing and the calculations in FLUENT are utilized to solve the governing equations e.g., Navier Stokes equation.

The numerical simulations have been carried out for Reynolds numbers of 1000 for laminar flow and 10000 for turbulent flow (Reynolds number of less than 2100 is considered laminar whereas above 4000 is considered as turbulent). Static pressure has been investigated using lamina and turbulent fluid flow models through these 8 different fluid flow geometries. Their results with pressure drop values and contours of static pressure have been shown and discussed in this chapter (Section 4.6). It is to be noted that velocity magnitude and velocity vectors colored by velocity for 7 of these 8 geometries were not carried out as their effect is not significant enough to cause much change in the turbulence or recirculation because of the nature of their design. Only the optimal design of square swirl slinky coil pipe has been shown with

pressure drop values, contours of static pressure, velocity magnitude and velocity vectors colored by velocity.

4.2 Basic Model Assumptions

In terms of physical and chemical phenomena which need to be considered at an adaptable level while preserving relevant features of the flow problem, assumptions need to be made to simplify the flow problem before setting up and running the CFD simulation (H.K.VeK. Versteeg W. Malalasekeraa, 2010). The models for numerical simulations are based on some of the following assumptions:

- The flow through the conduits is steady state, three dimensional and either laminar or turbulent;
- The flow is said to be single phase except stated otherwise;
- Based on the state of the flow, either laminar or turbulent, the inlet velocity is constant;
- The properties of the fluids simulated are constant.
- There is no slip wall which means the wall conduits are stationary

4.3 Laminar and Turbulent flow simulation set up

The simulations were run at Reynolds number of 1000 and 10000 for Laminar and Turbulent flow regimes respectively. The fluent settings for the simulations are; the Pipe Diameter, D = 0.0032m. The simulation was pressure based and run in steady state, the viscous laminar model was used due to the Reynolds number of 1000 which is in the laminar flow region while the standard K-ε, standard wall function model was used due to the Reynolds number of 10 000 which is in the turbulent flow region. The fluid considered is Oil with a density of 970kg/m^3 and viscosity of 0.1 kg/m-s. The cell zone is set to fluid; the inlet is set to Velocity inlet and the values are as calculated below; the outlet is set to pressure outlet at 0 Pascal. The specification method is the intensity and viscosity ratio with the backflow turbulent intensity at 5% and the

backflow turbulent viscosity ratio of 10. The solution is computed from the inlet with a reference temperature of 298.15K. Solution method is Simple for laminar cases and coupled for turbulent cases. Residual monitors are set to the value of 1e-05 and 1e-06 respectively, the solution is hybrid initialized and then 3000 iterations are run. The mass flow rates all balanced out and simulations attained convergence.

From the Reynolds number equation,

$Re = \frac{\rho V D}{\mu}$ (4.1)

For laminar flow (Re = 1000),

The velocity for oil is as follows; $V = 32.22\, m/s$

The velocity for water is as follows; $V = 0.16\, m/s$

The velocity for gas is as follows; $V = 0.06\, m/s$

For Turbulent flow (Re = 10 000),

The velocity for oil is as follows; $V = 322.2\, m/s$

The velocity for water is as follows; $V = 1.6\, m/s$

The velocity for gas is as follows; $V = 0.6\, m/s$

Table 4-1: Table of Fluid properties for numerical simulation

Fluid	Density kg/m^3	Viscosity kg/m-s	Inlet Velocities (Laminar) (m/s)	Inlet Velocities (Turbulent) (m/s)
Oil	970	1e-1	32.22	322.2
Water	1000	5e-4	0.16	1.6
Gas	100	2e-5	0.06	0.6

4.4 New designs and related numerical simulations

The cases selected aim to optimise pressure drop in the AICV without increasing the size or robustness of the device and heat transfer in solar water heaters. The cases

are based on fluid flow, oil, water at gas through various conduits at two Reynolds numbers, one thousand to cover laminar flow for the laminar flow element and ten thousand to cover turbulent flow for the turbulent flow element. The geometries used for the cases were all set up with same dimensions and units. The Number of turns varies for the different coil types in the coil geometry cases. Using ANSYS FLUENT 19.2 the configuration of the flow geometry to be modelled was created. Only a section of a model is made because a whole geometry would consume time and computational power. The cases are discussed below.

4.4.1 Straight pipe

A straight pipe which was chosen because straight pipes are every common and there are already existing standards and calculations for pressure drops in a straight pipe hence, there is a basis for comparison. It is to be noted that this geometry has been used to determine length interdependency with regards to the pressure drop of the CFD simulations. The result shows a linear relationship between pressure drop and length of the geometries which indicate that a smaller model can be utilised for simulations to reduce processing time. This model can be extrapolated for larger geometries. These settings will be utilised for all the remaining 7 geometries.

The volumetric flow rate through the straight pipe is calculated as

$$Q = \frac{\pi}{4} D^2 V \qquad (4.2)$$

Where D is the pipe diameter and v is the average velocity. The Reynolds number formula will be used to calculate the inlet velocity as one of the simulation parameters later in the paper. A special case of the Naiver-Stokes Equation that describes laminar flow in straight tubes is known as the Hagen-Poiseuille Law. From the Hagen-Poiseuille Law, change in pressure through a length of tubing can be related to characteristics of the fluid and tube dimensions, with the equation

$$\frac{\Delta P}{l} = \frac{32 \mu U}{d^2} \qquad (4.3)$$

Where l is the length of tubing, μ is the kinematic fluid viscosity, U is the fluid velocity, and d is the tube diameter.At the inlet of the pipe, an entrance region is formed and as the fluid flows through, it sticks to the pipe walls due to viscous effects (Young et al., 2010). This creates a boundary layer in which viscous effects are important. The fluid velocity changes with distance along pipe, $\varkappa$, until the fluid exits the entrance region. The velocity profile and entrance length ℓ_e is determined by the state of the flow that is either laminar or turbulent. The entrance lengths are determined as shown below; for laminar flow, $\frac{\ell_e}{D} = 0.06\,Re$ and for turbulent flow, $\frac{\ell_e}{D} = 4.4(Re)^{\frac{1}{6}}$.

The knowledge of the velocity profile is important to determine information such as pressure drop, head loss and flow rate (Kundu and Cohen, 2004). The full length of the full coil pipe geometry is 2.23m round a path of 0.024m. Varying the path length gives us varied coil lengths. This correlation is valuable to reduce geometry size, reduce computational requirements and conserve simulation time. To achieve similarity in fluid flow domains the straight pipe length is equated to the call pipe length. For a straight pipe length of 0.25m, a path length of 0.00269m is required. To run numerical simulations on the straight pipe, as shown in figure 4.1, the geometry had to first be created using ANSYS design modeller

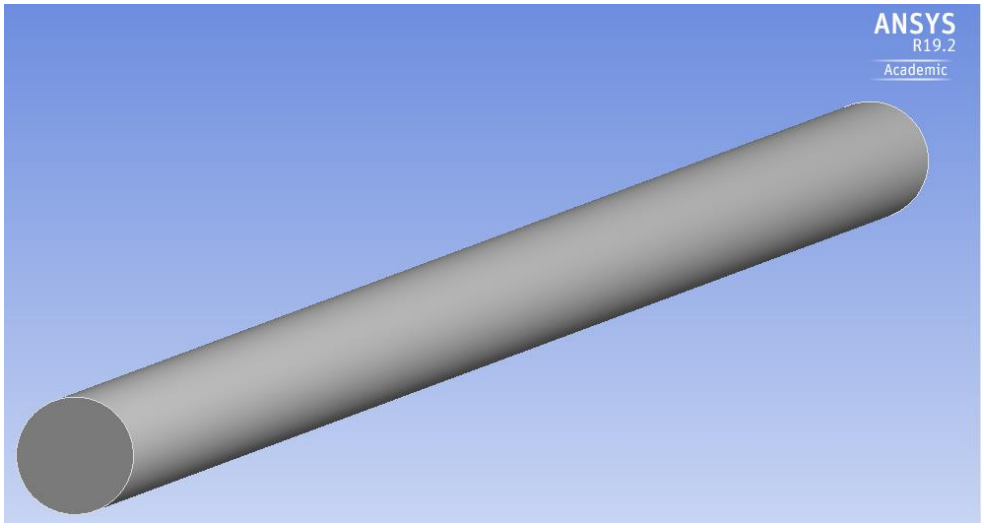

Figure 4.1: Straight pipe geometry

After the geometry creation and name selection process, the mesh grid is now generated as this must be done before numerical simulations can be carried out. The mesh or grid is generated using the same process and setting as used in the coil pipe. The findings and results achieved will be discussed in the following chapter.

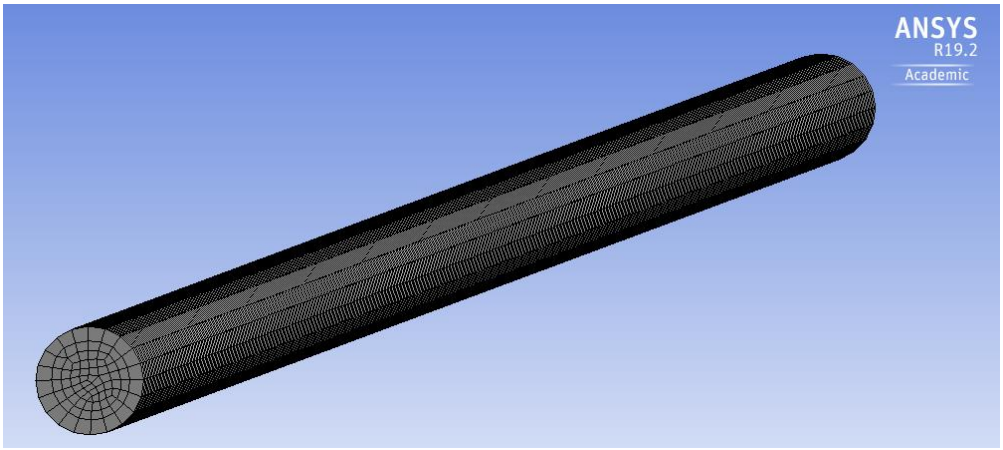

Figure 4.2: mesh grid generated for straight pipe

The CFD results were compared to the analytically calculated values as shown in the table using the Hagen-Poiseuille pressure drop equation.

$$\Delta P = \frac{32\mu LV}{d^2} \qquad (4.4)$$

The straight pipe case was used to validate the set up for laminar flow simulations. Various pipe lengths are run as shown in table and compared with their analytical calculated values. The results were seen to vary mostly by a factor of 2.05 which decreased to 1.05 with increase in pipe length. This suggests that the with increased pipe length, computational fluid simulation results are more reliable especially with simple geometries. Due to limitations on computation power, mesh elements on ANSYS fluent, this correlation is important as it allows you run minimal size models and equate them to full size designs. A correlation is also seen in the tabulated values in table 4-2. The CFD results obtained seem to match the previous pipe length of 0.05m differences. After finalising the settings for CFD, the laminar and turbulent simulations for all 8 geometries have been run and shown side by side for oil, water and gas.

4.4.1.1. Laminar and turbulent oil flow simulations

The pressure drop attained for the straight pipe geometry when simulating the flow of oil through the conduit was about 0.258 MPa as indicated in figure 4.3 below, the color map shows at the entrance region exhibits the highest-pressure coloration which dissipates as the flow goes through the pipe. On the other hand, the pressure drop attained for the straight pipe geometry when simulating the flow of oil through the conduit was about 13.54 MPa as indicated below, the color map shows at the entrance region exhibits the highest-pressure coloration which dissipates as the flow goes through the pipe.

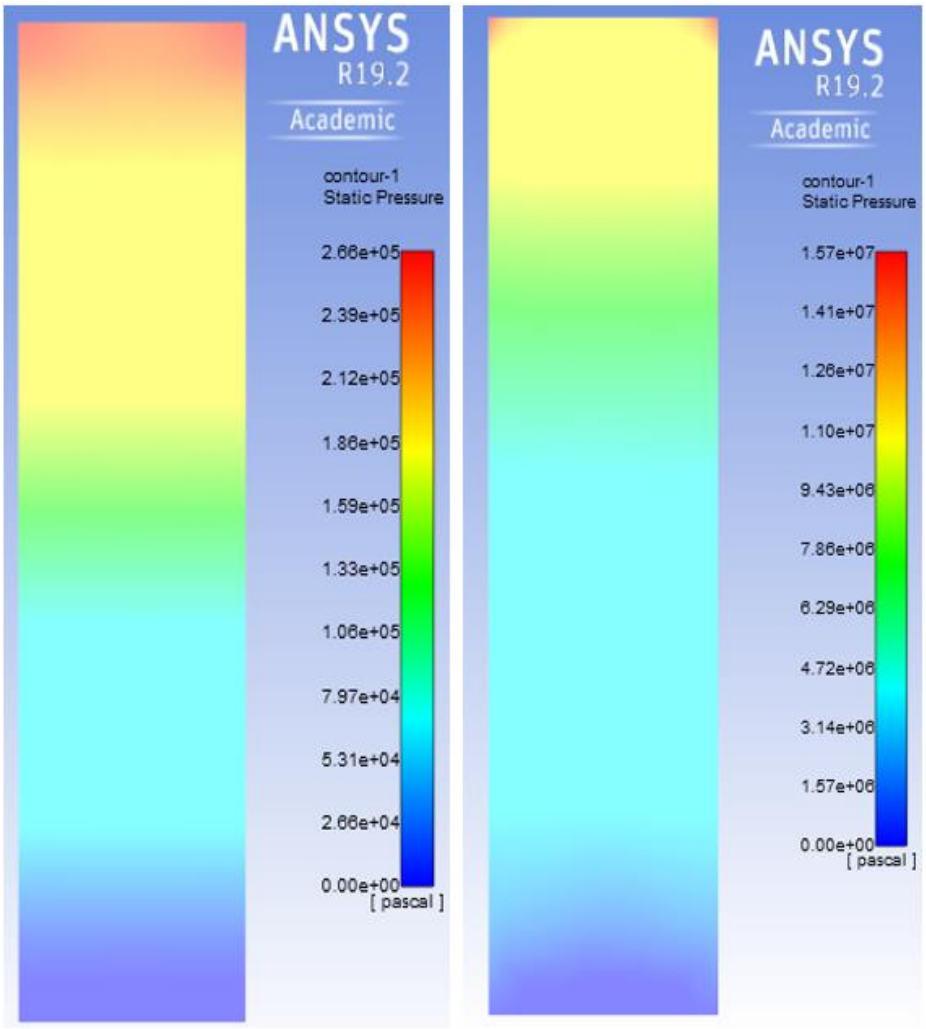

Figure 4.3: Laminar (left) and turbulent (right) oil flow - Contours of static pressure

4.4.1.2. Laminar and turbulent water flow simulations

The pressure drop attained for the straight pipe geometry when simulating the flow of water through the conduit was about 6.42 Pa as indicated in figure 4.4 below, the color map shows at the entrance region exhibits the highest-pressure coloration which dissipates as the flow goes through the pipe. On the other hand, the pressure drop attained for the straight pipe geometry when simulating the flow of water through the conduit was about 340.9 MPa as indicated below, the color map shows at the entrance region exhibits the highest-pressure coloration which dissipates as the flow goes through the pipe.

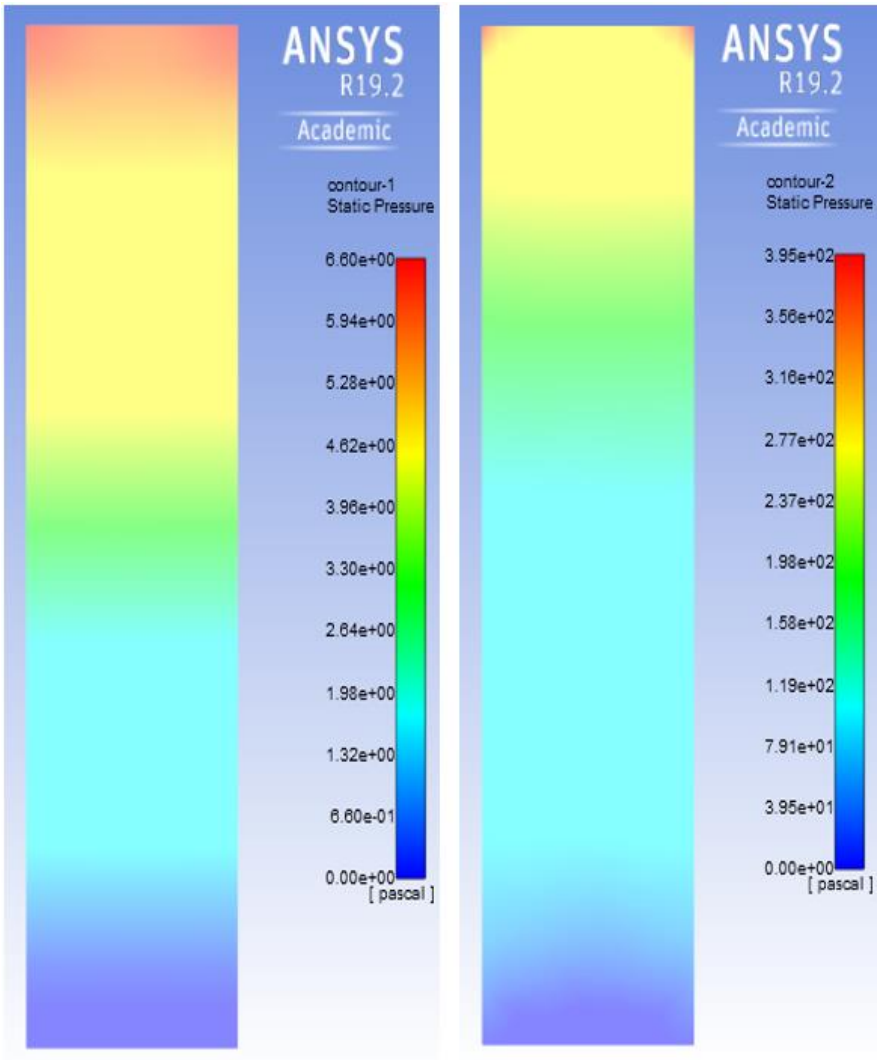

Figure 4.4: Laminar (left) and turbulent (right) water flow - Contours of static pressure

4.4.1.3. Laminar and turbulent gas flow simulations

The pressure drop attained for the straight pipe geometry when simulating the flow of gas through the conduit was about 0.1 Pa as indicated in figure 4.5 below, the color map shows at the entrance region exhibits the highest-pressure coloration which dissipates as the flow goes through the pipe. On the other hand, the pressure drop attained for the straight pipe geometry when simulating the flow of gas through the conduit was about 4.92Pa as indicated below, the color map shows at the entrance region exhibits the highest-pressure coloration which dissipates as the flow goes through the pipe.

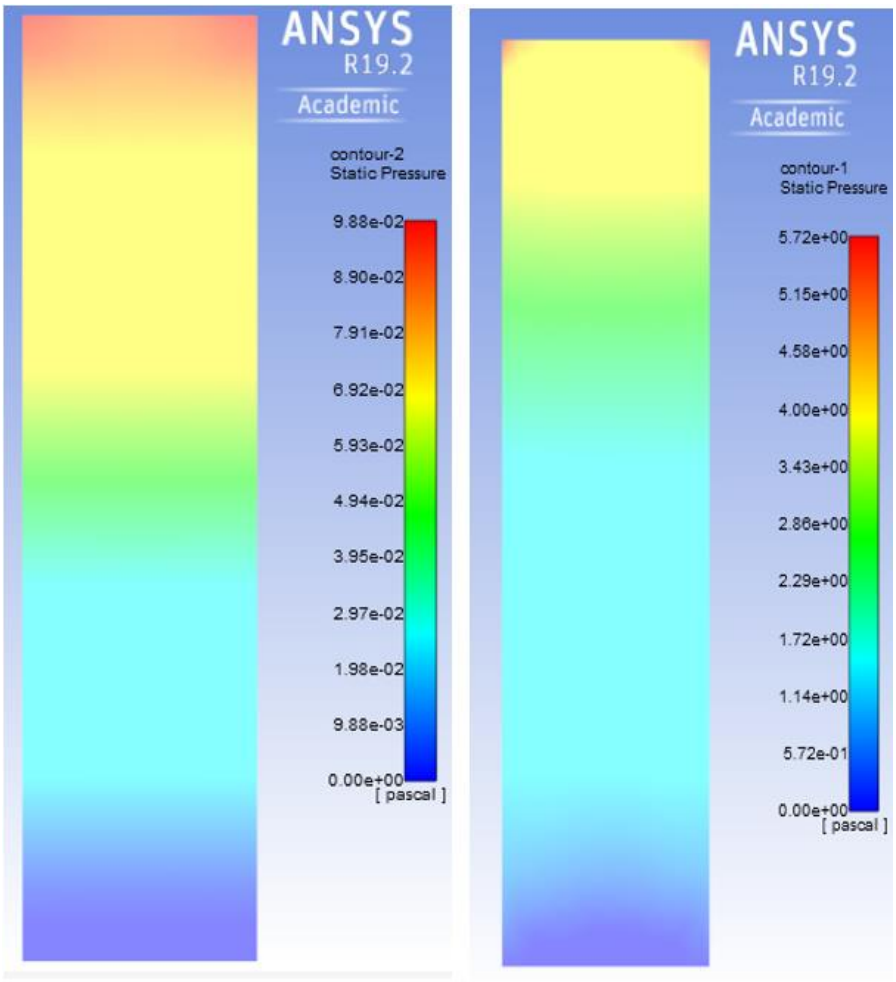

Figure 4.5: Laminar (left) and turbulent (right) gas flow simulations - Contours of static pressure

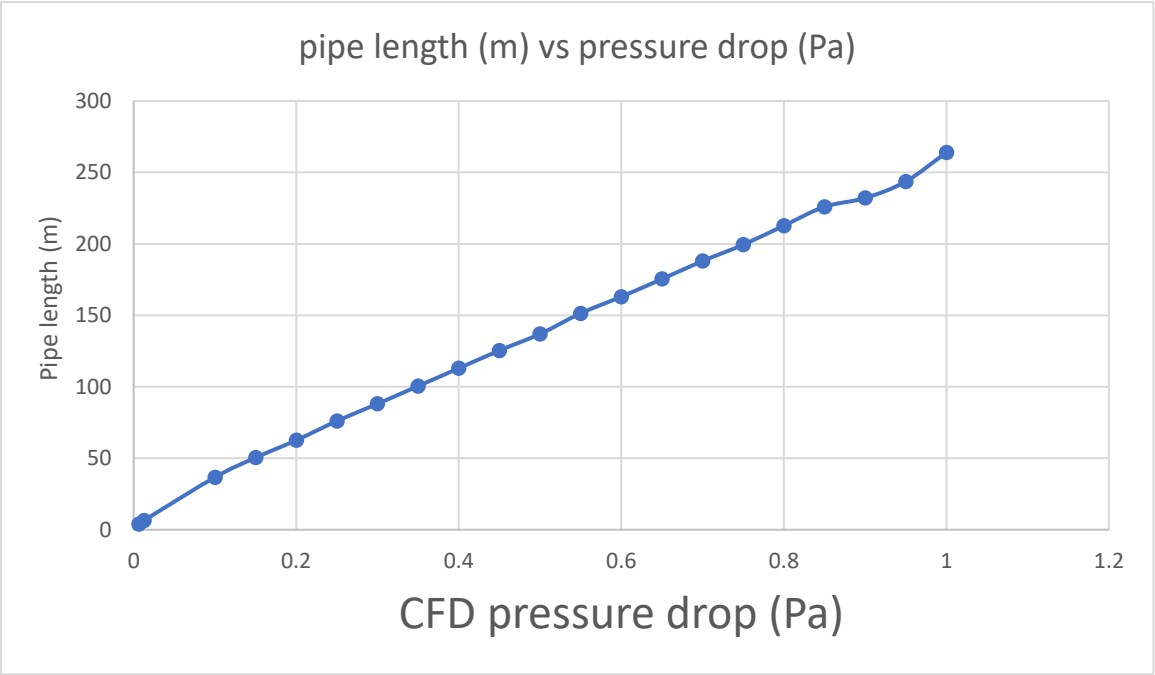

Figure 4.6: increase in pressure drop values with increase in pipe length

It is visible from the graph, that the pressure drops attained, increases in a way which could be said to be linear with an increase in pipe length. This means that, the longer the pipe, the higher the pressure drop which is in accordance to literature. It can now be assumed that to save computational time and resources, a smaller model can be run, and the results forecasted linearly to predict the drop-in pressure for larger scale models.

Table 4-2Table of values (pipe length, mesh elements, CFD, analytical pressure drop and correlation:

Pipe length (m)	pipe diameter (m)	Mesh elements	CFD pressure drop (Pa)	Analytical pressure drop (Pa)	Correlation factor
0.00625	0.0032	2261	3.97717	1.5625	2.545389
0.0125	0.0032	1800	6.4172	3.125	2.053504
0.1	0.0032	15522	36.7025	25	1.4681
0.15	0.0032	24219	50.4299	37.5	1.344797
0.2	0.0032	25870	62.5793	50	1.251586
0.25	0.0032	41832	76.0187	62.5	1.216299
0.3	0.0032	42387	88.0726	75	1.174301
0.35	0.0032	50881	100.497	87.5	1.148537
0.4	0.0032	55720	112.946	100	1.12946
0.45	0.0032	61824	125.396	112.5	1.114631
0.5	0.0032	58705	136.981	125	1.095848
0.55	0.0032	90885	151.378	137.5	1.100931
0.6	0.0032	83580	163.021	150	1.086807
0.65	0.0032	90580	175.381	162.5	1.079268
0.7	0.0032	108654	187.984	175	1.074194
0.75	0.0032	100031	199.423	187.5	1.063589

0.8	0.0032	108256	212.718	200	1.06359
0.85	0.0032	125208	225.973	212.5	1.063402
0.9	0.0032	77013	232.062	225	1.031387
0.95	0.0032	77490	243.607	237.5	1.025714
1	0.0032	151240	263.917	250	1.055668

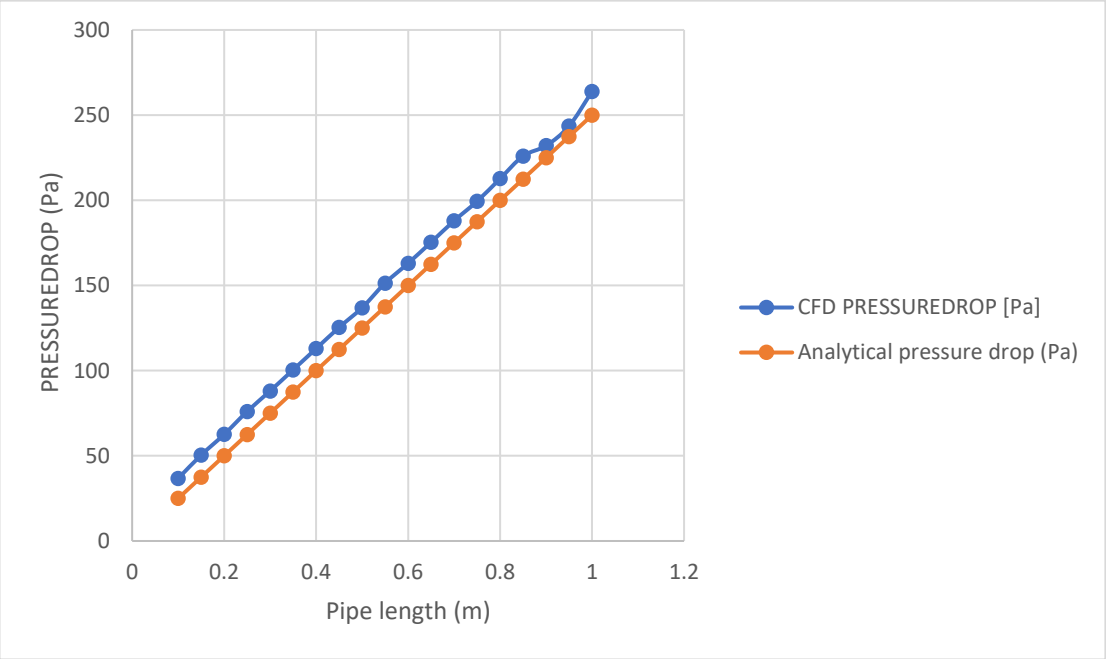

Figure 4.7: Graph comparing CFD and Analytical pressure drop values

4.4.2 Coil Pipe

Flow through straight tubes has been studied extensively over time, while flow through coiled tubing has been studied in significantly less detail. The Autonomous Inflow Control Valve (AICV) makes use of a coil pipe. The coil pipe has an internal diameter of 2r. The coil diameter which is also known as the pitch circle diameter (PCD) can be measured between the centres of the pipes is denoted by $2R_C$. The distance between two adjacent turns of the coil is known as the pitch, H. The curvature

ratio δ is the pipe diameter to coil diameter ratio ($\frac{r}{R_C}$). The ratio of the pitch to a developed length of one turn ($\frac{H}{2\pi R_C}$) is known as the non-dimensional pitch, λ. The flow in coil pipes is characterised by a dean number which is similar to the Reynolds number for flow in other pipes (Jayakumar et al., 2010). The dean number, De is defined as,

$$De = Re\sqrt{\frac{R}{A}} \quad (4.5)$$

Where Re is the Reynolds number, = $\frac{2ru_{av}\rho}{\mu}$ (4.6)

C.M White experimentally determined that the Dean Number can be related to the pressure drop in a tube, by a function of the Dean Number, defined as:

$$f(De) = 0.37De^{0.36} \quad (4.7)$$

When resistance of laminar flow in a straight tube is multiplied, the resulting equation is:

$$\frac{\Delta P}{l} = \frac{32\mu U}{d^2} f(De) = \frac{32\mu U}{d^2} 0.37De^{0.36} \quad (4.8)$$

Therefore, when the value of $\frac{\Delta P d^2}{l\mu U}$ is plotted against$0.37De^{0.36}$, the resulting graph should be a linear relationship with a slope of 32.

Research has shown that very complex flow patterns occur within a coil pipe. The centrifugal forces experienced within the coil are controlled by the coil curvature. These forces are responsible for the development of secondary flow (Darvid, Smith, Merril, & Brain, 1971). The effect of the curvature also means that the fluid flow at the outer side of the pipe moves much faster that the fluid flow in the inner pipe. This difference in flow speed results in secondary flow which changes with the dean number of the flow. During the flow in a coil pipe, the transition from laminar to turbulent flow occurs at a much higher Reynolds number (Critical Reynolds Number, Re_{cr}) than that of a straight pipe. The critical Reynolds number (Re_{cr}) can be estimated

using the correlations developed by Ito (1959), Schmidt (1967), Srinivasan, Nandapurkar, and Holland (1970) or Janssen and Hoogendoorn (1978).

To run numerical simulations on the coil pipe, as shown in figure 4.6, the geometry had to first be created using ANSYS design modeller. The geometry creation process is described below; the sketch of a circle and a path measuring 3.2mm in diameter and 24mm in length respectively are drawn on the XY plane. After proper dimensioning and constraints, the circle is swept along the path with a desired pitch to form the coil geometry. After the geometry has been successfully swept and created, named selection is now done before the next process of mesh generation is carried out. Hydraulic diameter

$$d_h = 3.2mm$$

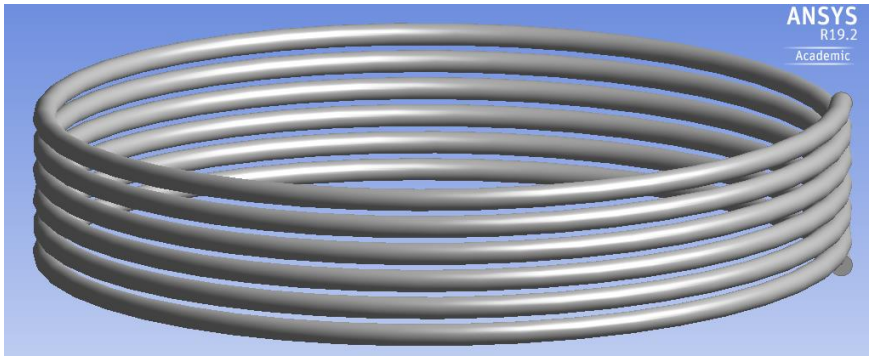

Figure 4.8: Coil pipe geometry

The pressure drop in the coil pipe is calculated analytically from the dean number correlation described in previous sections.

$$\Delta P = \frac{32\mu LV}{d^2}\ x\ 0.37(De^{0.36}) \qquad (4.9)$$

4.4.2.1. Laminar and turbulent oil flow simulations

The pressure drop attained for the coil pipe geometry when simulating the flow of oil through the conduit was about 0.26 MPa as indicated in figure 4.9 below, the color

map shows at the entrance region exhibits the highest-pressure coloration which dissipates as the flow goes through the pipe. On the other hand, The pressure drop attained for the coil pipe geometry when simulating the flow of oil through the conduit was about 13.62 MPa as indicated below, the color map shows at the entrance region exhibits the highest-pressure coloration which dissipates as the flow goes through the pipe

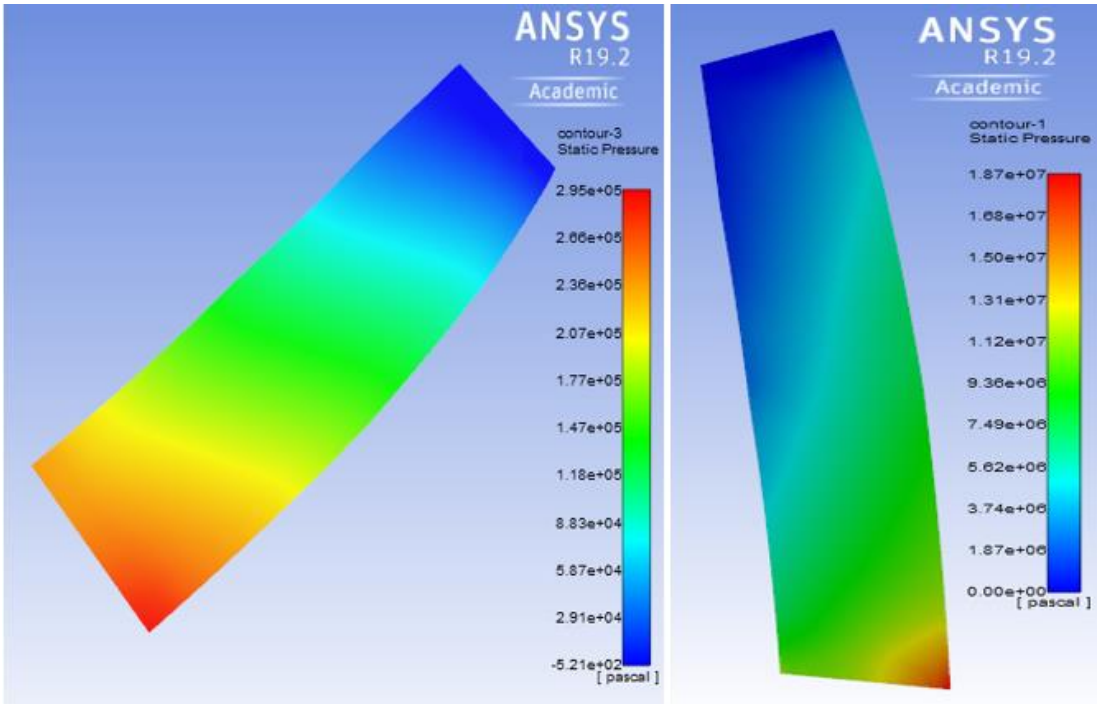

Figure 4.9: Laminar (left) and turbulent (right) oil flow - Contours of static pressure

4.4.2.2. Laminar and turbulent water flow simulations

The pressure drop attained for the coil pipe geometry when simulating the flow of oil through the conduit was about 13.62 MPa as indicated in figure 4.10 below, the color map shows at the entrance region exhibits the highest-pressure coloration which dissipates as the flow goes through the pipe. On the other hand, the pressure drop attained for the coil pipe geometry when simulating the flow of water through the conduit was about 6.54 Pa as indicated below, the color map shows at the entrance

region exhibits the highest-pressure coloration which dissipates as the flow goes through the pipe

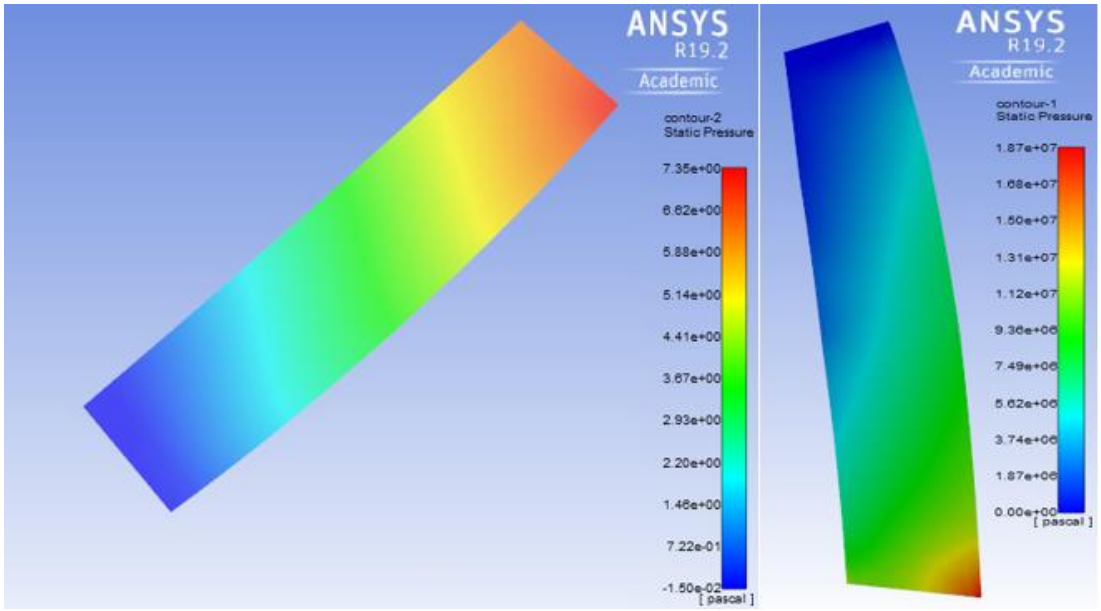

Figure 4.10: Laminar (left) and turbulent (right) water flow - Contours of static pressure

4.4.2.3. Laminar and turbulent gas flow simulations

The pressure drop attained for the coil pipe geometry when simulating the flow of gas through the conduit was about 0.09 Pa as indicated in figure 4.11 below, the color map shows at the entrance region exhibits the highest-pressure coloration which dissipates as the flow goes through the pipe. On the other hand, the pressure drop attained for the coil pipe geometry when simulating the flow of gas through the conduit was about 4.95 Pa as indicated below, the color map shows at the entrance region exhibits the highest-pressure coloration which dissipates as the flow goes through the pipe

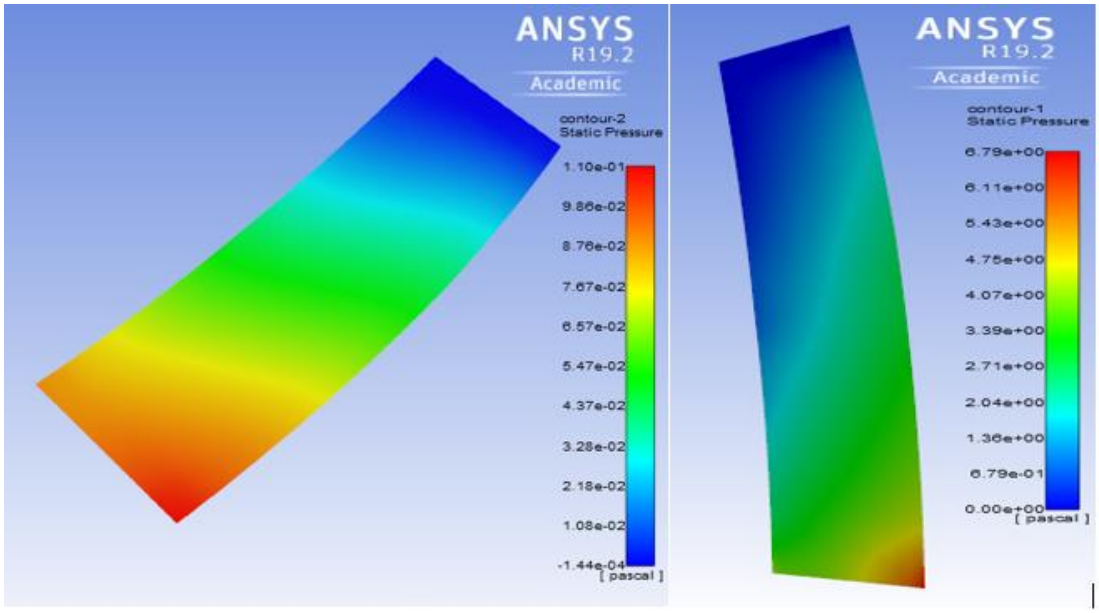

Figure 4.11: Laminar (left) and turbulent (right) gas flow - Contours of static pressure

4.4.3 Elliptical straight pipe

A variation of the straight circular pipe is the straight elliptical pipe. An important fact which was considered before creating the geometry for the ellipse was the relatability of results. This meant that both designs had to have the same properties such as the surface area to compare the results obtained after numerical simulations.

The surface area of a circle is calculated using the formula, $A = \pi r^2$ (4.10)

While the surface area of an ellipse is calculated using the formula,

$A = \pi \text{ x } r_a \text{ x } r_b$ (4.11)

$$r_a = 1.3\text{mm}$$

$$r_b = 1.96\text{mm}$$

The same principle is applied to the elliptical pipe; the sketch is drawn on the XY plane and swept along the path of a desired length to create the geometry.

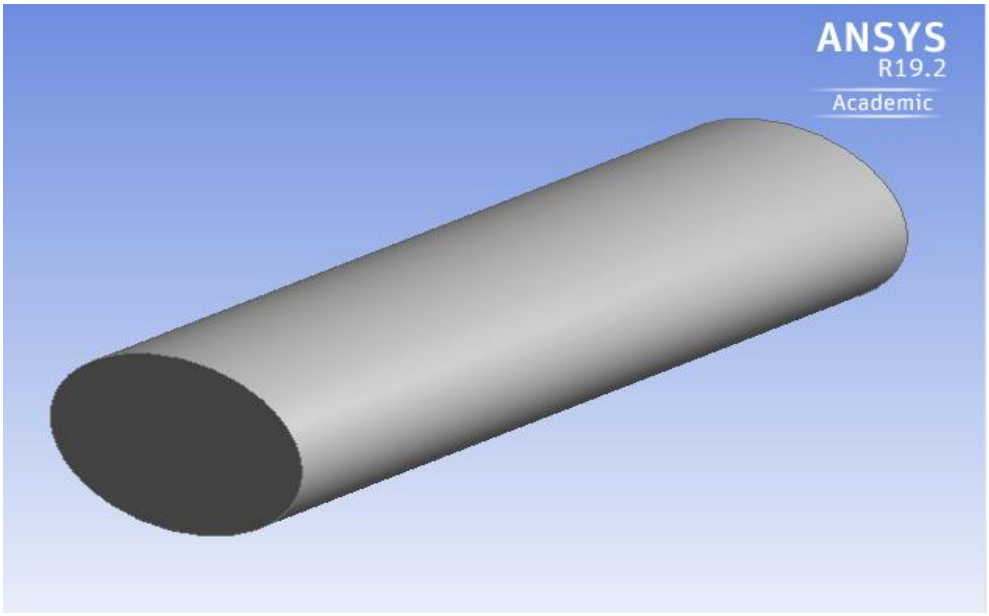

Figure 4.12: Elliptical Straight pipe geometry

4.4.3.1. Laminar and turbulent oil flow simulations

The pressure drop attained for the elliptical pipe geometry when simulating the flow of oil through the conduit was about 0.34 MPa as indicated in figure 4.13 below, the color map shows at the entrance region exhibits the highest-pressure coloration which dissipates as the flow goes through the pipe. On the other hand, the pressure drop attained for the elliptical pipe geometry when simulating the flow of oil through the conduit was about 14.59 MPa as indicated below, the color map shows at the entrance region exhibits the highest-pressure coloration which dissipates as the flow goes through the pipe.

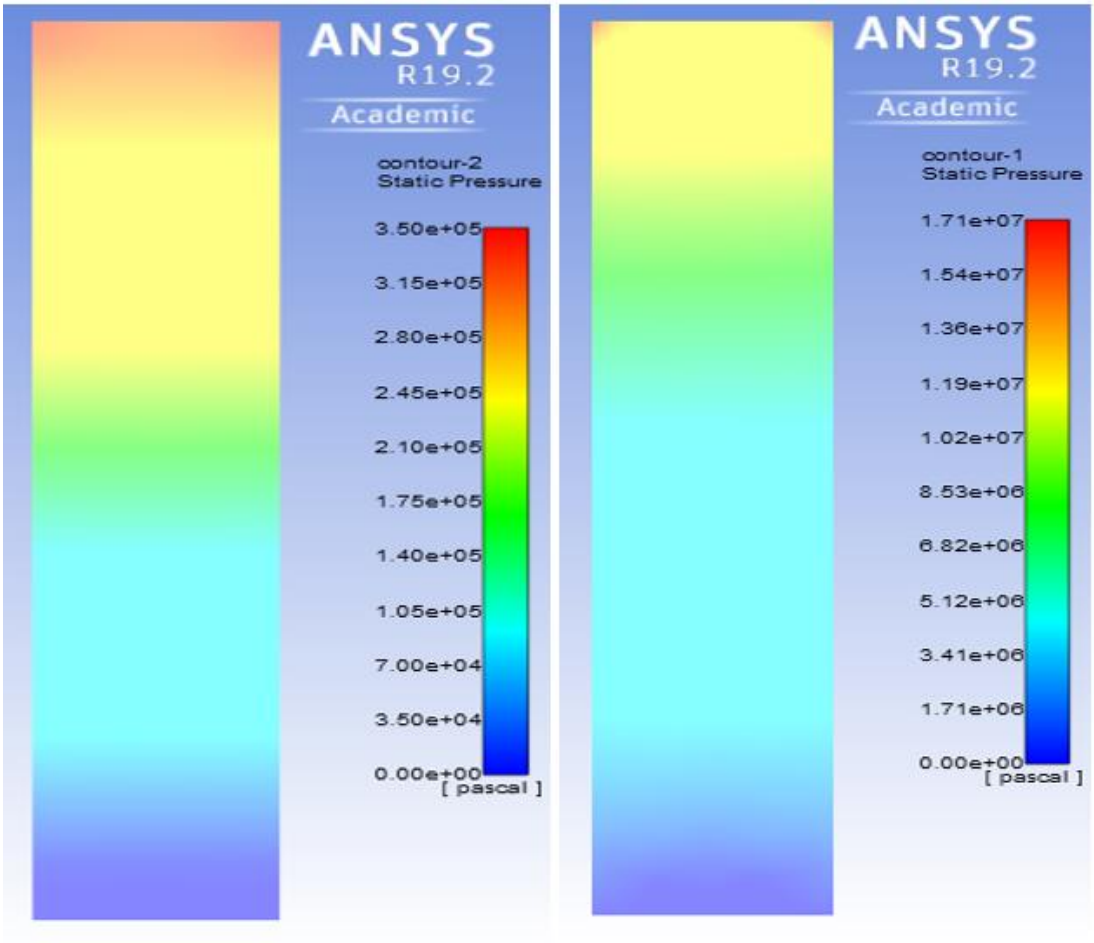

Figure 4.13: Laminar (left) and turbulent (right) oil flow - Contours of static pressure

4.4.3.2. Laminar and turbulent water flow simulations

The pressure drop attained for the elliptical pipe geometry when simulating the flow of water through the conduit was about 8.35 Pa as indicated in figure 4.14 below, the color map shows at the entrance region exhibits the highest-pressure coloration which dissipates as the flow goes through the pipe. On the other hand, the pressure drop attained for the elliptical pipe geometry when simulating the flow of water through the conduit was about 367.62 Pa as indicated below, the color map shows at the entrance region exhibits the highest-pressure coloration which dissipates as the flow goes through the pipe.

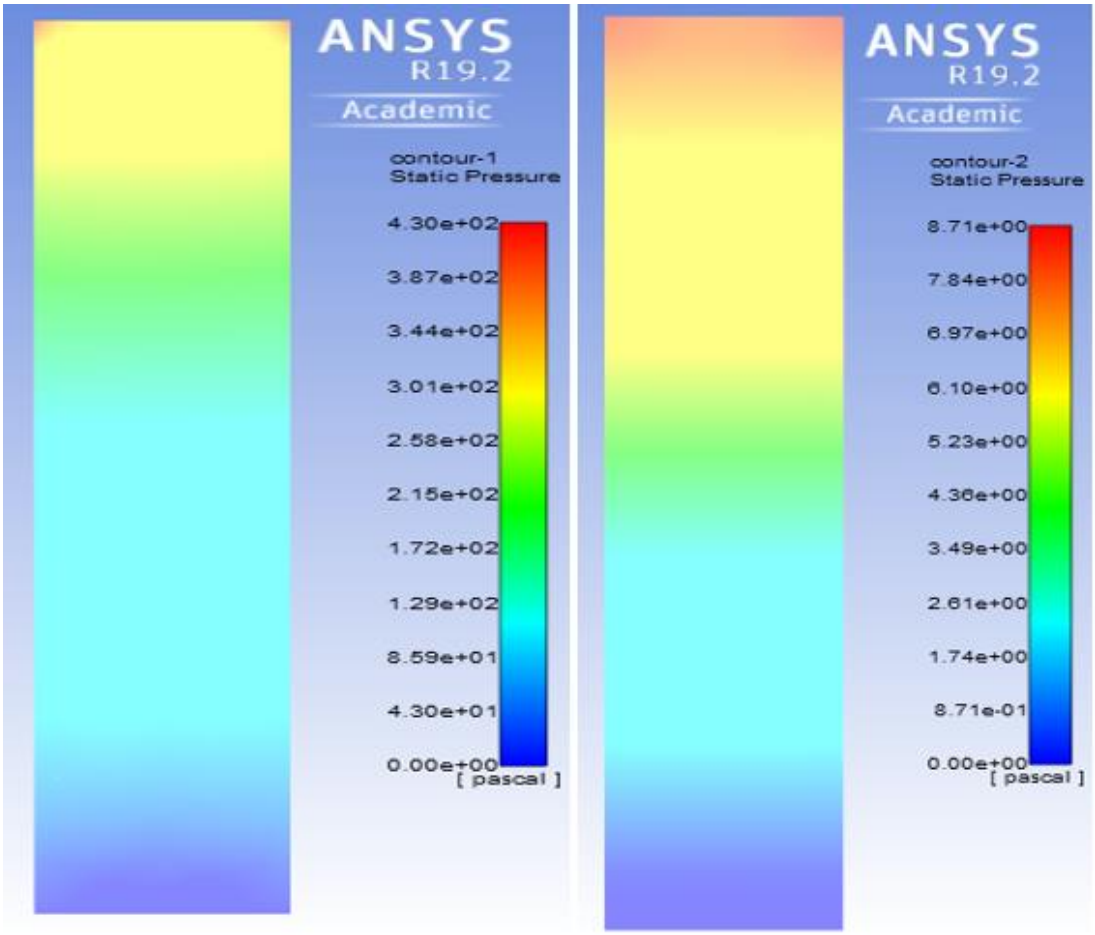

Figure 4.14: Laminar (left) and turbulent (right) water flow - Contours of static pressure

4.4.3.3. Laminar and turbulent gas flow simulations

The pressure drop attained for the elliptical pipe geometry when simulating the flow of gas through the conduit was about 0.16 Pa as indicated in figure 4.15 below, the color map shows at the entrance region exhibits the highest-pressure coloration which dissipates as the flow goes through the pipe. On the other hand, the pressure drop attained for the elliptical pipe geometry when simulating the flow of gas through the conduit was about 5.29 Pa as indicated below, the color map shows at the entrance region exhibits the highest-pressure coloration which dissipates as the flow goes through the pipe

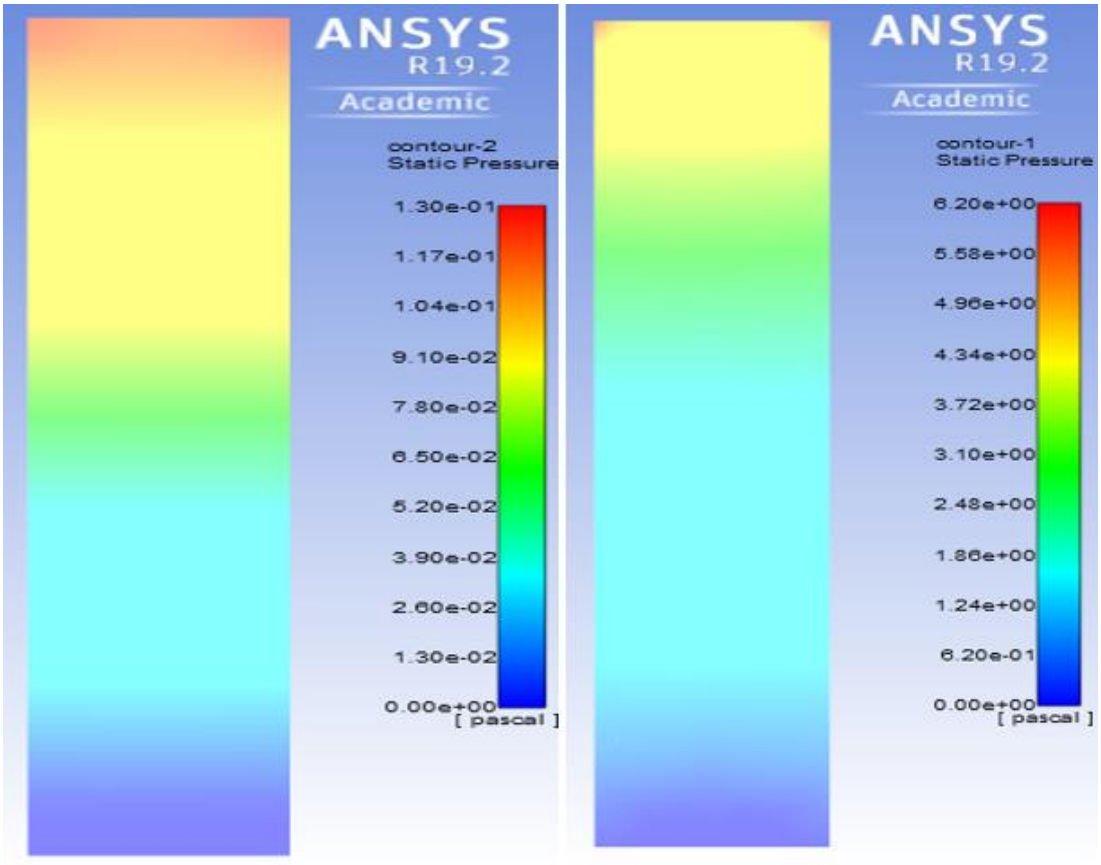

Figure 4.15: Laminar (left) and turbulent (right) gas flow - Contours of static pressure

4.4.4 Straight Square Pipe

Another variation of the straight circular pipe is the straight square pipe, giving more surface area and more turbulence. An important fact was considered before creating the geometry for the square straight pipe, the relatability of results. This meant that both designs had to have the same properties such as the surface area to compare the results obtained after numerical simulations.

The surface area of a circle is calculated using the formula, $A = \pi r^2$ (4.12)

While the surface area of a square is calculated using the formula, $A = L^2$ (4.13)

$$\mathrm{L} = 2.84mm$$

The same principle is applied to the square pipe; the sketch is drawn on the XY plane and swept along the path of a desired length to create the geometry. Manufacturability of the design was also taken into consideration although with advances in the area

such as 3D printing and additive manufacturing, any design is pretty much achievable. This design however features fillets measuring 0.5mm in radii on all four edges as opposed to sharp edges to cater or ensure manufacturability.

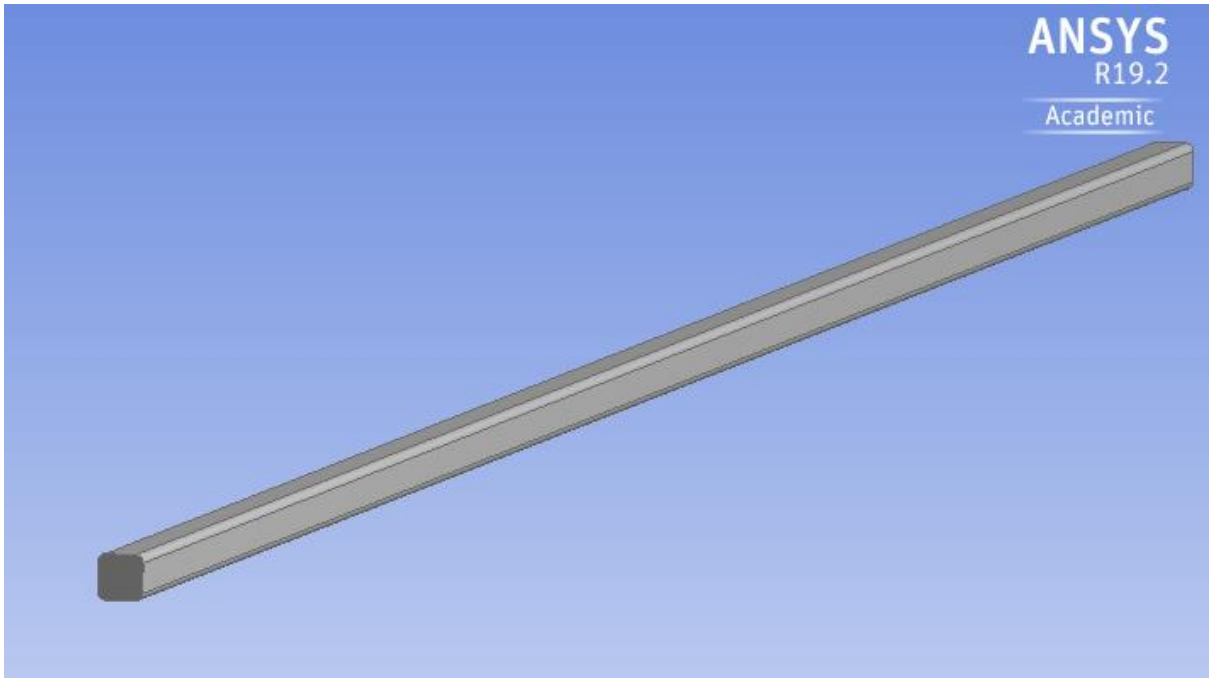

Figure 4.16: Square pipe geometry

4.4.4.1. Laminar and turbulent oil flow simulations

The pressure drop attained for the straight square pipe geometry when simulating the flow of oil through the conduit was about 0.428 MPa as indicated in figure 4.17 below, the color map shows at the entrance region exhibits the highest-pressure coloration which dissipates as the flow goes through the pipe. . On the other hand, the pressure drop attained for the straight square pipe geometry when simulating the flow of oil through the conduit was about 14.84 MPa as indicated below, the color map shows at the entrance region exhibits the highest-pressure coloration which dissipates as the flow goes through the pipe

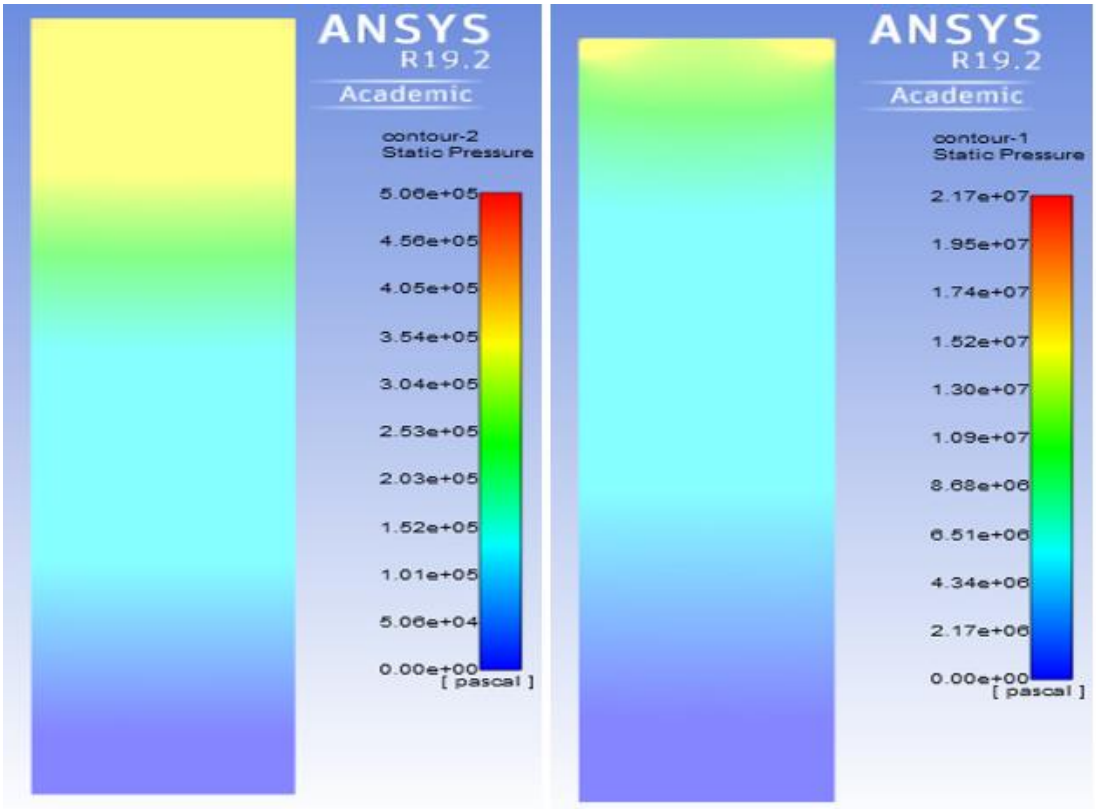

Figure 4.17: Laminar (left) and turbulent (right) oil flow - Contours of static pressure

4.4.4.2. Laminar and turbulent water flow simulations

The pressure drop attained for the straight square pipe geometry when simulating the flow of water through the conduit was about 10.73 Pa as indicated in figure 4.18 below, the color map shows at the entrance region exhibits the highest-pressure coloration which dissipates as the flow goes through the pipe. On the other hand, the pressure drop attained for the straight square pipe geometry when simulating the flow of water through the conduit was about 374 Pa as indicated below, the color map shows at the entrance region exhibits the highest-pressure coloration which dissipates as the flow goes through the pipe

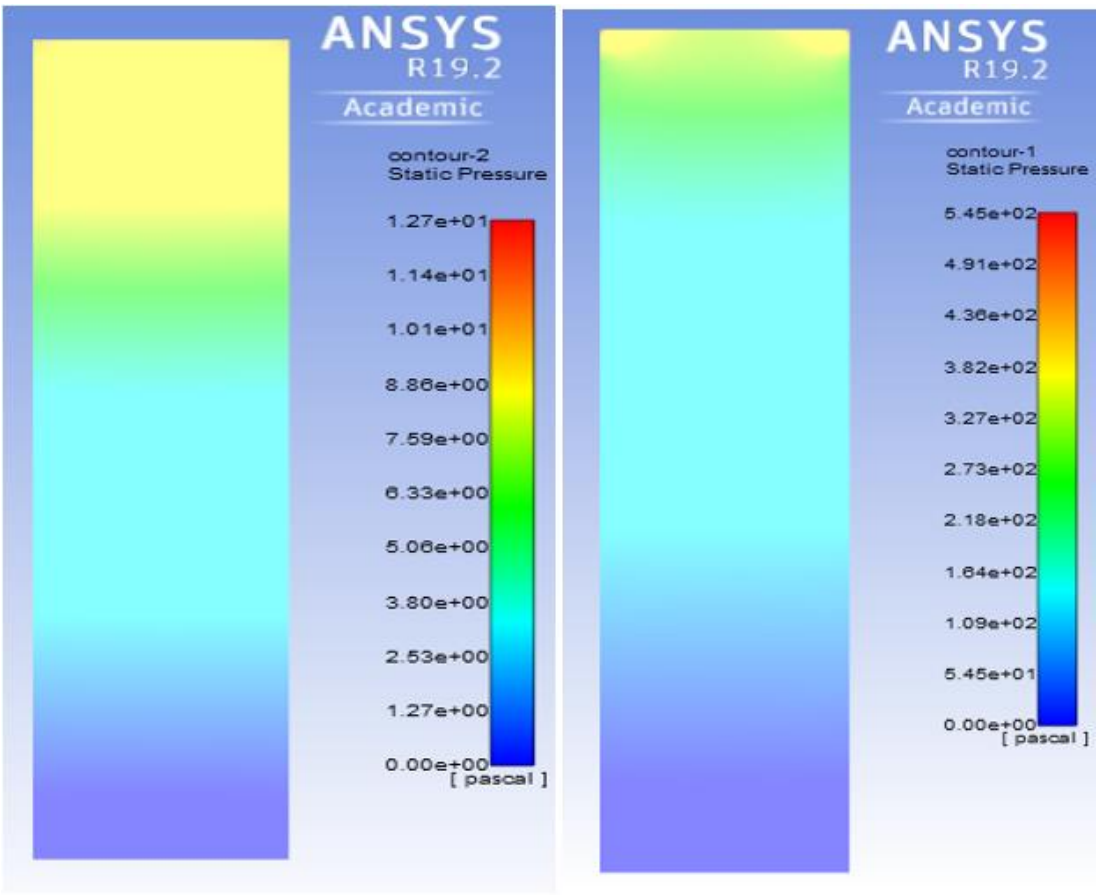

Figure 4.18: Laminar (left) and turbulent (right) water flow - Contours of static pressure

4.4.4.3. Laminar and turbulent gas flow simulations

The pressure drop attained for the straight square pipe geometry when simulating the flow of gas through the conduit was about 0.16 Pa as indicated in figure 4.19 below, the color map shows at the entrance region exhibits the highest-pressure coloration which dissipates as the flow goes through the pipe. On the other hand, the pressure drop attained for the straight square pipe geometry when simulating the flow of gas through the conduit was about 5.39 Pa as indicated below, the color map shows at the entrance region exhibits the highest-pressure coloration which dissipates as the flow goes through the pipe

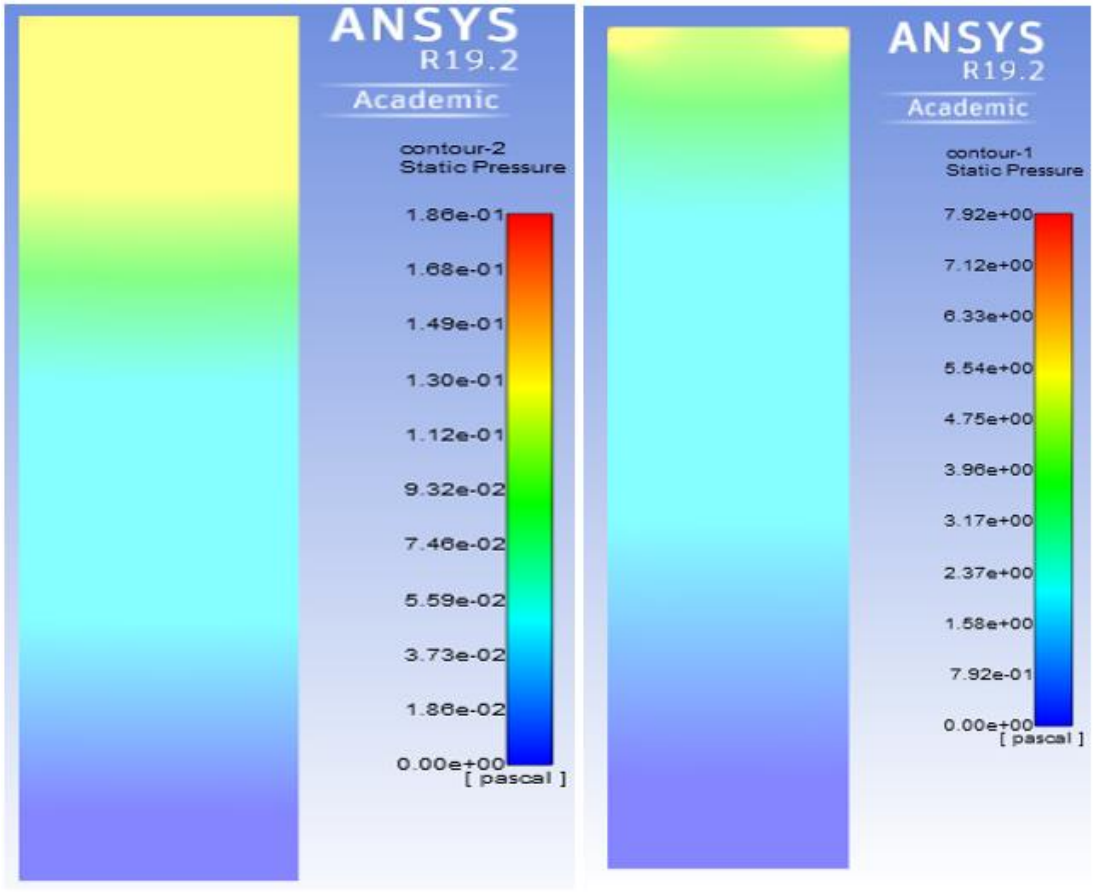

Figure 4.19: Laminar (left) and turbulent (right) gas flow - Contours of static pressure

4.4.5 Square coil

A square coil pipe is a variation of the coil pipe using a quadrilateral shape. To run the same simulation around all geometry cases, it also had to be ensured that they all had same dimensions. For the square coil, the surface area of the square had to be the same with the circle and this was achieved by equating both surfaces areas. Therefore, the length of the square that would give same surface area as the circle is 2.835mm.

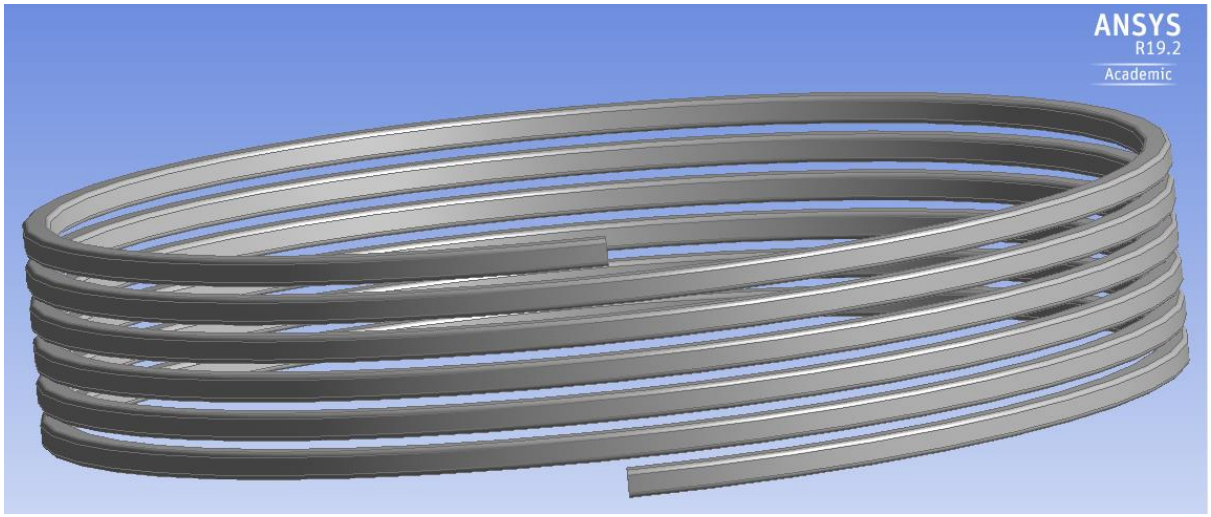

Figure 4.20: Square coil geometry

4.4.5.1. Laminar and turbulent oil flow simulations

The pressure drop attained for the square coil geometry when simulating the flow of oil through the conduit was about 0.43 MPa as indicated in figure 4.21 below, the color map shows at the entrance region exhibits the highest-pressure coloration which dissipates as the flow goes through the pipe. On the other hand, the pressure drop attained for the straight square pipe geometry when simulating the flow of oil through the conduit was about 14.86 MPa as indicated below, the color map shows at the entrance region exhibits the highest-pressure coloration which dissipates as the flow goes through the pipe

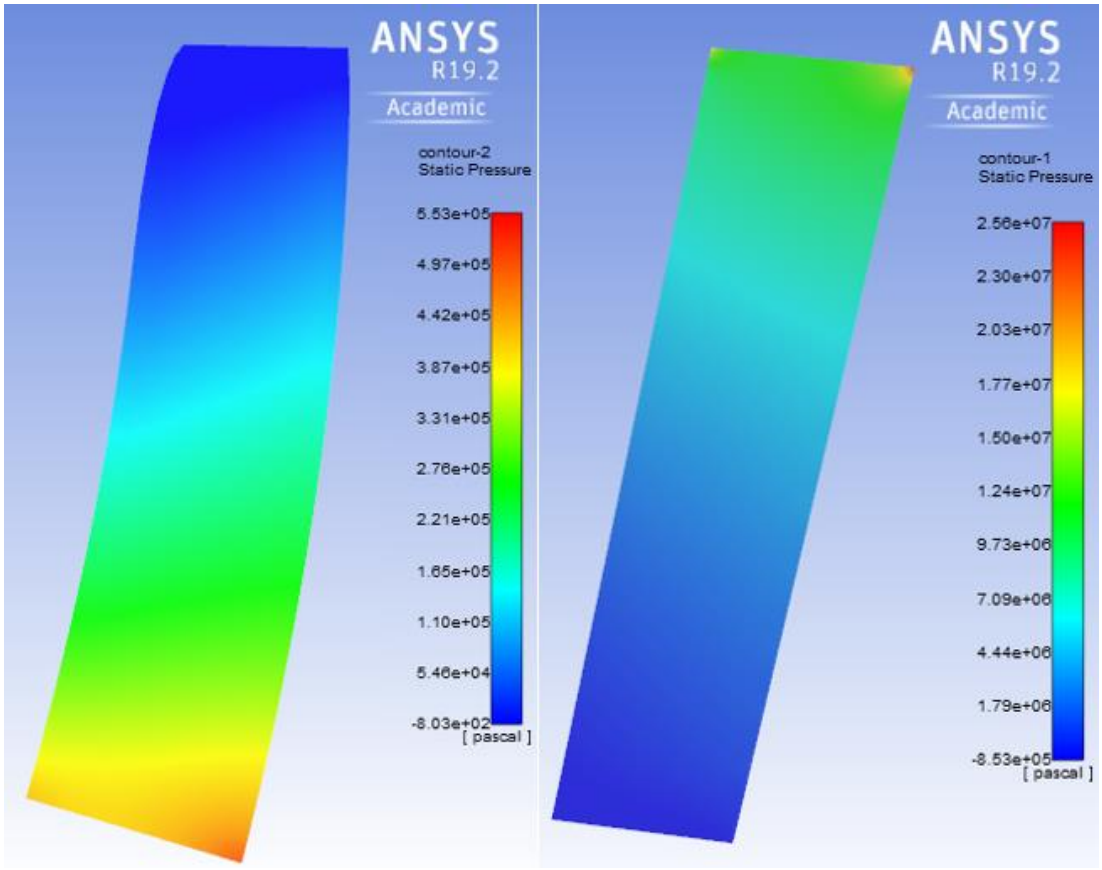

Figure 4.21: Laminar (left) and turbulent (right) oil flow - Contours of static pressure

4.4.5.2. Laminar and turbulent water flow simulations

The pressure drop attained for the straight square pipe geometry when simulating the flow of water through the conduit was about 10.85 Pa as indicated in figure 4.22 below, the color map shows at the entrance region exhibits the highest-pressure coloration which dissipates as the flow goes through the pipe. On the other hand, the pressure drop attained for the straight square pipe geometry when simulating the flow of water through the conduit was about 374.32 Pa as indicated below, the color map shows at the entrance region exhibits the highest-pressure coloration which dissipates as the flow goes through the pipe

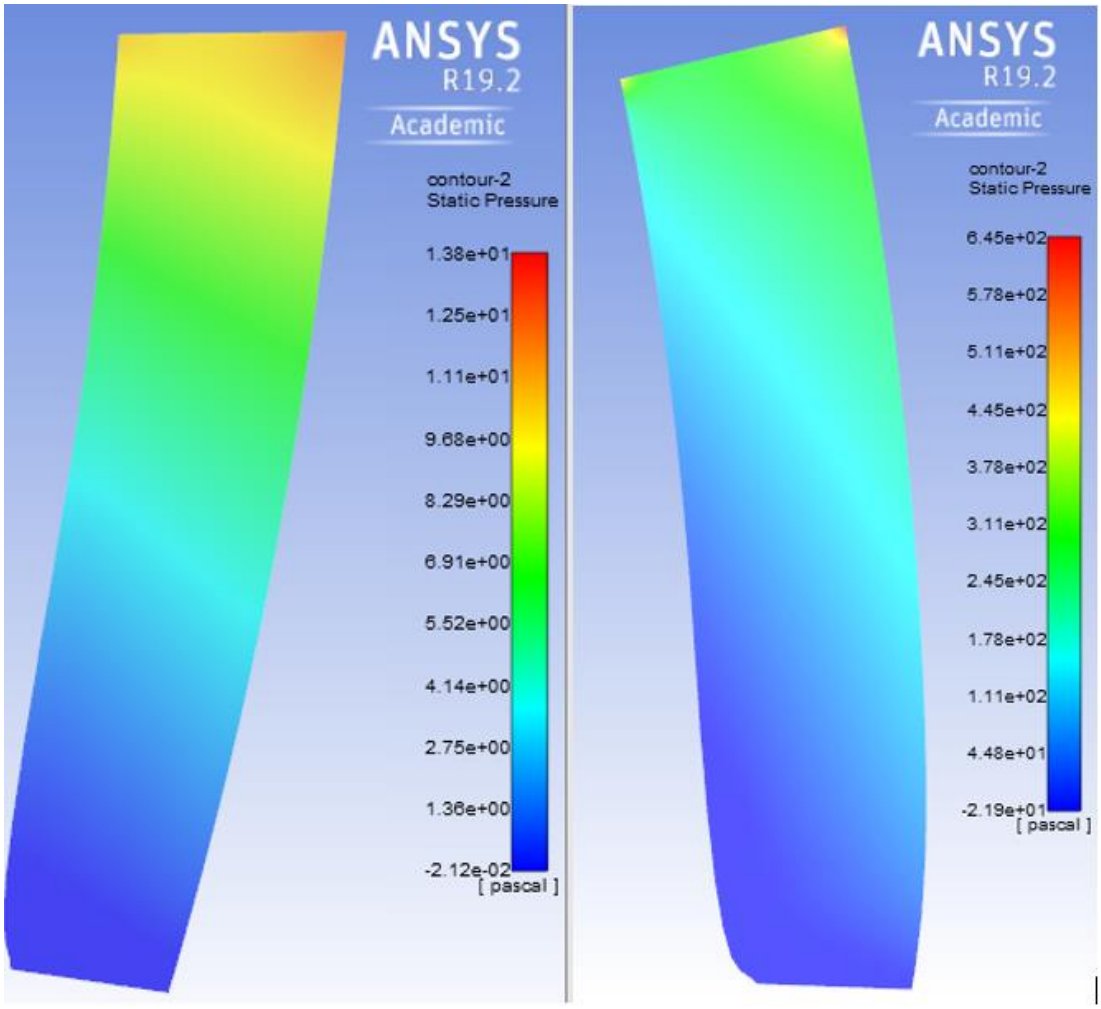

Figure 4.22: Laminar (left) and turbulent (right) water flow - Contours of static pressure

4.4.5.3. Laminar and turbulent gas flow simulations

The pressure drop attained for the straight square pipe geometry when simulating the flow of gas through the conduit was about 0.2 Pa as indicated in figure 4.23 below, the color map shows at the entrance region exhibits the highest-pressure coloration which dissipates as the flow goes through the pipe. On the other hand, the pressure drop attained for the straight square pipe geometry when simulating the flow of gas through the conduit was about 5.4 Pa as indicated below, the color map shows at the entrance region exhibits the highest-pressure coloration which dissipates as the flow goes through the pipe

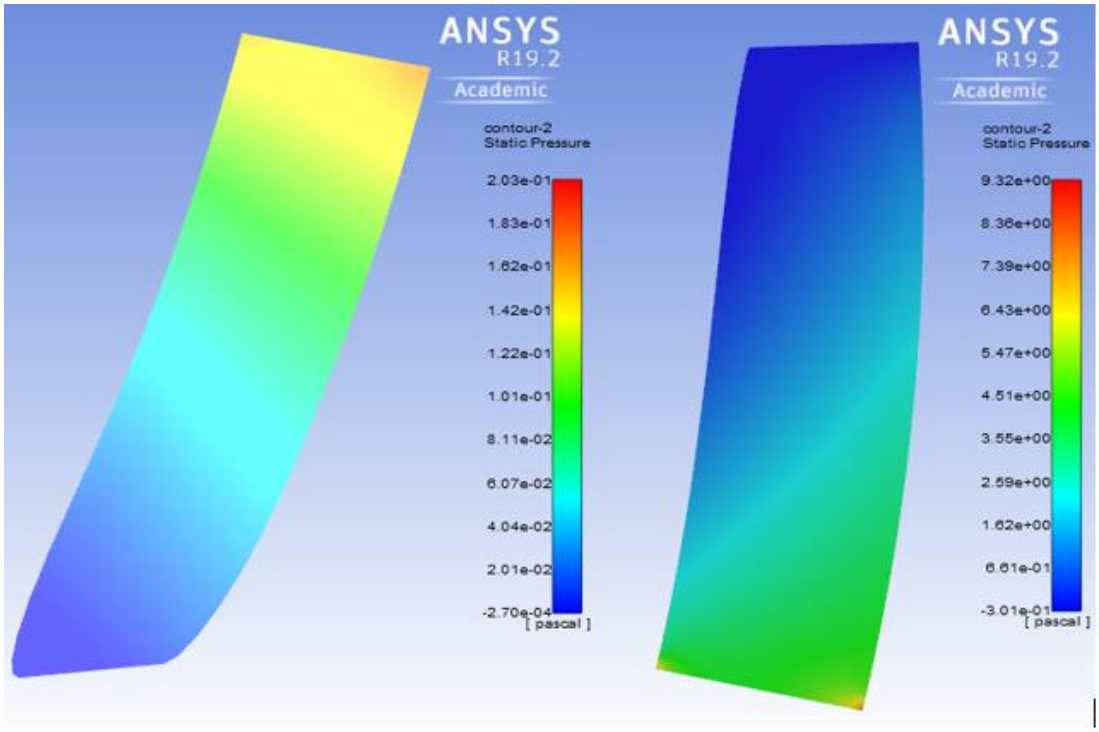

Figure 4.23: Laminar (left) and turbulent (right) gas flow - Contours of static pressure

4.4.6 Slinky Coil Pipe

A slinky coil pipe, which as the name implies, assumes the shape of a slinky. It looks to still maintain the shape, size and robustness of the original design but to achieve design optimization, the geometry is created using the diameter of the original coil as the design path and then a circle sketch of the same diameter as the coil, 3.2mm, is swept round the design path to create the desired geometry. The findings and results achieved will be discussed in the following chapter.

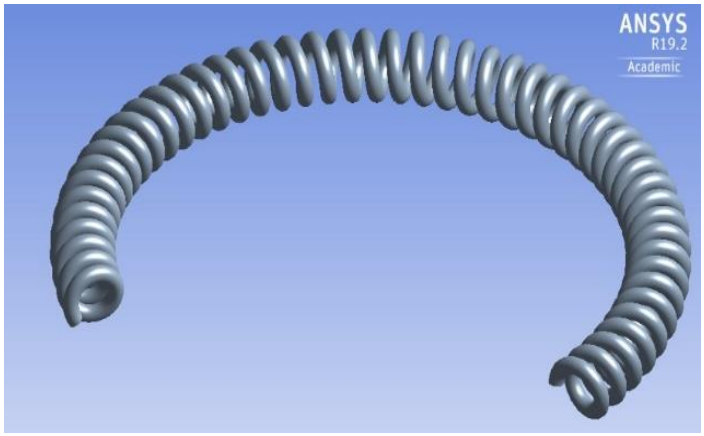

Figure 4.24: Optimised slinky coil geometry

4.4.6.1. Laminar and turbulent oil flow simulations

The pressure drop attained for the straight square pipe geometry when simulating the flow of oil through the conduit was about 2.2 MPa as indicated in figure 4.25 below, the color map shows at the entrance region exhibits the highest-pressure coloration which dissipates as the flow goes through the pipe. On the other hand, the pressure drop attained for the straight square pipe geometry when simulating the flow of oil through the conduit was about 117.55 MPa as indicated below, the color map shows at the entrance region exhibits the highest-pressure coloration which dissipates as the flow goes through the pipe

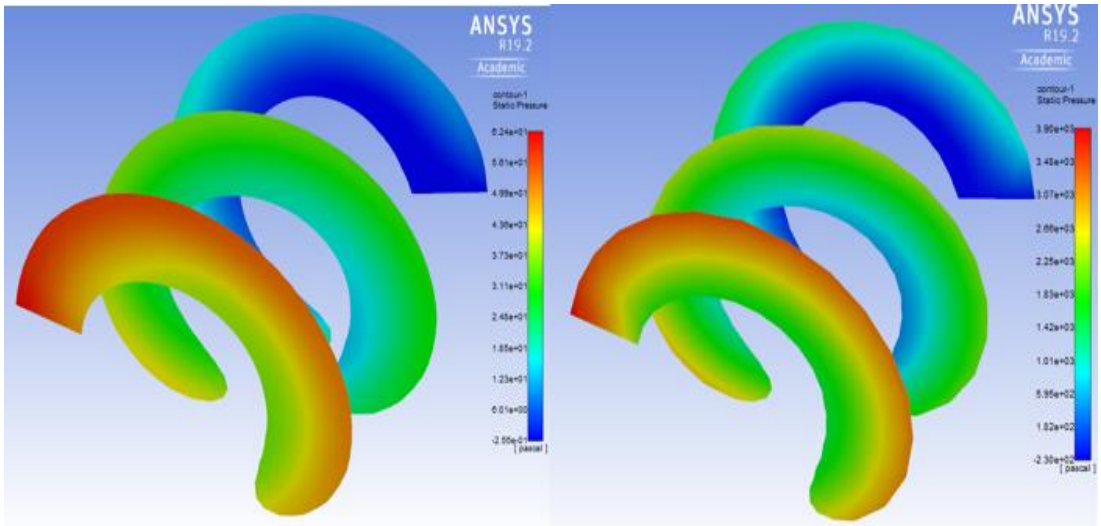

Figure 4.25: Laminar (left) and turbulent (right) oil flow - Contours of static pressure

4.4.6.2. Laminar and turbulent water flow simulations

The pressure drop attained for the straight square pipe geometry when simulating the flow of water through the conduit was about 55.15 Pa as indicated in figure 4.26 below, the color map shows at the entrance region exhibits the highest-pressure coloration which dissipates as the flow goes through the pipe. On the other hand, the pressure drop attained for the straight square pipe geometry when simulating the flow of water through the conduit was about 2956 Pa as indicated below, the color map shows at the entrance region exhibits the highest-pressure coloration which dissipates as the flow goes through the pipe

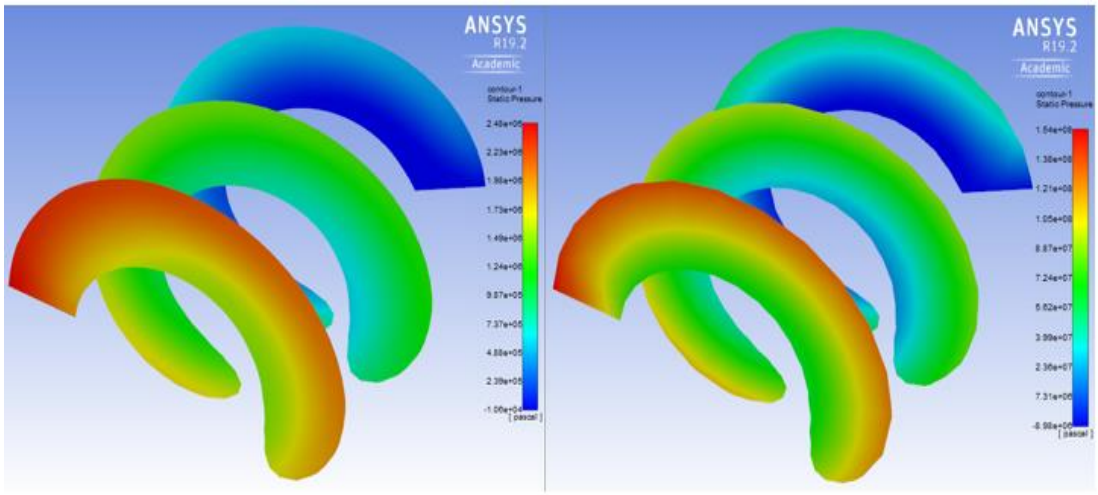

Figure 4.26: Laminar (left) and turbulent (right) water flow - Contours of static pressure

4.4.6.3. Laminar and turbulent gas flow simulations

The pressure drop attained for the straight square pipe geometry when simulating the flow of gas through the conduit was about 0.8 Pa as indicated in figure 4.27 below, the color map shows at the entrance region exhibits the highest-pressure coloration which dissipates as the flow goes through the pipe. On the other hand, the pressure drop attained for the straight square pipe geometry when simulating the flow of gas through the conduit was about 42.82 Pa as indicated below, the color map shows at the entrance region exhibits the highest-pressure coloration which dissipates as the flow goes through the pipe

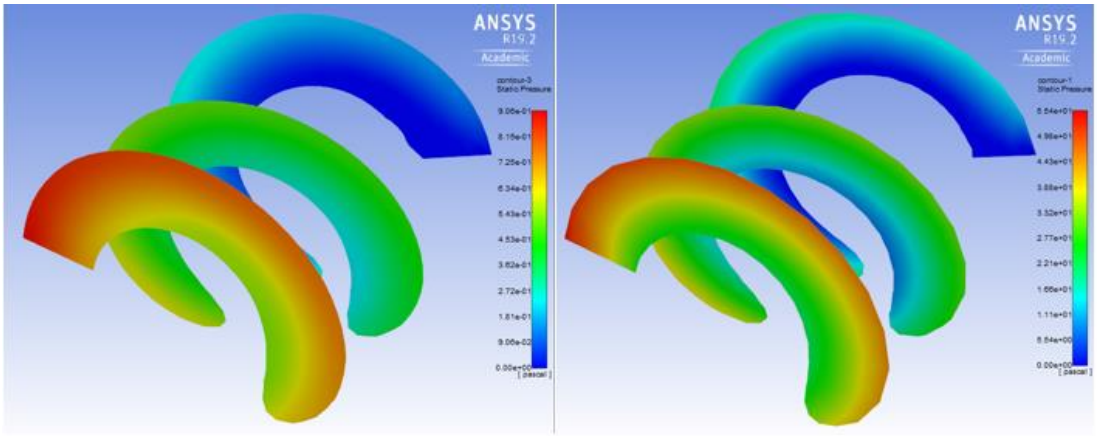

Figure 4.27: Laminar (left) and turbulent (right) gas flow - Contours of static pressure

4.4.7 Square slinky coil pipe

Applying the square fluid flow geometry to the slinky coil pipe created the square slinky coil pipe.

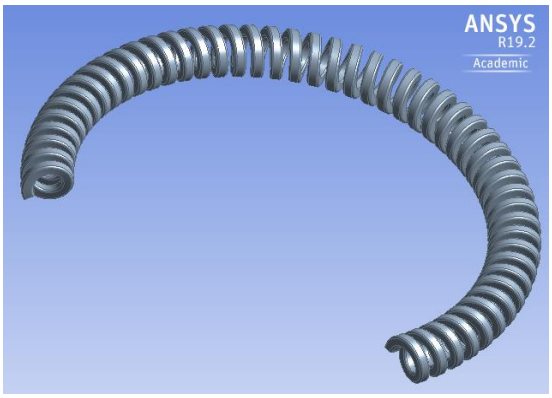

Figure 4.28: Square slinky coil pipe

4.4.6.1. Laminar and turbulent oil flow simulations

The pressure drop attained for the straight square pipe geometry when simulating the flow of oil through the conduit was about 2.8 MPa as indicated in figure 4.29 below, the color map shows at the entrance region exhibits the highest-pressure coloration which dissipates as the flow goes through the pipe. On the other hand, the pressure drop attained for the straight square pipe geometry when simulating the flow of oil through the conduit was about 119.4 MPa as indicated below, the color map shows at the entrance region exhibits the highest-pressure coloration which dissipates as the flow goes through the pipe

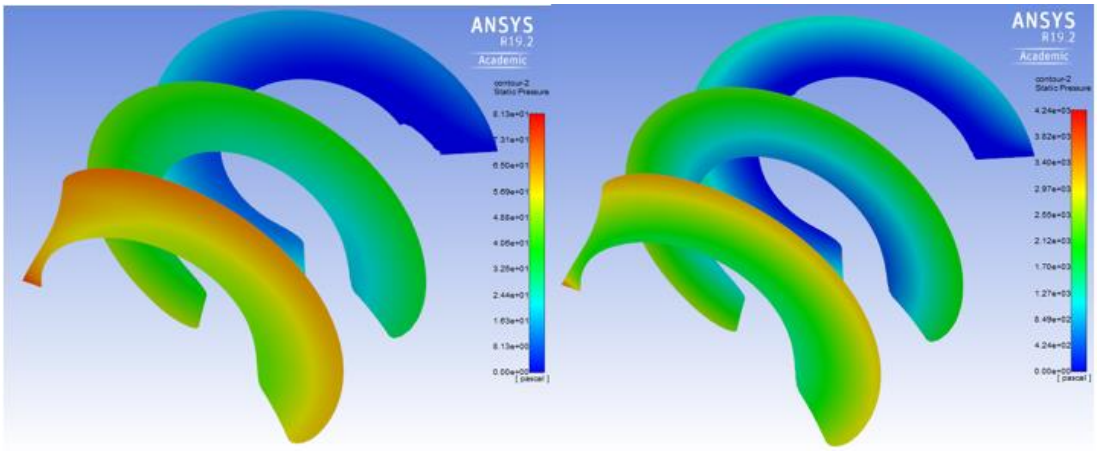

Figure 4.29: Laminar (left) and turbulent (right) oil flow - Contours of static pressure

4.4.6.2. Laminar and turbulent water flow simulations

The pressure drop attained for the straight square pipe geometry when simulating the flow of water through the conduit was about 69.7 Pa as indicated in figure 4.30 below, the color map shows at the entrance region exhibits the highest-pressure coloration which dissipates as the flow goes through the pipe. On the other hand, the pressure drop attained for the straight square pipe geometry when simulating the flow of water through the conduit was about 3021 Pa as indicated below, the color map shows at the entrance region exhibits the highest-pressure coloration which dissipates as the flow goes through the pipe

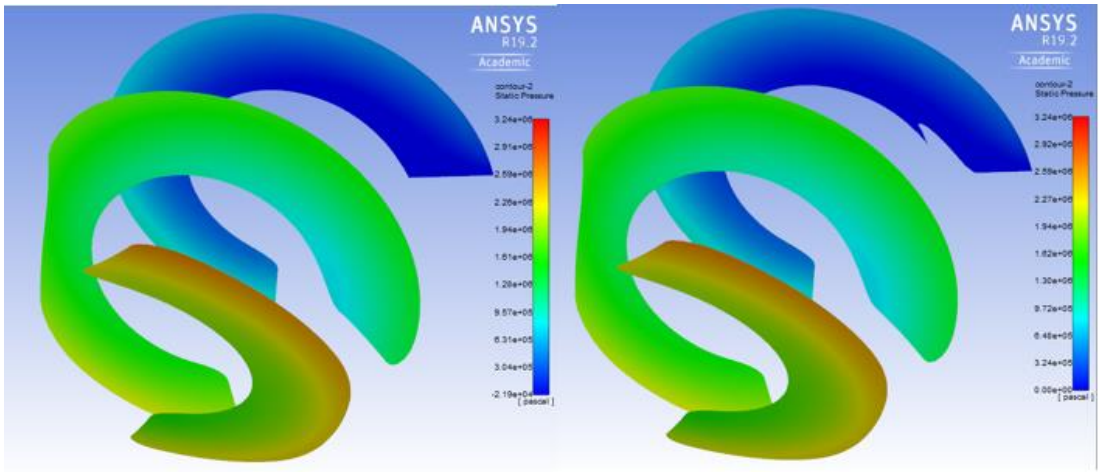

Figure 4.30: Laminar (left) and turbulent (right) water flow - Contours of static pressure

4.4.6.3. Laminar and turbulent gas flow simulations

The pressure drop attained for the straight square pipe geometry when simulating the flow of gas through the conduit was about 1.02 Pa as indicated in figure 4.31 below, the color map shows at the entrance region exhibits the highest-pressure coloration which dissipates as the flow goes through the pipe. On the other hand, the pressure drop attained for the straight square pipe geometry when simulating the flow of gas through the conduit was about 43.03 Pa as indicated below, the color map shows at the entrance region exhibits the highest-pressure coloration which dissipates as the flow goes through the pipe.

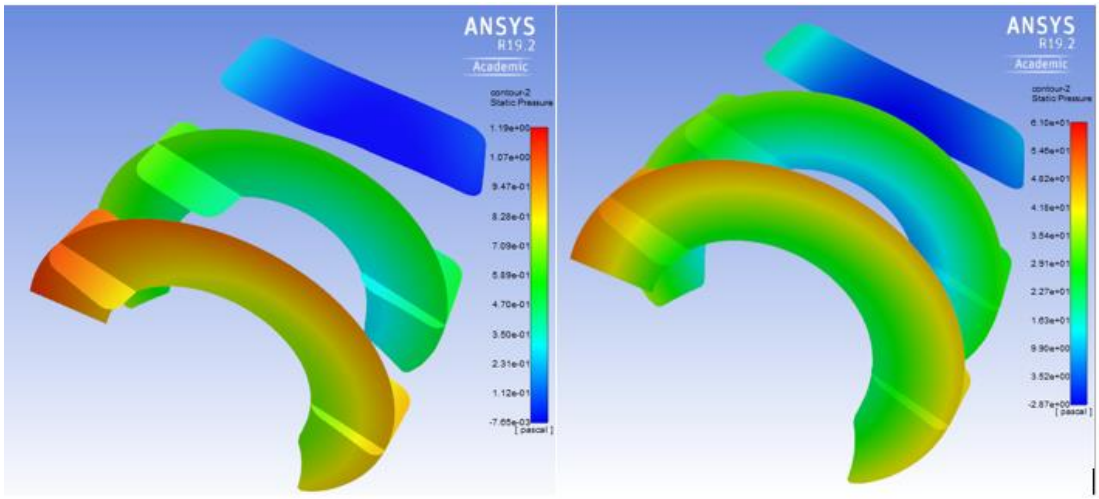

Figure 4.31: Laminar (left) and turbulent (right) gas flow - Contours of static pressure

4.4.8 Square swirl coil pipe

This has been identified as the optimal geometry for pressure drop and therefore shows the simulation results for pressure drop values, contours of static pressure, velocity magnitude and velocity vectors colored by velocity.

This design is a variation of the square coil pipe using a quadrilateral shape. To run the same simulation around all geometry cases, it also had to be ensured that they all had same dimensions. For the square swirl coil, the surface area of the square had to be the same with the circle and this was achieved by equating both surfaces areas. Therefore, the length of the square that would give same surface area as the

circle is 2.835mm. The geometry is created the same way as the coil. However, in this scenario, the sketch of the square is created and swept along the line body path created to create the swirl. This fluid flow geometry is a step up from the previous design as it incorporates the element of swirl. The effects of this will be examined in the next chapter.

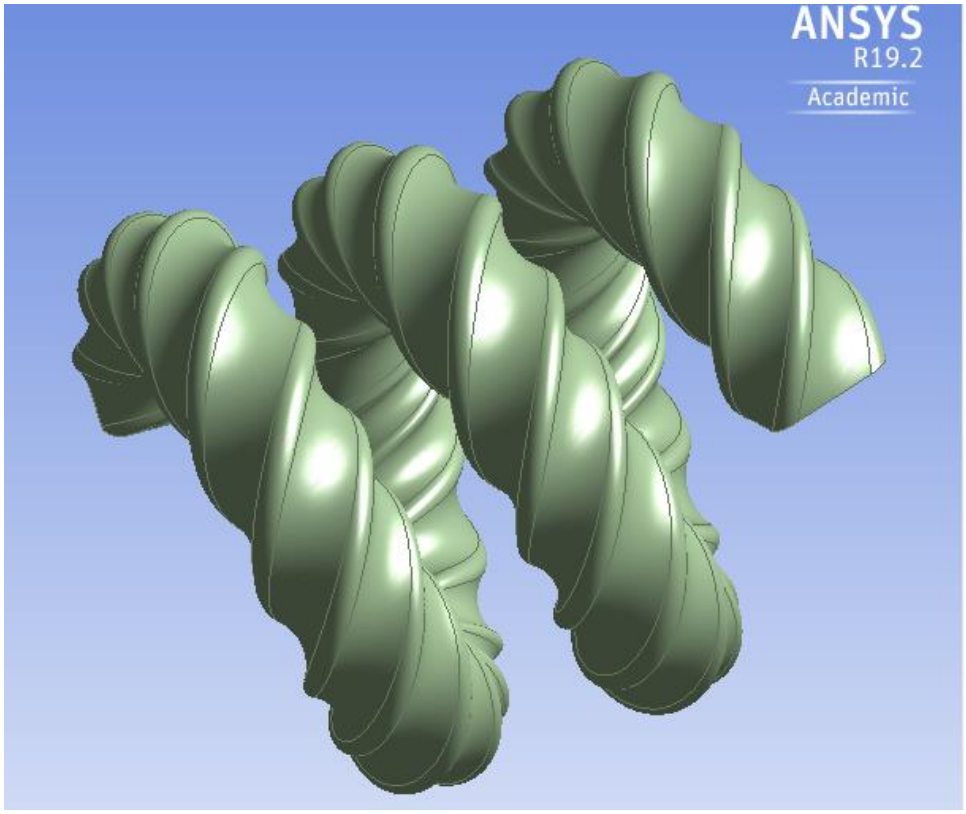

Figure 4.32: Optimised square swirl coil geometry

4.4.8.1. Laminar and turbulent oil flow simulations

The pressure drops attained for the square swirl coil pipe geometry when simulating the flow of oil through the conduit was about 6.1 MPa as indicated in figure 4.33 below, the color map shows at the entrance region exhibits the highest-pressure coloration which dissipates as the flow goes through the pipe experiencing turbulence due to the swirl effect the geometry creates and experiencing recirculation in some areas. On the other hand, the pressure drop attained for the square swirl coil pipe geometry when simulating the flow of oil through the conduit was about 191 MPa as indicated

below, the color map shows at the distinct coloration of entrance region exhibits the highest-pressure coloration which dissipates as the flow goes through the pipe experiencing turbulence due to the swirl effect the geometry creates and experiencing recirculation in some areas. This is the maximum pressure drop attained amongst all geometry cases. It shows the effect the fluid flow geometry has on the physics of flow regarding pressure drop considered important in valve operation.

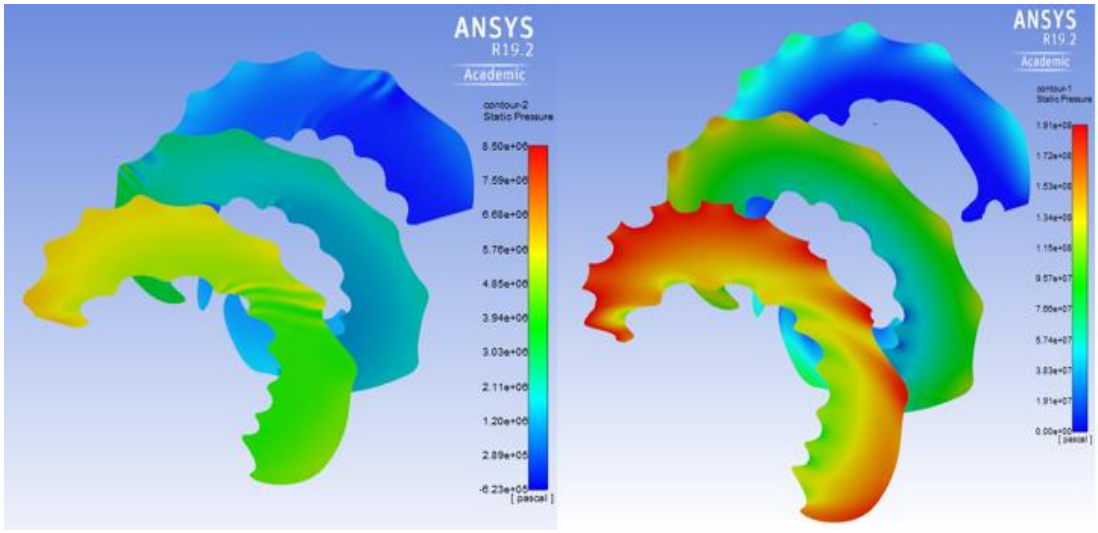

Figure 4.33: Laminar (left) and turbulent (right) oil flow - Contours of static pressure

4.4.8.2. Velocity contour magnitude for oil flow

The velocity vectors show us how the fluid flows or moves through the geometry and the colour map shows us the how the magnitude of velocity varies along different areas of the design. In figure 5.2, the laminar boundary wall layer is visible, but the centrifugal forces acting on the fluid as it flows through the geometry makes the higher velocity flow move to the outer part of the pipe while the slower fluid flow is on the inner part of the coil. The figure shows us the laminar layer acting as a lubrication layer hence allowing the fluid close to the wall due to centrifugal forces move as a much faster velocity of about 35 m/s compared to the inner fluids layer's velocity of about 12m/s.

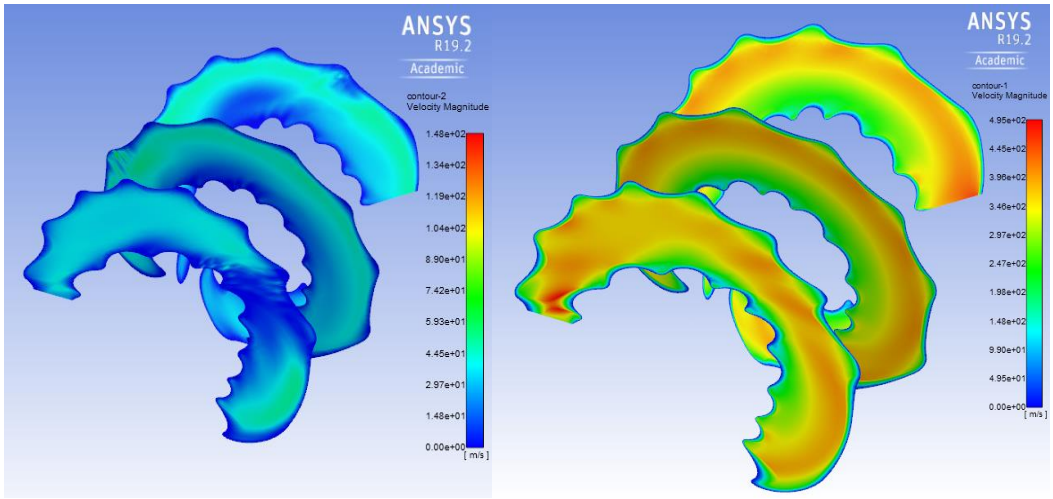

Figure 4.34: Laminar (left) and turbulent (right) oil flow - Contours of velocity magnitude

The velocity vectors coloured by velocity magnitude are used to view using 3D arrows, the fluid flow through the geometry in more detail, below in figure 5.3, it is seen that the square swirl slinky coil fluid flow geometry creates some disturbances to the fluid flow and some zones where recirculation might occur. These physics factors are applicable to heat transfer enhancement hence, the square swirl slinky coil pipe geometry will be applied to enhance heat transfer.

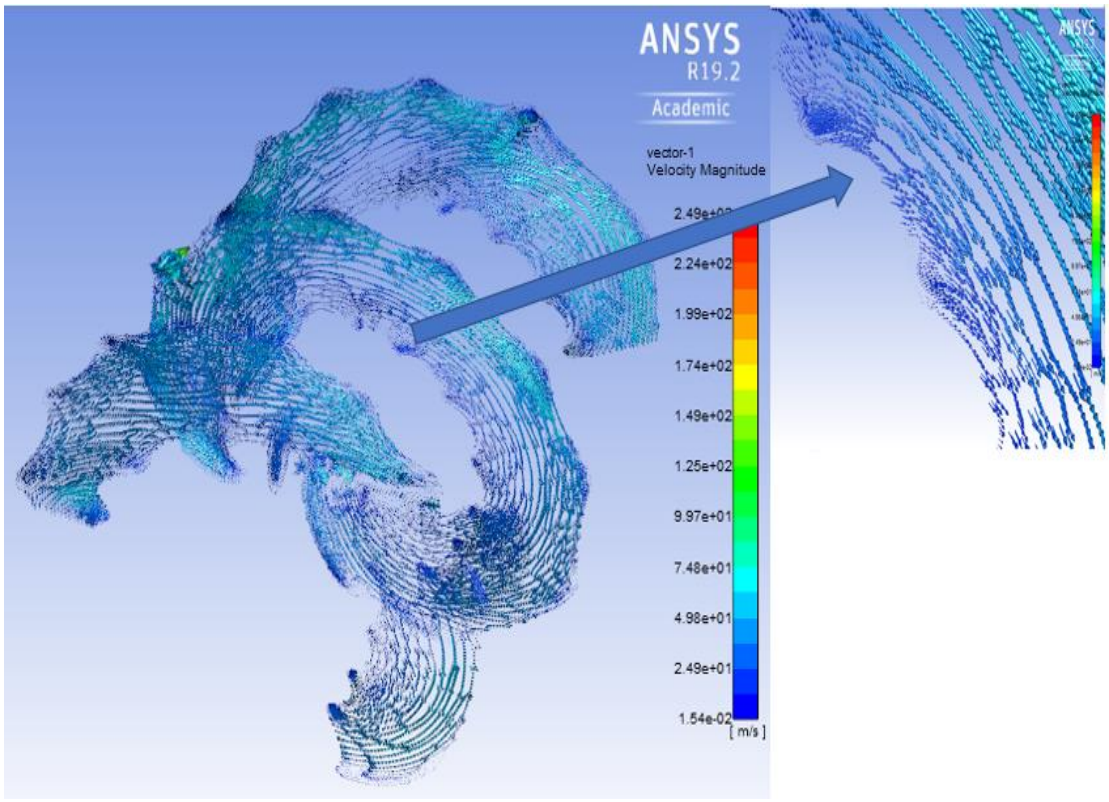

Figure 4.35: Vectors of velocity magnitude showing turbulence and recirculation zones observed

4.4.8.3. Laminar and turbulent water flow simulations

The pressure drop attained for the square swirl coil pipe geometry when simulating the flow of water through the conduit was about 135.761 Pa as indicated in figure 4.34 below, the color map shows at the entrance region exhibits the highest-pressure coloration which dissipates as the flow goes through the pipe experiencing turbulence due to the swirl effect the geometry creates and also experiencing recirculation in some areas. On the other hand, the pressure drop attained for the square swirl coil pipe geometry when simulating the flow of water through the conduit was about 4850Pa as indicated below, the color map shows at the entrance region exhibits the highest-pressure coloration which dissipates as the flow goes through the pipe experiencing turbulence due to the swirl effect the geometry creates and experiencing recirculation in some areas. This is the maximum pressure drop attained amongst all geometry cases. It shows the effect the fluid flow geometry has on the physics of flow regarding pressure drop considered important in valve operation

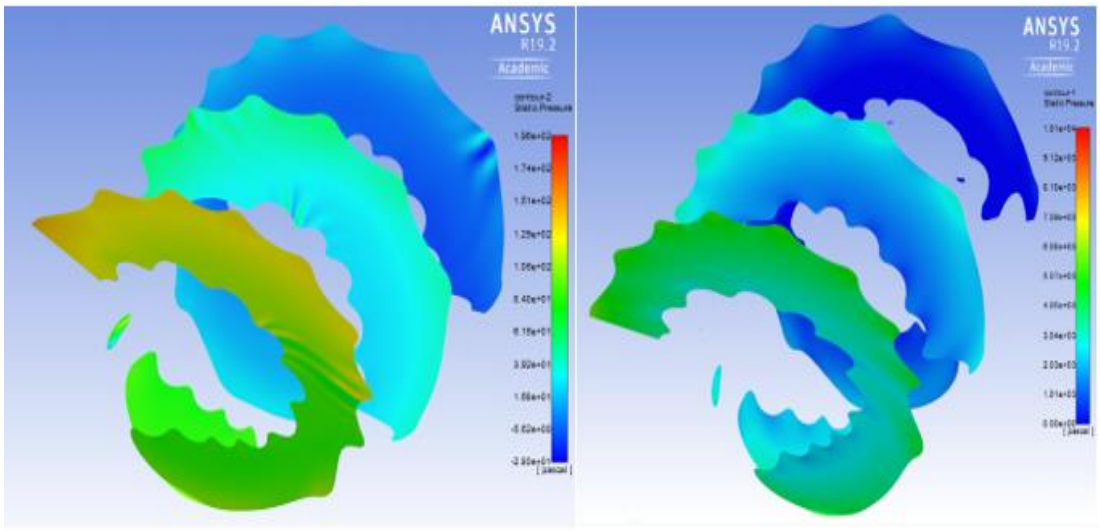

Figure 4.36: Laminar (left) and turbulent (right) water flow - Contours of static pressure

4.4.8.4. Velocity contour magnitude for water flow

The velocity vectors show us how the fluid flows or moves through the geometry and the colour map shows us the how the magnitude of velocity varies along different areas of the design. In figure 4.37, the laminar boundary wall layer is visible, but the centrifugal forces acting on the fluid as it flows through the geometry makes the higher velocity flow move to the outer part of the pipe while the slower fluid flow is on the inner part of the coil. The figure shows us the laminar layer acting as a lubrication layer hence allowing the fluid close to the wall due to centrifugal forces move at a much faster velocity of about 0.37m/s compared to the inner fluids layer's velocity of about 0.061m/s.

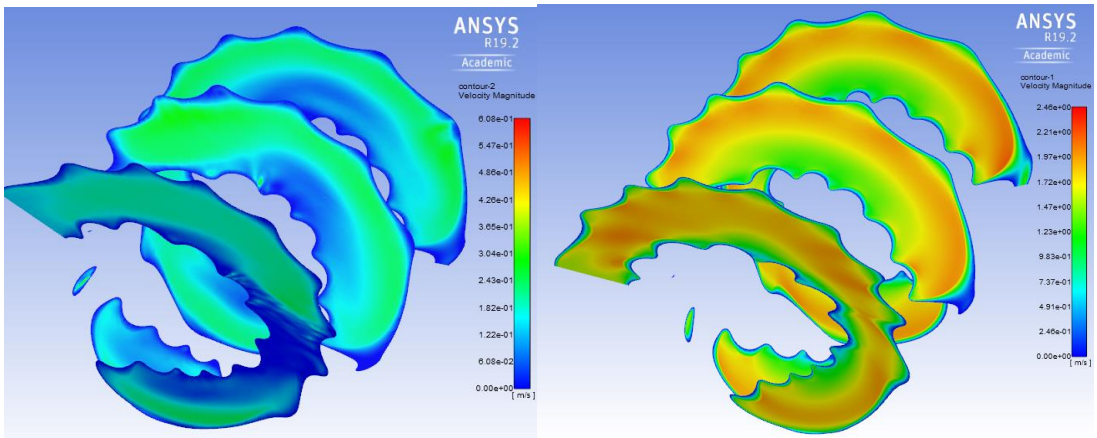

Figure 4.37: Laminar (left) and turbulent (right) water flow - Contours of velocity magnitude

The velocity vectors coloured by velocity magnitude are used to view using 3D arrows, the fluid flow through the geometry in more detail, below in figure 4.38, it is seen that the square swirl slinky coil fluid flow geometry creates some disturbances to the fluid flow and some zones where recirculation might occur. These physics factors are applicable to heat transfer enhancement hence, the square swirl slinky coil pipe geometry will be applied to enhance heat transfer.

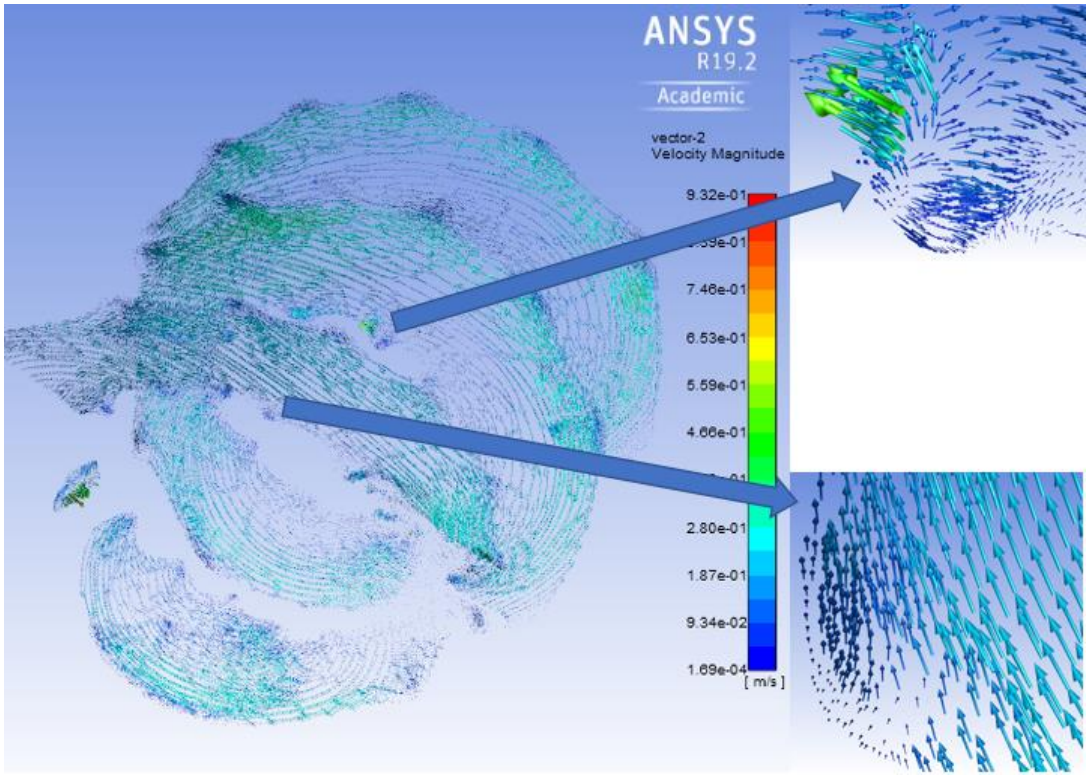

Figure 4.38: Vectors of velocity magnitude showing turbulence and recirculation zones observed

4.4.8.5. Laminar and turbulent gas flow simulations

The pressure drop attained for the square swirl coil pipe geometry when simulating the flow of gas through the conduit was about 1.65Pa as indicated in figure 4.35 below, the color map shows at the entrance region exhibits the highest-pressure coloration which dissipates as the flow goes through the pipe experiencing turbulence due to the swirl effect the geometry creates and experiencing recirculation in some areas. On the other hand, the pressure drop attained for the square swirl coil pipe

geometry when simulating the flow of oil through the conduit was about 68.87 Pa as indicated below, the color map shows at the distinct coloration of entrance region exhibits the highest-pressure coloration which dissipates as the flow goes through the pipe experiencing turbulence due to the swirl effect the geometry creates and experiencing recirculation in some areas. This is the maximum pressure drop attained amongst all geometry cases. It shows the effect the fluid flow geometry has on the physics of flow regarding pressure drop considered important in valve operation

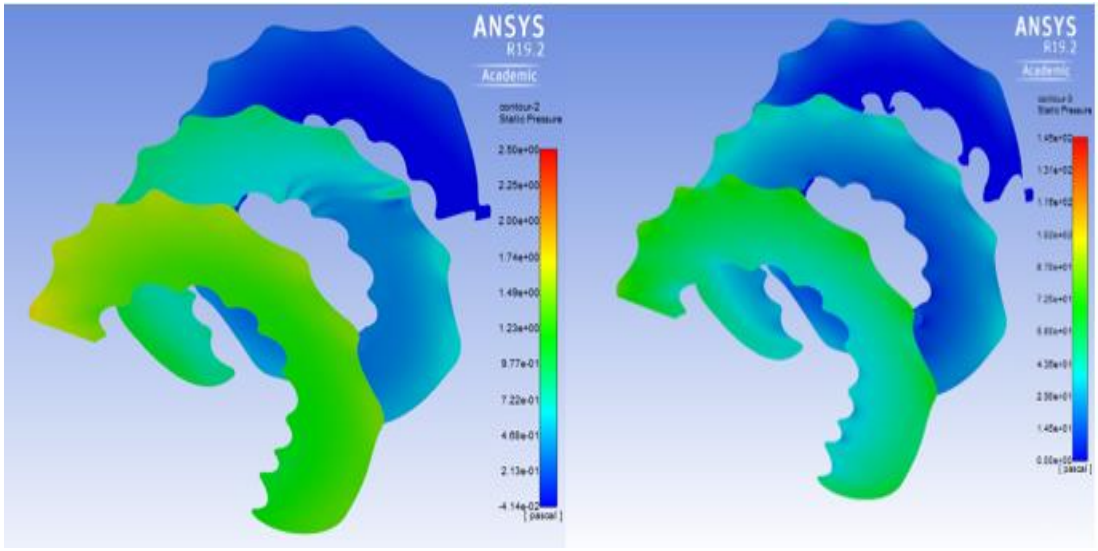

Figure 4.39: Laminar (left) and turbulent (right) gas flow - Contours of static pressure

4.4.8.6. Velocity contour magnitude for gas flow

The velocity vectors show us how the fluid flows or moves through the geometry and the colour map shows us the how the magnitude of velocity varies along different areas of the design. In figure 4.40, the laminar boundary wall layer is visible, but the centrifugal forces acting on the fluid as it flows through the geometry makes the higher velocity flow move to the outer part of the pipe while the slower fluid flow is on the inner part of the coil. The figure shows us the laminar layer acting as a lubrication layer hence allowing the fluid close to the wall due to centrifugal forces move at a much faster velocity of about 0. 086m/s compared to the inner fluids layer's velocity of about 0.014m/s

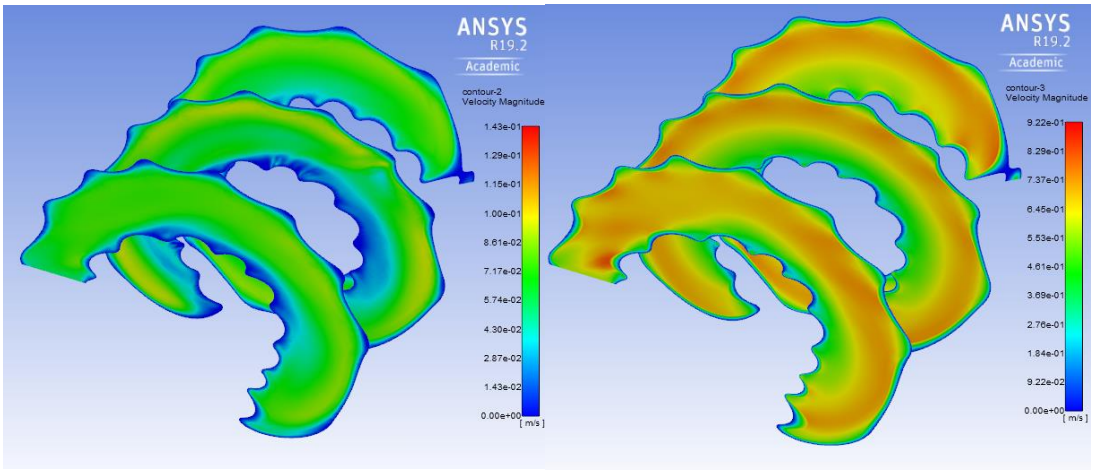

Figure 4.40: laminar and turbulent gas flow (Square swirl slinky pipe) - Contours of velocity magnitude

The velocity vectors coloured by velocity magnitude are used to view using 3D arrows, the fluid flow through the geometry in more detail, below in figure 4.41, it is seen that the square swirl slinky coil fluid flow geometry creates some disturbances to the fluid flow and some zones where recirculation might occur. These physics factors are applicable to heat transfer enhancement hence, the square swirl slinky coil pipe geometry will be applied to enhance heat transfer.

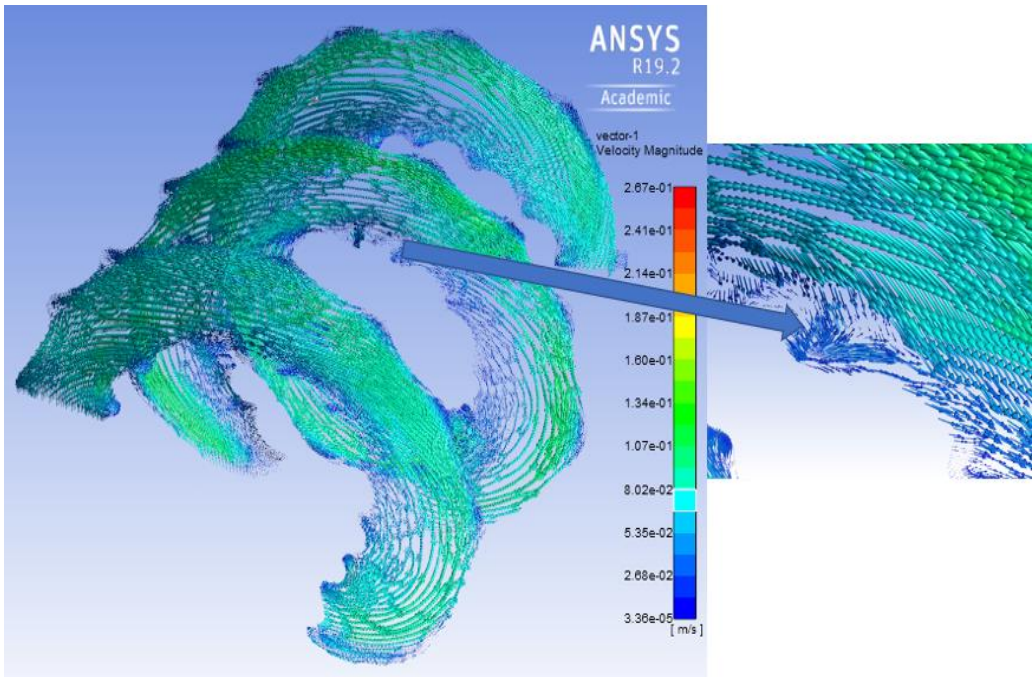

Figure 4.41: Vectors of velocity magnitude showing turbulence and recirculation zones observed

4.5. Summary of simulation results

The CFD simulation result shave been shown in Section 4.4 for the 8 newly proposed designs of AICV. All of them have been analysed for pressure drop and velocity. The square swirl slinky col pipe showed the maximum pressure drop for all three fluids (i.e., oil, water and gas) and hence has been shown with the velocity contours as well. The following two tables show the summary of the pressure drop for all the 8 designs in laminar and turbulent flow regimes.

Table 4-3: Summary of laminar flow pressure drop values attained for each fluid flow geometry case

	Laminar water (Pa)	Laminar gas (Pa)	Laminar oil (MPa)
Straight pipe	6.4172	0.0961651	0.258375
coil pipe	6.53654	0.0978852	0.263112
Elliptical pipe	8.34576	0.124376	0.33536
Straight square pipe	10.7256	0.157555	0.428701
Square coil pipe	10.85	0.159154	0.433447
Slinky Pipe	55.1554	0.803645	2.19796
Square slinky coil	69.6982	1.02197	2.78382
square swirl slinky coil (10 pitch)	135.761	1.65029	6.12266

Table 4-4: Summary of turbulent flow pressure drop values attained for each fluid flow geometry case

	Turbulent water (Pa)	Turbulent gas (Pa)	Turbulent oil (MPa)
Straight pipe	340.866	4.92118	13.54133
coil pipe	343.01033	4.9476204	13.61718
Elliptical pipe	367.61536	5.2986183	14.58985
Straight square pipe	374.0127	5.3946793	14.84783
Square coil pipe	374.31908	5.395632	14.86027
Slinky Pipe	2956.383	42.820684	117.545
Square slinky coil	3020.696	43.031702	119.3965
square swirl slinky coil (10 pitch)	4850.0221	68.869182	191.4455

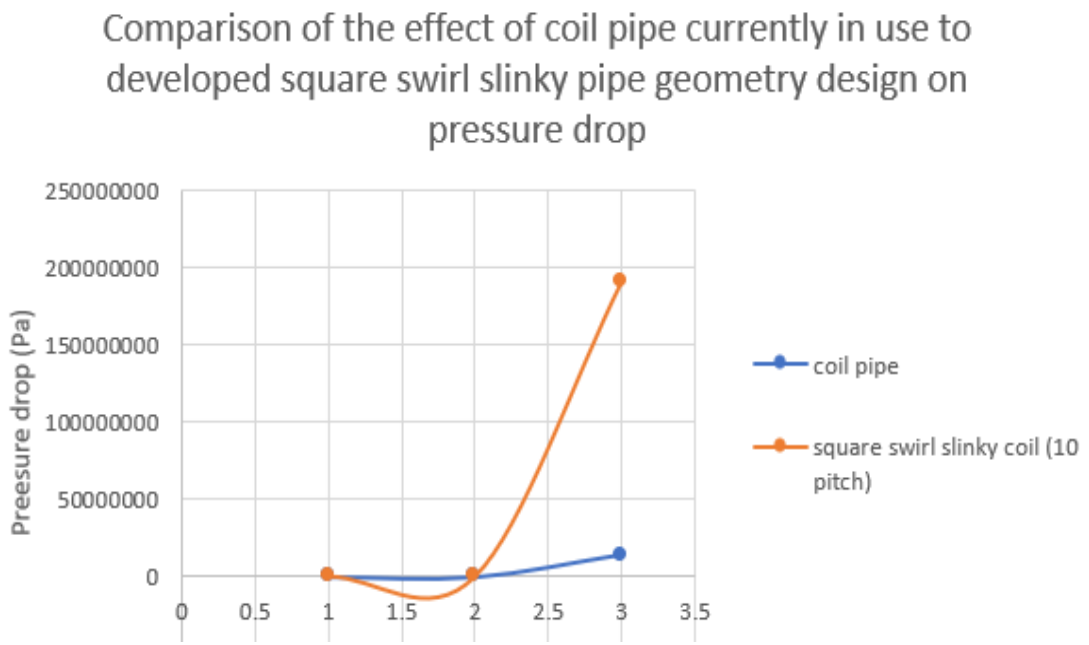

Figure 4.42: Comparison of the effect of coil pipe currently in use to developed square swirl slinky pipe geometry design on pressure drop

4.6. Design Rights related to this research

The work done in this research has led to the following two design rights been filed at the UK Intellectual Property Office (further details at: https://www.gov.uk/search-registered-design).

Square swirl Pipe

Design number: 6021625

Class 23 - Fluid distribution equipment, sanitary, heating, ventilation and air-conditioning equipment, solid fuel

Spiralled coil Pipe

Design number: 6021642

Class 23 - Fluid distribution equipment, sanitary, heating, ventilation and air-conditioning equipment, solid fuel

Chapter 5 Conclusions and Recommendations

In this chapter, conclusions regarding the relative performance of all fluid flow geometry cases designed and simulated have been presented. The conclusions drawn are based on the results analysed in Chapter 4.

5.1 Conclusions

The main purpose of this research was to design fluid flow geometry capable of achieving optimal pressure drop for oil recovery by understanding the effect the fluid flow geometry had on the physics of fluid flow with regard to, the drop-in pressure as this factor majorly determined the mechanical actuation of the valves through the laminar and turbulent flow elements in the AICV and the heat transfer in a solar water heater. The fluid flow geometry cases selected are based on fluid flow especially oil through various conduits at various Reynolds numbers. The study was carried out through extensive literature review, computational fluid dynamics (CFD) and its validations through either direct experiment or peer reviewed experimental research. One of the objectives set for this research was to determine fluid flow geometry parameters which affect the physics of flow with regards to mechanical actuation to prevent premature water and or gas breakthrough. This was achieved as seen through the simulations, discussions and results. The fluid flow geometry parameters considered which affect the physics flow about the drop-in pressure, assuming negligible pipe wall roughness, were seen to be the length or path of the fluid flow geometry, the shape of the fluid flow geometry and the amount of swirl impacted on the fluid flow by the geometry. These parameters have been optimised through simulations and analytical calculations to design a fluid flow geometry (square swirl slinky coil pipe) which affects the physics of flow and optimise the for pressure drop.

This design was then utilised to enhance heat transfer applications and then simulated results were compared with published literature

The tables below show the pressure drop values equated using the correlation factor of 2.0535 to the analytical result values as demonstrated in chapter 4.

5.2 Achievement of aim and objectives

The aim of this research was to design a fluid flow geometry capable of achieving optimal pressure drop for oil recovery. This aim was achieved as is evident in section 4.2. An optimum fluid flow geometry was design with the capability of achieving optimal pressure drop for oil recovery.

The objectives of this work were:

1. To undertake literature review of fluid flow parameters and their effect on the physics of flow.

   This objective was met through the extensive literature review carried out in chapter 2 and further utilised for new geometry designs in Chapter 4.

2. To identify geometry parameters for AICV that can avoid premature water and or gas breakthrough

   This research met the objective through study of literature and published work, the valve operation, understanding the underlying physics and numerical simulations to determine what parameters affected the physics of flow regarding pressure drop in chapters 1 through to 4.

3. To propose new designs for the AICV that can lead to optimum pressure drop

   After numerical simulations were carried out, the square swirl design proved to be the optimum fluid flow geometry thereby meeting this objective as a proposed new design which leads to optimum pressure drop.

4. To compare the CFD results of the circular coil pipe of the AICV with the newly proposed designs

   In the results sections in chapter 4, the result of the new design is compared with that of the current design as shown in figures 4.42

5. To optimise the design with the best results compared to the circular coil pipe of the AICV

   During the research, the various designs were optimised, and the square geometry proved to be the most efficient design for enhancing pressure drop in all fluid simulated. The swirl design was also tested which also proved to work best on the square geometry

6. To compare the simulation results of the optimal design with analytical values

   As discussed in chapter 4 under the cases for numerical simulation, analytical methods were used to validate the numerical simulation results before using those setting to run the other simulations. A correlation factor was discovered which reduced with an increase ion pipe length. This leads to the assumption that with a longer length of pipe, the numerical fluid flow analysis becomes more accurate as shown in table 4.2. The correlated pressure drop values are also displayed below in tables 5-1 and 5-2.

Table 5-1 Correlated Laminar flow pressure drop values

	Laminar water (Pa)	Laminar gas (Pa)	Laminar oil (MPa)
Straight pipe	3.125	0.04683	0.125822
coil pipe	3.1831153	0.047667	0.128128
Elliptical pipe	4.064155707	0.060568	0.163311
Straight square pipe	5.223072368	0.076725	0.208766
Square coil pipe	5.283651748	0.077504	0.211077
Slinky Pipe	26.85916365	0.391353	1.070346
Square slinky coil	33.94110749	0.497671	1.355644
square swirl slinky coil (10 pitch)	66.11187512	0.803646	2.981567

Table 5-2: Correlated turbulent flow pressure drop values

	Turbulent water (Pa)	Turbulent gas (Pa)	Turbulent oil (MPa)
Straight pipe	165.9923721	2.396479	6.594254
coil pipe	167.0366018	2.409355	6.631191
Elliptical pipe	179.0185751	2.580281	7.104856

Straight square pipe	182.1339038	2.627061	7.230487
Square coil pipe	182.2831024	2.627524	7.236543
Slinky Pipe	1439.677254	20.8525	57.2412
Square slinky coil	1470.995917	20.95526	58.14279
square swirl slinky coil (10 pitch)	2361.827442	33.5374	93.2287

The pressure drop created by the Laminar Flow Element is shown by the below equation: $\Delta P = \frac{32\mu VL}{D^2}$ The graphs below show in detail the vast difference in pressure drop generated due to altering the fluid flow geometry to affect the fluid flow between the coil design and the final square swirl slinky pipe design for laminar flow. The graph in figure 5.1 shows the effect of flow geometry on the physics of flow regarding pressure drop in the laminar flow regime while figure 5.2 details the effect of the optimised fluid flow geometry enhancing oil recovery

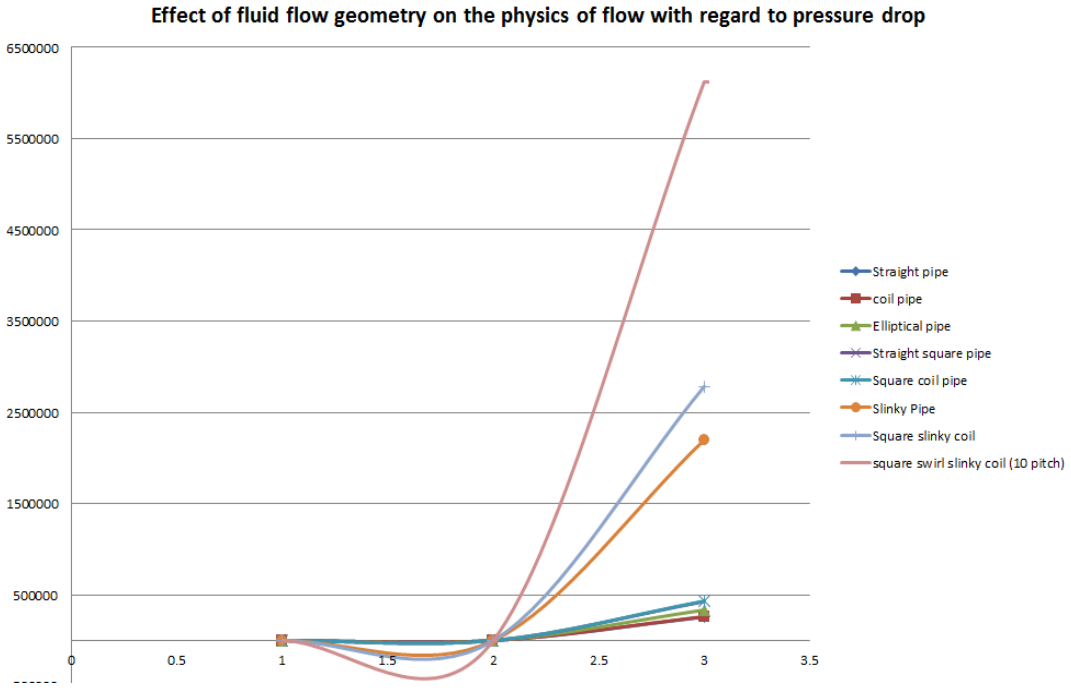

Figure 5.1: effect of flow geometry on the physics of flow regarding pressure drop in the laminar flow regime

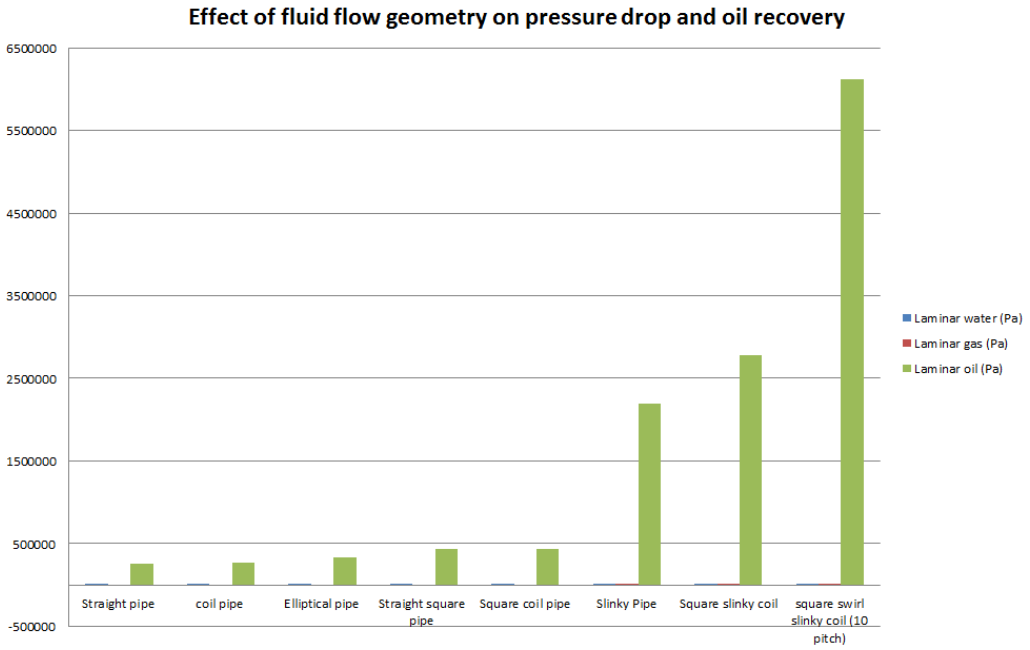

Figure 5.2: the effect of the optimised fluid flow geometry enhancing oil recovery (LFE)

Where: ΔP = differential pressure, μ = 0.1, V = 32.22m/s, L = 0.0125m (2.23m full flow path), D = 0.0032 The pressure drop through the laminar flow element for the 0.0125m path length is as follows;

ΔP From CFD simulation = 0.25 MPa Analytical pressure drop value = 0.125MPa

ΔP at full length = 22.5MPa

In comparison to the simulated pressure drop it can be assumed the calculated values correlate to about twice the simulated values. From the above calculations that the fluid flow geometry, Square swirl slinky coil shows an apparent increase in the flow path which is due to the shape of the fluid flow geometry, this increase in the flow path affects the physics of flow by already creating a further pressure drop which is then further enhanced by the addition of swirl which optimises the fluid flow geometry as evidenced by the results. This fluid flow geometry from simulations, coil and swirl ensures flow separation according to their viscosities and then the drop is pressure which governs the laminar flow element will ensure proper valve operation even with multiphase or emulsion flows.

Due to higher flow rate per unit area through the orifice, when the fluid leaves the laminar flow element, there is a higher rate of flow through the turbulent element which results in turbulent flow. The pressure differential in the chamber changes with reference to the fluid properties such as:

- flow rate,
- density of the fluid,
- Inlet or outlet orifice sizes.

The drop-in pressure for this section is depicted by the equation:

$$\Delta P = K \frac{1}{2} \rho V^2$$

The graphs below show in detail the vast difference in pressure drop generated due to altering the fluid flow geometry to affect the fluid flow between the coil design and the final square swirl slinky pipe design for turbulent flow. The graph in figure 5.3 shows the effect of flow geometry on the physics of flow with regard to pressure drop in the turbulent flow regime while figure 5.4 details the effect of the optimised fluid flow geometry enhancing oil recovery.

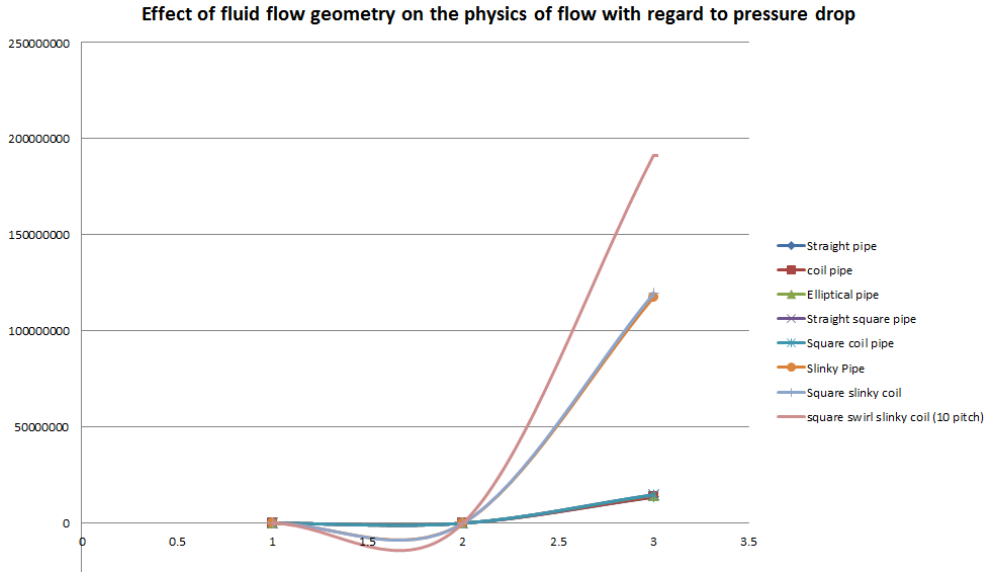

Figure 5.3: effect of flow geometry on the physics of flow regarding pressure drop in the turbulent flow regime

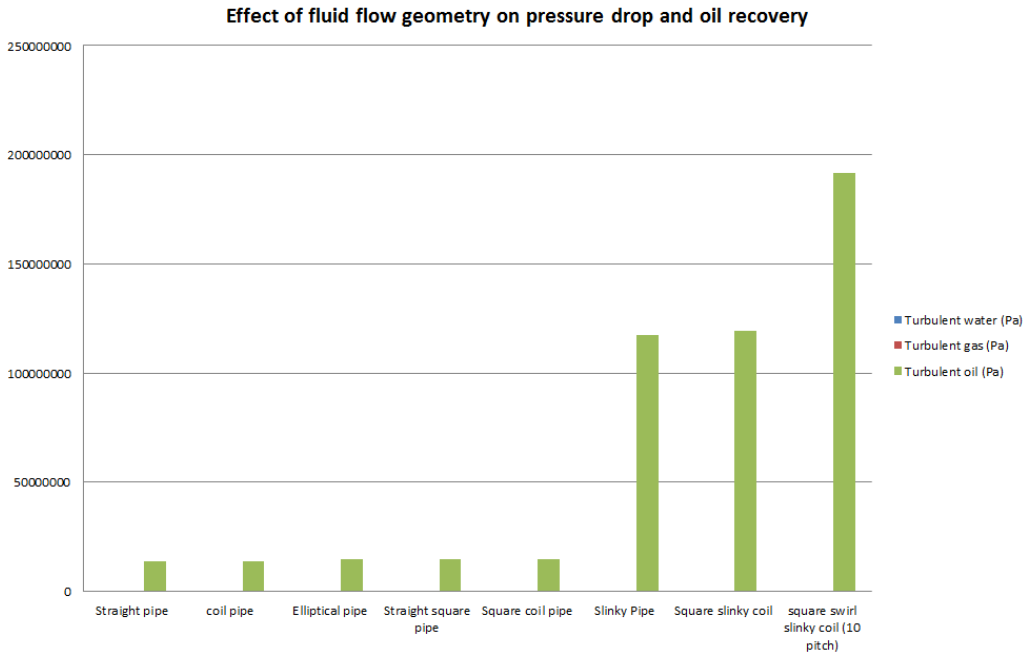

Figure 5.4: the effect of the optimised fluid flow geometry enhancing oil recovery (TFE)

Where: ΔP = differential pressure, K = Geometrical constant, ρ = density, V = velocity, ρ_{oil} = 970 kg/m^3, V_{oil} = 322.2m/s

For the Coil pipe; $0.27 = K$, For the square swirl slinky coil pipe; $3.8 = K$

The geometrical constant K is an important parameter when considering the effect of fluid flow geometry in a turbulent flow regime on physics of flow. The equation above shows us the increase in K from 0.27 for the coil pipe to 3.8 for the square swirl slinky pipe.

Table 5-3: K factor values

Fluid flow geometry	K factors
Straight pipe	0.268948
coil pipe	0.270455
Elliptical pipe	0.289773
Straight square pipe	0.294897
Square coil pipe	0.295144
Slinky Pipe	2.334595
Square slinky coil	2.371366
square swirl slinky coil	3.802352

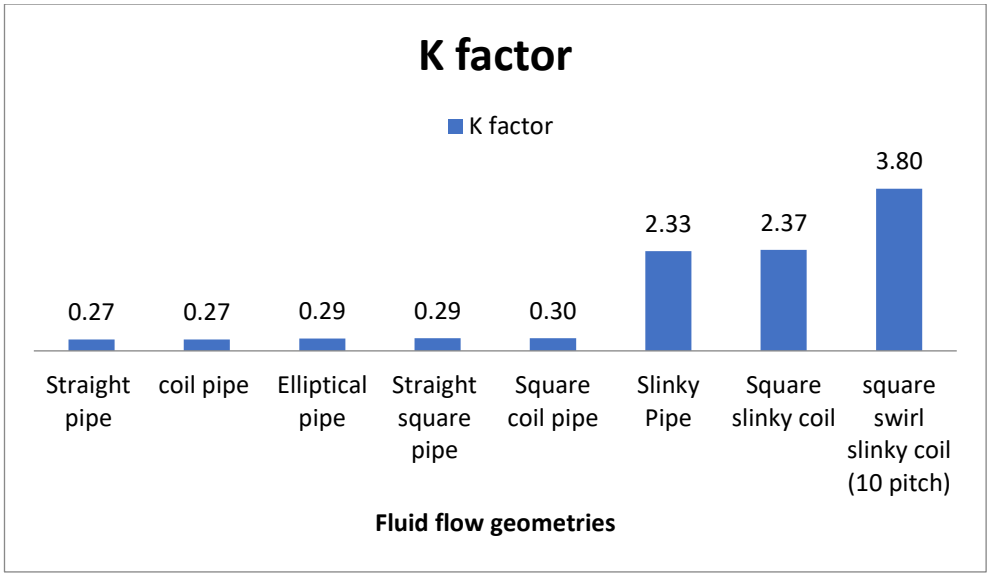

Figure 5.5: Graph showing K factor values for various fluid flow geometry cases

5.3 Novel contribution to knowledge

The effect the discovered and designed square swirl fluid flow geometry design has on the physics of flow regarding creating optimum pressure drop for the recovery of oil. In conclusion, the fluid flow geometry design has been optimised to affect the physics of the flow and produce optimum flow. This will serve to stop premature water breakthrough using mechanical actuation of the valve. The research has shown from review and current design and optimised design the practicality of the inflow valve design solution. It also shows the orifice and nozzle type enhancing and producing maximum flow. Maintaining the same fluid flow geometry size or even smaller but increasing efficiency and pressure drop necessary for operation was achieved as well. During the above research, the square swirl design discovered, and design righted was seen to improve heat transfer due to the obstruction of the boundary layer and the generation of recirculation zones in the fluid flow conduit. This means that due to turbulence generated by the swirl, the heat transfer is more efficient, and the recirculation zones maintain the heat in the hot stream or the fluid with a higher temperature which led to better transfer of heat between hot and cold fluids and less

energy requirements due to heat temperature being maintained. The design could also be applied to oil transportation in the pipeline which currently required heating or the pipeline or heating jackets.

5.4 Concluding Remarks

The approaches described in this thesis are supported by literature and numerical simulations. The working models and calculations have shown the principles have resulted in positive effects on the fluid flow geometry that can lead to greater pressure drops capable of extracting more oil when used in AICV. The effect of swirl on the multiphase flow (oil and water) has also been shown in Appendix B but was not the focus of this work. Multiphase flow simulations are extremely time consuming and can lead to accurate flow configurations in the presence of multiple fluids.

This new square slinky coil pipe geometry has shown large areas of recirculation that lead to pressure drop. This recirculation phenomenon can also help in creating turbulent flow which is one of the prime factors for heat transfer applications. This geometry has therefore been analysed for heat transfer in a flat plate thermal solar panel and has shown increased rate of heat transfer (Appendix A).

References

Aadnoy, B. (2008) *Autonomous Flow Control Valve or 'intelligent' ICD*. Available at: http://www.hansenenergy.biz/HANSEN_Energy_Solutions/InflowControl2008B.pdf (Accessed: 2 July 2015).

Aadnoy, B. (2010) *A Short Note on Inflow Performance Related to ICD's and Facts and Fiction about Inflow Control Devices*. Available at: http://www.hansenenergy.biz/HANSEN_Energy_Solutions/ICDPerformance.pdf (Accessed: 10 October 2015).

Abdel Azim, R. (2015) 'Evaluation of water coning phenomenon in naturally fractured oil reservoirs', *Journal of Petroleum Exploration and Production Technology*, . doi: 10.1007/s13202-015-0185-7.

Adkisson, C. (1997) *USGS fact sheet FS-003-97 figure 2*. Available at: http://pubs.usgs.gov/fs/1997/fs003-97/Fig.2.html (Accessed: 18 February 2016).

AICV® Ultra Light Oil (2014) Available at: http://www.inflowcontrol.no/aicv-product-range/aicv-ultra-light-oil/ (Accessed: 24 July 2015).

Al-Hashimy, Z.I., Al-Kayiem, H.H., Kadhim, Z.K. and Mohmmed, & A.O. (2015) 'Numerical simulation and pressure drop prediction of slug flow in oil/gas pipelines computational methods in Multiphase flow VIII 57', *WIT Transactions on Engineering Sciences*, 89. doi: 10.2495/MPF150051.

AlKhelaiwi, F.T.M. (2013) *A Comprehensive Approach to the Design of Advanced Well Completions*. Available at: http://www.ros.hw.ac.uk/bitstream/handle/10399/2644/AlkhelaiwiFTM_0313_pe(1).pdf;jsessionid=9EA3EFB230A0FE130A2778A3EECB54BE?sequence=3 (Accessed: 13 October 2015).

Amini, G. (2015) 'International journal of Multiphase flow liquid flow in a simplex swirl nozzle', *International Journal of Multiphase Flow*, 79, pp. 225–235. doi: 10.1016/j.ijmultiphaseflow.2015.09.004.

An Introduction To Fluid Mechanics: CIVE1400 SCHOOL OF CIVIL ENGINEERING (2009) Available at: http://www.efm.leeds.ac.uk/CIVE/FluidsLevel1/Unit00/index.html (Accessed: 23 July 2015).

Andrews, R. (2003) *Research Questions (Continuum Research Methods)*. LONDON: Continuum International Publishing Group.

Ansys (2009) *ANSYS Meshing Application Introduction*. Available at: http://www.racfd.com/mesh/AM_12_Appendix%20A.ppt (Accessed: 12 October 2016).

ANSYS (no date) *ANSYS FLUENT 12.0 user's guide - 14.3.6 setting the pressure-drop parameters and effectiveness*. Available at: http://www.afs.enea.it/project/neptunius/docs/fluent/html/ug/node500.htm (Accessed: 2 June 2016).

Ariyaratne, C. and Beng (2016) *DESIGN AND OPTIMISATION OF SWIRL PIPES AND TRANSITION GEOMETRIES FOR SLURRY TRANSPORT*. Available at: http://eprints.nottingham.ac.uk/11570/1/Ariyaratne_Thesis.pdf (Accessed: 11 February 2016).

Arslan, O. (2005) *OPTIMAL OPERATING STRATEGY FOR WELLS WITH DOWNHOLE WATER SINK COMPLETIONS TO CONTROL WATER PRODUCTION AND IMPROVE PERFORMANCE*. Available at: http://etd.lsu.edu/docs/available/etd-01132005-144724/unrestricted/Arslan_dis.pdf (Accessed: 18 February 2016).

Bahrami, M. (2009) *The angular momentum energy equation*. Available at: http://www.sfu.ca/~mbahrami/ENSC%20283/Notes/Integral%20Relations%20for%20CV_Part%202.pdf (Accessed: 25 February 2016).

Bailey, B., Crabtree, M., Aberdeen, J.T., Scotland, Caracas, C.R., Roodhart, V.L., Burdylo, L., Chang, K.S., Hegeman, P., Land, S., Goligher, A. and Montrouge, F. ; (no date) *Water control*. Available at: https://www.slb.com/~/media/Files/resources/oilfield_review/ors00/spr00/p30_51.pdf (Accessed: 10 March 2016).

Bakker, A. (2002) *Lecture 10 -turbulence models applied computational fluid dynamics*. Available at: http://www.bakker.org/dartmouth06/engs150/10-rans.pdf (Accessed: 17 June 2016).

BBC (2006) *GCSE Bitesize: Refining crude oil*. Available at: http://www.bbc.co.uk/schools/gcsebitesize/science/21c/materials_choices/crude_oil_usesrev2.shtml (Accessed: 8 March 2016).

Biodiesel Basics (2015) Available at: http://biodiesel.org/what-is-biodiesel/biodiesel-basics (Accessed: 2 September 2015).

Bionas Ghaba USA - Jatropha Curcas (2011) Available at: http://ghabainternational.com/bionasghaba/jatropha.html (Accessed: 2 September 2015).

Birchenko, V. (2010) *Analytical Modelling of Wells with Inflow Control Devices*. PHD thesis. Available at: http://www.ros.hw.ac.uk/bitstream/10399/2349/1/BirchenkoV_0710_pe.pdf (Accessed: 25 June 2015).

Birchenko, V.M., Bejan, A.I., Usnich, A.V. and Davies, D.R. (2011) 'Application of inflow control devices to heterogeneous reservoirs', *Journal of Petroleum Science and Engineering*, 78(2), pp. 534–541. doi: 10.1016/j.petrol.2011.06.022.

Birchenko, V.M., Muradov, K.M. and Davies, D.R. (2010) 'Reduction of the horizontal well's heel–toe effect with inflow control devices', *Journal of Petroleum Science and Engineering*, 75(s 1–2), pp. 244–250. doi: 10.1016/j.petrol.2010.11.013.

Bohra, L.K. (2004) *FLOW AND PRESSURE DROP OF HIGHLY VISCOUS FLUIDS IN SMALL APERTURE ORIFICES*. Available at: https://smartech.gatech.edu/bitstream/handle/1853/7269/bohra_lalit_k_200407_ms.pdf (Accessed: 13 July 2016).

Bouchard, M. (2008) *Flow Control Issues relating to heavy oil*. Available at: http://www.slb.com/~/media/Files/industry_challenges/heavy_oil/other/feature_articles/ho_flow_control_issues.pdf (Accessed: 11 October 2015).

Cable, M. (2009) *An evaluation of turbulence models for the numerical study of forced and natural Convective flow in Atria*. Available at: http://www.collectionscanada.gc.ca/obj/thesescanada/vol2/OKQ/TC-OKQ-1884.pdf (Accessed: 24 October 2016).

Chapter 3_Lect Notes_Turbulent flow and moody diagram (no date) Available at: http://faculty.kfupm.edu.sa/CHE/alshami/teaching/Che%20204/Lecture%20Notes/Chapter%203_Lect%20Notes_Turbulent%20Flow%20and%20Moody%20Diagram.htm (Accessed: 2 June 2016).

CHAPTER-4 RESERVOIR FLUID PROPERTIES (no date) Available at: http://users.metu.edu.tr/kok/pete110/PETE110_CHAPTER4.pdf (Accessed: 8 March 2016).

Chu, K.W., Wang, B., Yu, A.B. and Vince, A. (2009) 'CFD-DEM modelling of multiphase flow in dense medium cyclones', *Powder Technology*, 193, pp. 235–247. doi: 10.1016/j.powtec.2009.03.015.

CIVE2400 fluid mechanics section 1: Fluid flow in pipes (2006) Available at: http://www.efm.leeds.ac.uk/CIVE/CIVE2400/pipe_flow2.pdf (Accessed: 13 July 2016).

Colombo, M., Cammi, A., Guédon, G.R., Inzoli, F. and Ricotti, M.E. (2015) 'CFD study of an air–water flow inside helically coiled pipes', *Progress in Nuclear Energy*, 85, pp. 462–472. doi: 10.1016/j.pnucene.2015.07.006.

COLORADO OIL AND GAS PRODUCTION – UPDATE (april 2013) (2013) Available at: http://cogcc.state.co.us/Announcements/ColoradoOilProd.pdf (Accessed: 18 February 2016).

COMM (2015) *European commission: CORDIS: Projects & results service: 'A novel, autonomous and rEVersible inflow control vALve to increase oil production and reservoir recovery rate by stopping the production of unwanted water and gas locally in the reservoirs'*. Available at: http://cordis.europa.eu/project/rcn/109490_en.html (Accessed: 31 May 2016).

COMSOL (2005) *Swirl flow around a rotating disk*. Available at: http://www.comsol.com/model/download/268471/models.cfd.rotating_disk.pdf (Accessed: 10 February 2016).

Coning - Schlumberger oilfield glossary (2016) Available at: http://www.glossary.oilfield.slb.com/en/Terms/c/coning.aspx (Accessed: 21 January 2016).

Cresting - Schlumberger oilfield glossary (2016) Available at: http://www.glossary.oilfield.slb.com/en/Terms/c/cresting.aspx (Accessed: 21 January 2016).

Davailles, A., Climent, E. and Bourgeois, F. (2012) 'Fundamental understanding of swirling flow pattern in hydrocyclones', *Separation and Purification Technology*, 92, pp. 152–160. doi: 10.1016/j.seppur.2011.12.011.

Developing a flow control system for a well (2006) Available at: http://www.google.com/patents/US20080149203 (Accessed: 17 August 2015).

Digital, F.R. (2015) *Inflow Control – Product ranges – Tendeka*. Available at: http://www.tendeka.com/product-ranges/inflow-control/ (Accessed: 24 July 2015).

Dogan, T., Conger, M., Mousaviraad, M., Xing, T. and Stern, F. (2014) *Verification of Laminar and validation of turbulent pipe flows 58: 160 intermediate mechanics of fluids CFD LAB 1*. Available at: http://user.engineering.uiowa.edu/~me_160/lab/intermediate-2013/lab%201-pipe/intermediate%20lab%201%20manual.pdf (Accessed: 29 February 2016).

Downhole tool systems 2-1 Downhole tool systems (2005) Available at: http://www.halliburton.com/public/cps/contents/books_and_catalogs/web/sandcontrol/section2_downhole_tool_systems.pdf (Accessed: 5 September 2016).

Dusseault, M. (2001) *Comparing Venezuelan and Canadian heavy oil and tar sands. Calgary, Canada. Canadian International Petroleum Conference (June 12-14, 2001)*. Available at: http://www.energy.gov.ab.ca/OilSands/pdfs/RPT_Chops_app3.pdf (Accessed: 2 July 2015).

Dwire, O.S. (1949) *A study of pressure drop in helical coils*. Available at: http://adsabs.harvard.edu/abs/1949PhDT.....16D (Accessed: 19 May 2016).

Dynamics, N. (2012) *Pressure loss in pipe – Neutrium*. Available at: https://neutrium.net/fluid_flow/pressure-loss-in-pipe/ (Accessed: 2 October 2016).

Dynamics, N. (2013) *Terminal velocity of particles for gravity separation – Neutrium*. Available at: https://neutrium.net/unit-operations/terminal-velocity-of-particles-for-gravity-separation/ (Accessed: 24 October 2016).

Dyson, S. and USGS (2013) *USGS fact sheet FS-003-97*. Available at: http://pubs.usgs.gov/fs/1997/fs003-97/FS-003-97.html (Accessed: 18 February 2016).

Eesa, M. (2009) *CFD STUDIES OF COMPLEX FLUID FLOWS IN PIPES*. Available at: https://core.ac.uk/download/files/121/77180.pdf (Accessed: 2 March 2016).

Efficiency of ICV/ICD systems MASTER'S THESIS (2012) Available at: https://brage.bibsys.no/xmlui/bitstream/handle/11250/182088/Gimre,%20Jeanette.pdf?sequence=1 (Accessed: 5 September 2016).

Eiamsa-ArdS and Seemawute, P. (2012) 'Decaying swirl flow in round tubes with short-length twisted tapes ☆', *International Communications in Heat and Mass Transfer*, 39, pp. 649–656. doi: 10.1016/j.icheatmasstransfer.2012.03.021.

El Drainy, Y.A., Saqr, K.M., Aly, H.S. and Nazri Mohd. Jaafar, M. (2009) 'CFD analysis of Incompressible turbulent swirling flow through Zanker plate', *Engineering Applications of Computational Fluid Mechanics*, 3(4), pp. 562–572. doi: 10.1080/19942060.2009.11015291.

El Xia J, ', B Smith L, Benim3, A.C., Schmidlp, J. and ', Yadigaroglu G (1997) 'EFFECT OF INLET AND OUTLET BOUNDARY CONDITIONS ON SWIRLING FLOWS', *Computers & Fhids*, 26(8), pp. 81–823.

Ellis, T., Goh, G. and Jokela, T. (2010) *Inflow Control Devices - Raising profiles*. Available at: https://www.slb.com/~/media/Files/resources/oilfield_review/ors09/win09/03_inflow_control_devices.pdf (Accessed: 2 July 2015).

Engineers, S. of P. (2012) *Controlling excess water production* -. Available at: http://petrowiki.org/Controlling_excess_water_production (Accessed: 5 September 2016).

Enhanced Oil Recovery | Department of Energy (2015) Available at: http://energy.gov/fe/science-innovation/oil-gas-research/enhanced-oil-recovery (Accessed: 8 July 2015).

EquiFlow® autonomous inflow control device (2014) Available at: http://www.halliburton.com/en-US/ps/completions/sand-control/screens/inflow-control/equiflow-autonomous-inflow-control-device.page?nav=en-US_stimulation_public&node-id=hgyyxpul (Accessed: 22 February 2016).

EquiFlow® Autonomous Inflow Control Device (2015) Available at: http://www.halliburton.com/en-US/ps/completions/sand-control/screens/inflow-control/equiflow-autonomous-inflow-control-device.page (Accessed: 6 August 2015).

Escue, A. and Cui, J. (no date) 'Comparison of turbulence models in simulating swirling pipe flows', *Applied Mathematical Modelling*, 34(10), pp. 2840–2849. doi: 10.1016/j.apm.2009.12.018.

Eswaran, V. (2002) *Turbulent Flows: Fundamentals, Experiments and Modeling*. Available at: https://books.google.co.uk/books?id=BBsdQPhrXugC&pg=PA180&lpg=PA180&dq=turbulent+flow+element&source=bl&ots=4Ws7E1Kwjb&sig=WAwXmqUG0x66skc50reHyPLKW4M&hl=en&sa=X&ved=0CEAQ6AEwBWoVChMI_On3-

OmjxwIVQbYaCh2Jtg9X#v=onepage&q=turbulent%20flow%20element&f=false (Accessed: 12 August 2015).

Evseev, N. and Shvab, A. (2014) 'Modeling of a two-phase swirling turbulent flow in the separation chamber of the centrifugal apparatus', *EPJ Web of Conferences*, 76. doi: 10.1051/epjconf/20147601036.

F L O W I N P I P E S (no date) Available at: https://www.uio.no/studier/emner/matnat/math/MEK4450/h11/undervisningsmaterial e/modul-5/Pipeflow_intro.pdf (Accessed: 22 October 2016).

File: Vol5 page 0877 image 0001.png - (2013) Available at: http://petrowiki.org/File%3AVol5_Page_0877_Image_0001.png (Accessed: 21 January 2016).

Fluid flow fundamentals (2015) Available at: http://wiki.aapg.org/Fluid_flow_fundamentals (Accessed: 10 July 2015).

Fluid Flow in the Subsurface (Darcy's Law) (2015) Available at: https://fracfocus.org/groundwater-protection/fluid-flow-subsurface-darcys-law (Accessed: 6 August 2015).

Fluid flow through permeable media - (2015) Available at: http://petrowiki.org/Fluid_flow_through_permeable_media (Accessed: 10 July 2015).

Fluid mechanics for drilling - (2015) Available at: http://petrowiki.org/Fluid_mechanics_for_drilling (Accessed: 28 August 2015).

Fracking Manual Chapter 5 (no date) Available at: https://docs.google.com/document/d/1muwjhw6j3EguLQ-WuFWckZE-7p6y79lqPFbiUgVusrA/edit?pli=1 (Accessed: 17 August 2015).

Fundamentals of Pressure Sensor Technology | Sensors (2015) Available at: http://www.sensorsmag.com/sensors/pressure/fundamentals-pressure-sensor-technology-846 (Accessed: 28 August 2015).

Glover, P. (no date) *Formation evaluation MSc course notes reservoir fluids chapter 2: Reservoir fluids 2.1 introduction*. Available at: http://homepages.see.leeds.ac.uk/~earpwjg/PG_EN/CD%20Contents/Formation%20Evaluation%20English/Chapter%202.PDF (Accessed: 8 March 2016).

Graham, E. (2014) *Introduction to Multiphase & wet gas flows*. Available at: http://www.tuvnel.com/assets/content_images/Intro%20to%20Muph%20and%20wet%20gas.pdf (Accessed: 20 June 2016).

Halliburton (2012) *Maximizing the value of mature fields solving challenges. ™ mature fields*. Available at: http://www.halliburton.com/public/solutions/contents/Mature_Fields/related_docs/11BDSOL0080_Maturefield_bro_web4.pdf (Accessed: 18 February 2016).

Help (2015) *Pressure drop prediction in a long straight pipe*. Available at: https://knowledge.autodesk.com/support/cfd/learn-explore/caas/CloudHelp/cloudhelp/2014/ENU/SimCFD/files/GUID-FAF6581B-5FFB-4BAB-91DF-10BA8D35CC62-htm.html (Accessed: 19 October 2016).

Hossain, N. and profile, V. my complete (2012) *Computational mechanics*. Available at: http://naimhossain.blogspot.co.uk/2012/08/turbulence-modeling.html (Accessed: 7 June 2016).

How It Works | Alicat Scientific (2015) Available at: http://www.alicat.com/knowledge/how-it-works/ (Accessed: 12 August 2015).

Inc, F. (no date) *FLUENT 6.3 user's guide - 12.4.3 Realizable - model*. Available at: https://www.sharcnet.ca/Software/Fluent6/html/ug/node480.htm (Accessed: 24 October 2016).

Inc, F.A. (2012) *Reservoir fluid properties*. Available at: http://fekete.com/SAN/TheoryAndEquations/HarmonyTheoryEquations/Content/HTML_Files/Reference_Material/General_Concepts/Reservoir_Fluid_Properties.htm (Accessed: 8 March 2016).

Inflow control device with passive shut-off feature (2005) Available at: https://www.google.com/patents/US7290606 (Accessed: 20 July 2015).

Inikori, S.O. (2002) 'Numerical study of water coning control with Downhole water sink (DWS) completions in vertical and horizontal wells', .

InSitu Density Reservoir Fluid Density, Schlumberger (2015) Available at: http://www.slb.com/services/characterization/reservoir/wireline/insitu_family/insitu_density.aspx (Accessed: 26 August 2015).

Introduction of computational fluid dynamics (2005) Available at: http://wwwmayr.informatik.tu-muenchen.de/konferenzen/Jass05/courses/2/Zuo/Zuo_paper.pdf (Accessed: 29 September 2016).

Islek, A.A. (2004) *The impact of swirl in turbulent pipe flow*. Available at: https://smartech.gatech.edu/bitstream/handle/1853/4955/islek_akay_a_200412_mast.pdf (Accessed: 10 February 2016).

Jansen, J. (2001) *Smart wells*. Available at: http://www.citg.tudelft.nl/fileadmin/Faculteit/CiTG/Over_de_faculteit/Afdelingen/Afdel

ing_Geotechnologie/secties/Sectie_Petroleum_Engineering/staff/Jansen,_J._D./Publications/doc/Smartwells.pdf (Accessed: 2 July 2015).

Jayakumar, J.S., Mahajani, S.M., Mandal, J.C., Iyer, K.N. and Vijayan, P.K. (2010) 'CFD analysis of single-phase flows inside helically coiled tubes', *Computers & Chemical Engineering*, 34(4), pp. 430–446. doi: 10.1016/j.compchemeng.2009.11.008.

Kahawalage, A.C., Energy, Halvorsen, B.M., AS, I. and Mathiesen, V. (2015) 'Proceedings of the 56th conference on simulation and Modelling (SIMS 56), October, 7-9, 2015, Linköping university, Sweden', (119), pp. 247–254.

Kahawalage, A.C., Halvorsen, B.M. and Mathiesen, V. (2015) 'Near well CFD simulation of SAGD extra heavy oil production', *Proceedings Name*, . doi: 10.3384/ecp15119247.

Kalpakli, A. (2012) *Experimental study of turbulent flows through pipe bends*. Available at: http://kth.diva-portal.org/smash/get/diva2:515647/FULLTEXT02 (Accessed: 29 February 2016).

Kanarachos, S. and Flouros, M. (2014) *Simulation of the air-oil mixture flow in the Scavenge pipe of an Aero engine using generalized Interphase momentum exchange models*. Available at: http://www.wseas.org/multimedia/journals/fluid/2014/a125713-132.pdf (Accessed: 9 March 2016).

Kang, J. and Services, H.E. (2013) *Patent WO2014109773A1 - remote-open inflow control device with swellable actuator*. Available at: http://www.google.com/patents/WO2014109773A1?cl=en (Accessed: 5 September 2016).

Karthik, T.S.D. and Durst, F. (2011) *TURBULENCE MODELS AND THEIR APPLICATIONS*. Available at: http://www.leb.eei.uni-erlangen.de/winterakademie/2011/report/content/course01/pdf/0112.pdf (Accessed: 9 October 2016).

King, H. (2015) *Horizontal Drilling & Directional Drilling: Natural Gas Wells*. Available at: http://geology.com/articles/horizontal-drilling/ (Accessed: 2 July 2015).

Kitoh, O. (1991) 'Experimental study of turbulent swirling flow in a straight pipe', *Journal of Fluid Mechanics*, 225, pp. 445–479. doi: 10.1017/S0022112091002124.

Kuang, S., Qi, Z., Yu, A.B., Vince, A., Barnett, G.D. and Barnett, P.J. (2014) 'CFD modeling and analysis of the multiphase flow and performance of dense medium cyclones', *Minerals Engineering*, 62, pp. 43–54. doi: 10.1016/j.mineng.2013.10.012.

Kumar, A. (no date) 'SIMULATION AND FLOW ANALYSIS THROUGH A STRAIGHT PIPE SASWAT SAMBIT 110CE0056 UNDER THE GUIDANCE OF', (1).

Laminar and turbulent flow (2000) Available at: http://www.efm.leeds.ac.uk/CIVE/CIVE1400/Section4/laminar_turbulent.htm (Accessed: 13 July 2016).

Liang, F., Chen, J., Wang, J., Yu, H. and Cao, X. (2014) 'Gasâ€"liquid two-phase flow equal division using a swirling flow distributor', *EXPERIMENTAL THERMAL AND FLUID SCIENCE*, 59, pp. 43–50. doi: 10.1016/j.expthermflusci.2014.07.013.

Liu, H.-F., Xu, J.-Y., Wu, Y.-X. and Zheng, Z.-C. (2010) 'Numerical study on oil and water two-phase flow in a cylindrical cyclone', *Journal of Hydrodynamics*, 22(5), pp. 832–837. doi: 10.1016/S1001-6058(10)60038-8.

Liu, H.-F., Xu, J.-Y., Zhang, J., Sun, H.-Q. and Wu, Y.-X. (2012) 'OIL/WATER SEPARATION IN A LIQUID-LIQUID CYLINDRICAL CYC- LONE *', *Journal of Hydrodynamics*, 24(1), pp. 116–123. doi: 10.1016/S1001-6058(11)60225-4.

Liu, W. and Bai, B. (2015) 'Swirl decay in the gasâ€"liquid two-phase swirling flow inside a circular straight pipe', *EXPERIMENTAL THERMAL AND FLUID SCIENCE*, 68, pp. 187–195. doi: 10.1016/j.expthermflusci.2015.04.018.

Losses in pipes (no date) Available at: http://my.me.queensu.ca/People/Sellens/LossesinPipes.html (Accessed: 10 October 2016).

Mcgovern, J. (2016) *Technical note: Friction factor diagrams for pipe flow*. Available at: http://arrow.dit.ie/cgi/viewcontent.cgi?article=1030&context=engschmecart (Accessed: 2 June 2016).

Muggeridge, A., Cockin, A., Webb, K., Frampton, H., Collins, I., Moulds, T. and Salino, P. (2014) *Recovery rates, enhanced oil recovery and technological limits*. Available at: http://rsta.royalsocietypublishing.org/content/372/2006/20120320 (Accessed: 23 July 2015).

Mukhaimer, A., Al-Sarkhi, A., Nakla, E.M., Ahmed, W.H. and Al-Hadhrami, L. (2015) 'Pressure drop and flow pattern of oil–water flow for low viscosity oils: Role of mixture viscosity', *International Journal of Multiphase Flow*, 73, pp. 90–96. doi: 10.1016/j.ijmultiphaseflow.2015.02.018.

Munson, B.R., Young, D.F., Okiishi, T.H. and Huebsch, W.W. (2009) *Fundamentals of fluid mechanics, international student version*. 6th edn. Chichester, United Kingdom: Wiley, John & Sons.

Nearyt, V.S. and Sotiropoulos, F. (1996) ‘numerical investigation of laminar flows through go-degree diversions of rectangular cross-section’, *Computers & Fluids*, 25(295), pp. 95–18.

numerical study of water coning control with downhole water sink (dws) well completions in vertical and horizontal wells (2002) Available at: http://etd.lsu.edu/docs/available/etd-0610102-080619/unrestricted/Inikori_dis.pdf (Accessed: 18 February 2016).

Nurmi, R. (1995) *Horizontal Highlights*. Available at: http://www.slb.com/~/media/Files/resources/mearr/wer16/rel_pub_mewer16_1.pdf (Accessed: 2 July 2015).

Oil density - (2015) Available at: http://petrowiki.org/Oil_density (Accessed: 17 August 2015).

Oil fluid properties - (2015) Available at: http://petrowiki.org/Oil_fluid_properties (Accessed: 17 August 2015).

Oil viscosity - (2015) Available at: http://petrowiki.org/Oil_viscosity (Accessed: 17 August 2015).

OilfieldTechnology (2014) *EU project aims to revolutionise oil extraction*. Available at: http://www.energyglobal.com/upstream/drilling-and-production/19022014/EU_project_testing_autonomous_inflow_control_valves_aims_revolutionise_oil_extraction/ (Accessed: 10 March 2016).

OMEGA ENGINEERING - Flow Control (2015) Available at: https://www.omega.co.uk/techref/flowcontrol.html (Accessed: 12 August 2015).

OnePetro, Hatzignatiou, D.G. and Mohamed, F. (1994) *Water and gas coning in horizontal and vertical wells*. Available at: https://www.onepetro.org/conference-paper/PETSOC-94-26 (Accessed: 22 January 2016).

OnePetro, Krasnov, V., Zimin, S., Ali, A. and Guo, B. (2012) *Inflow-control-device design: Revisiting objectives and techniques*. Available at: https://www.onepetro.org/journal-paper/SPE-133234-PA (Accessed: 25 February 2016).

OnePetro, Zhu, D., Li, Z. and Fernandes, P. (2009) *Understanding the roles of inflow-control devices in optimizing horizontal-well performance*. Available at: https://www.onepetro.org/conference-paper/SPE-124677-MS (Accessed: 22 February 2016).

OnePetro, Zimin, S., Guo, B., Ali, A. and Krasnov, V. (2010) *ICD design: Revisiting objectives and techniques*. Available at: https://www.onepetro.org/conference-paper/SPE-133234-MS (Accessed: 26 January 2016).

Panzariu, O. (2009) *How does CFD (computational fluid dynamics) work?* Available at: http://www.autoevolution.com/news/how-does-cfd-computational-fluid-dynamics-work-6400.html (Accessed: 21 December 2016).

Park, Y. and Chang, S.H. (no date) 'Swirl flow analysis in a helical wire inserted tube using CFD code', *Nuclear Engineering and Design*, 240(10), pp. 3405–3412. doi: 10.1016/j.nucengdes.2010.07.015.

Pažanin, I. (2014) 'On the helical pipe flow with a pressure-dependent viscosity', *Theoretical and Applied Mechanics Letters*, 4(6). doi: 10.1063/2.1406206.

Petroleum reservoir fluid properties (2015) Available at: http://wiki.aapg.org/Petroleum_reservoir_fluid_properties (Accessed: 17 August 2015).

PetroWiki (2012) *Preventing formation of hydrate plugs* -. Available at: http://petrowiki.org/Preventing_formation_of_hydrate_plugs (Accessed: 7 June 2016).

PetroWiki (2012) *Water and gas coning* -. Available at: http://petrowiki.org/Water_and_gas_coning (Accessed: 2 July 2015).

PetroWiki (2015) *Horizontal wells* -. Available at: http://petrowiki.org/Horizontal_wells (Accessed: 2 July 2015).

Pitla, S.S., Groll, E.A. and Ramadhyani, S. (2002) 'New correlation to predict the heat transfer coefficient during in-tube cooling of turbulent supercritical CO2', *International Journal of Refrigeration*, 25(7), pp. 887–895. doi: 10.1016/s0140-7007(01)00098-6.

Posted and Loaiza, J. (2012) *Inflow Control Devices: Extending the Life of Mature Field Wells - Halliburton*. Available at: http://halliburtonblog.com/inflow-control-devices-extending-the-life-of-mature-field-wells/ (Accessed: 12 August 2015).

Prakasa, B., Haghighat, M., Muradov, K. and Davies, D. (2015) *Eltazy Khalid production enhancement and uncertainty reduction by optimum use of flow control devices*. Available at: https://www.spe-uk.org/aberdeen/wp-content/uploads/2015/10/Khalid-Heriot-Watt-Production-enhancement-and-uncertainty-reduction.pdf (Accessed: 31 May 2016).

Pressure drop evaluation along pipelines - (2015) Available at: http://petrowiki.org/Pressure_drop_evaluation_along_pipelines (Accessed: 6 August 2015).

Pressure drop in pipes.... PRESSURE DROP CALCULATIONS (2009) Available at: http://www.adpf.ae/images/Page-A.pdf (Accessed: 10 October 2016).

Production problems - AAPG Wiki (2016) Available at: http://wiki.aapg.org/Production_problems (Accessed: 5 September 2016).

Qualitative and quantitative research - data analysis | ATLAS.ti (2002) Available at: http://atlasti.com/quantitative-vs-qualitative-research/ (Accessed: 21 December 2016).

Reservoir pressure data interpretation - (2012) Available at: http://petrowiki.org/Reservoir_pressure_data_interpretation (Accessed: 26 August 2015).

Rizzo, G. (2015) *What is a brief description of how computational fluid dynamics (CFD) work?* Available at: https://www.quora.com/What-is-a-brief-description-of-how-computational-fluid-dynamics-CFD-work (Accessed: 21 December 2016).

Saha, S.K., Bhattacharyya, S. and Pal, P.K. (2012) 'Thermohydraulics of laminar flow of viscous oil through a circular tube having integral axial rib roughness and fitted with center-cleared twisted-tape', *Experimental Thermal and Fluid Science*, 41, pp. 121–129. doi: 10.1016/j.expthermflusci.2012.04.004.

SAS IP, Inc (2013) *ANSYS fluid dynamics verification manual*. Available at: http://148.204.81.206/Ansys/150/Fluid%20Dynamics%20Verification%20Manual.pdf (Accessed: 2 March 2016).

Schlumberger (2016) *Inflow control devices (ICDs)*. Available at: http://www.slb.com/services/completions/sand_control/sandscreens/inflow_control_devices.aspx (Accessed: 10 March 2016).

Shevchenko, E. (2013) *Experimental study of water coning phenomenon in perforated pipes geometry*. Available at: http://www.diva-portal.org/smash/get/diva2:656726/FULLTEXT01.pdf (Accessed: 25 June 2015).

Shi, S.-Y., Wu, Y.-X., Zhang, J., Guo, J. and Wang, S.-J. (2010) 'A study on separation performance of a vortex finder in a liquid-liquid cylindrical cyclone', *Journal of Hydrodynamics*, 22(5), pp. 391–397. doi: 10.1016/S1001-6058(09)60225-0.

Shirvan, S.S. (2011) *Experimental study of complex pipe flows*. Available at: http://kth.diva-portal.org/smash/get/diva2:430330/FULLTEXT01 (Accessed: 29 February 2016).

SHTORK, S.I., OKULOV, V.L., KUIBIN, P.A. and ALEKSEENKO, S.V. (1999) 'Helical vortices in swirl flow', *Journal of Fluid Mechanics*, 382, pp. 195–243. doi: 10.1017/S0022112098003772.

Shvab, A.V. and Khairullina, V.Y. (2011) 'Effect of an unsteady swirled turbulent flow on the motion of a single solid particle', *Journal of Applied Mechanics and Technical Physics*, 52(1), pp. 37–42. doi: 10.1134/s0021894411010068.

Shvab, A.V., Zyatikov, P.N., Sadretdinov, S.R. and Chepel', A.G. (2010) 'Numerical study of a swirled turbulent flow in the separation zone of a centrifugal air separator', *Journal of Applied Mechanics and Technical Physics*, 51(2), pp. 174–181. doi: 10.1007/s10808-010-0026-x.

Sister, V.G. and Ivannikova, E.M. (2004) 'Analysis of direct-flow centrifugal separation of dual-phase systems', *Chemical and Petroleum Engineering*, 40(3-4), pp. 123–127. doi: 10.1023/BCAPE.0000033660.90881.1f.

SlidePlayer (2016) *Presentation on theme: '1 lecture 10 - turbulence models applied computational fluid dynamics instructor: André Bakker © André Bakker (2002-2005)*

© *fluent Inc. (2002)'— presentation transcript:* Available at: http://slideplayer.com/slide/4235281/ (Accessed: 3 October 2016).

Smith, W.R. (2007a) 'Modulation equations and Reynolds averaging for finite-amplitude non-linear waves in an incompressible fluid', *IMA Journal of Applied Mathematics*, 72(6), pp. 923–945. doi: 10.1093/imamat/hxm054.

Smith, W.R. (2007b) *Modulation equations and Reynolds averaging for finite-amplitude non-linear waves in an incompressible fluid*. Available at: https://www.researchgate.net/publication/31314174_Modulation_equations_and_Reynolds_averaging_for_finite-amplitude_non-linear_waves_in_an_incompressible_fluid (Accessed: 25 February 2016).

Sodja, J. (2007) *Turbulence models in CFD*. Available at: http://www-f1.ijs.si/~rudi/sola/Turbulence-models-in-CFD.pdf (Accessed: 3 October 2016).

Steenbergen, W. and Voskamp, J. (1998) 'The rate of decay of swirl in turbulent pipe flow', *Flow Measurement and Instrumentation*, 9, pp. 67–78.

Stewart, M. (2016) '6 – fluid flow and pressure drop', *Surface Production Operations*, , pp. 343–470. doi: 10.1016/B978-1-85617-808-2.00006-7.

Sukri, M., Ali, M., Doolan, C.J. and Wheatley, V. (2009) *GRID CONVERGENCE STUDY FOR A TWO-DIMENSIONAL SIMULATION OF FLOW AROUND A SQUARE CYLINDER AT A LOW REYNOLDS NUMBER*. Available at: http://www.cfd.com.au/cfd_conf09/PDFs/136ALI.pdf (Accessed: 10 October 2016).

Sustaining production by limiting water cut and gas breakthrough with autonomous inflow control technology (2015) Available at: http://www.oilandgastechnology.net/upstream-news/sustaining-production-limiting-water-cut-gas-breakthrough-autonomous-inflow-control (Accessed: 6 August 2015).

Sutherland, K.S. and Chase, G. (2011) *Filters and Filtration Handbook*. Available at: https://books.google.co.uk/books?id=qwZDG-GsUW8C&pg=PA303&lpg=PA303&dq=mechanical+filtering+solutions&source=bl&ots=KVTPaPlmeI&sig=0NAlBL4-u_uNcQl7nZksqhvuBKM&hl=en&sa=X&ved=0CDQQ6AEwBGoVChMIhpzOrr38xwIVhL0aCh1luA27#v=onepage&q=mechanical%20filtering%20solutions&f=false (Accessed: 16 September 2015).

Team, L.C. (2014) *Tips & tricks: Turbulence part 1 - introduction to turbulence Modelling*. Available at: http://www.computationalfluiddynamics.com.au/turbulence-modelling/ (Accessed: 3 October 2016).

Terminology - Bluetooth (2016) Available at: https://casestudy-itgs.wikispaces.com/Terminology+-+Bluetooth (Accessed: 29 March 2016).

The k-epsilon model in the theory of turbulence (2004) Available at: http://d-scholarship.pitt.edu/10241/1/cdsp-new.pdf (Accessed: 1 March 2016).

Tryggvason, G. (2011) *Computational fluid dynamics! ' Classical ' ! Turbulence modeling!* Available at: http://www3.nd.edu/~gtryggva/CFD-Course/2011-Lecture-35.pdf (Accessed: 9 October 2016).

Turki, F. and Al-Khelaiwi, M. (2013) *A comprehensive approach to the design of advanced well*. Available at: http://www.ros.hw.ac.uk/bitstream/handle/10399/2644/AlkhelaiwiFTM_0313_pe.pdf?sequence=1 (Accessed: 31 May 2016).

Validation 3. Laminar flow around a circular cylinder 3.1 introduction (2002) Available at: http://www.calpoly.edu/~kshollen/ME554/Labs/validation_example.pdf (Accessed: 2 March 2016).

Virtual labs (no date) Available at: http://uorepc-nitk.vlabs.ac.in/exp1/index.html (Accessed: 29 February 2016).

Wan, P. (2013) *Optimizing MEG Recovery systems on Long Subsea Tiebacks*. Available at: http://www.subseauk.com/documents/presentations/asia2013%20patrick%20wan_intecsea.pdf (Accessed: 7 June 2016).

Wang, L.-P. and Du, M.H. (2008) 'Direct simulation of viscous flow in a wavy pipe using the lattice Boltzmann approach', *Int. J. Engineering Systems Modelling and Simulation*, 1(1), pp. 20–29.

Water Breakthrough Monitoring (2015) Available at: http://www.resman.no/products-and-services/water-breakthrough-monitoring/ (Accessed: 6 August 2015).

Wellbore Stability (Drilling Well): Oil and Natural Gas (2014) Available at: http://www.jogmec.go.jp/english/oil/technology_012.html (Accessed: 28 August 2015).

Widmann, J.F., Charagundla, R.S. and Presser, C. (1999) *Benchmark experimental database for Multiphase combustion model input and validation: Characterization of the inlet combustion air*. Available at: http://webbook.nist.gov/chemistry/special/spray-combust/pdf/nistir-6370.pdf (Accessed: 10 February 2016).

Winch, C. (2016) *Research methodologies*. Available at: http://www.socscidiss.bham.ac.uk/methodologies.html (Accessed: 21 December 2016).

Wolfram, E. (2016a) *AICV® extra heavy oil*. Available at: http://www.inflowcontrol.no/aicv-product-range/aicv-extra-heavy-oil/ (Accessed: 31 May 2016).

Wolfram, E. (2016b) *AICV® heavy oil*. Available at: http://www.inflowcontrol.no/aicv-product-range/aicv-heavy-oil/ (Accessed: 31 May 2016).

Wolfram, E. (2016c) *AICV® light oil*. Available at: http://www.inflowcontrol.no/aicv-product-range/aicv-light-oil/ (Accessed: 31 May 2016).

Wolfram, E. (2016d) *AICV® medium oil*. Available at: http://www.inflowcontrol.no/aicv-product-range/aicv-medium-oil/ (Accessed: 31 May 2016).

Wolfram, E. (2016e) *Inflow control*. Available at: http://www.inflowcontrol.no/aicv-product-range/aicv-gas/ (Accessed: 31 May 2016).

WordPress (2012) *Posts about Kickoff Point (KOP) on directionaldrilling*. Available at: https://directionaldrilling.wordpress.com/tag/kickoff-point-kop/ (Accessed: 2 July 2015).

Xiong, Z., Lu, M., Wang, M., Gu, H. and Cheng, X. (2013) 'Study on flow pattern and separation performance of airâ€"water swirl-vane separator', *Annals of Nuclear Energy*, 63, pp. 138–145. doi: 10.1016/j.anucene.2013.07.026.

Yildiz, C., Biçer, Y. and Pehlivan, D. (1995) 'Heat transfers and pressure drops in rotating helical pipes', *Applied Energy*, 50(1), pp. 85–94. doi: 10.1016/0306-2619(95)90765-9.

Young, D.F., Munson, B.R., Okiishi, T.H. and Huebsch, W.W. (2010) *A brief introduction to fluid mechanics*. 5th edn. Chichester, United Kingdom: Wiley, John & Sons.

Zambrano, H., Di G. Sigalotti, L., Klapp, J., Peña-Polo, F. and Bencomo, A. (2016) ‘Heavy oil slurry transportation through horizontal pipelines: Experiments and CFD simulations’, *International Journal of Multiphase Flow*,. doi: 10.1016/j.ijmultiphaseflow.2016.04.013.

Zeng, Q., Wang, Z., Wang, X., Wei, J., Zhang, Q. and Yang, G. (2015) ‘A novel autonomous inflow control device design and its performance prediction’, *Journal of Petroleum Science and Engineering*, 126, pp. 35–47. doi: 10.1016/j.petrol.2014.12.003.

Appendix A

Effect of the square swirl fluid flow on heat exchange

The square swirl design is applied to a heat exchanger and the results are analysed. The cold water is fed in at a temperature of 303K while the hot water goes into the hot inlet at 351.2K according to experiments carried out by (Shrikant and Limaye, 2016). The temperature of the cold fluid at the outlet is 306K while the hot fluid temperature at the hot outlet becomes about 349K. the cold fluid has increased in temperature by about 3K.

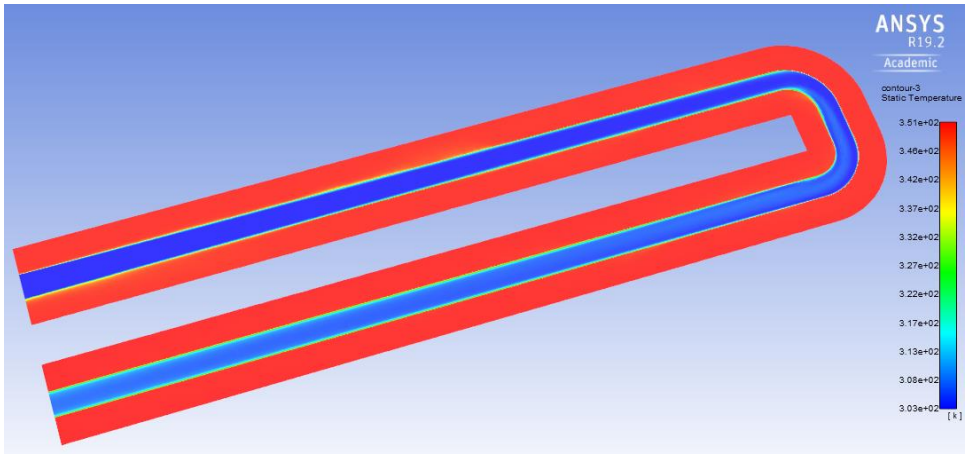

Contours of static temperature for a heat exchanger

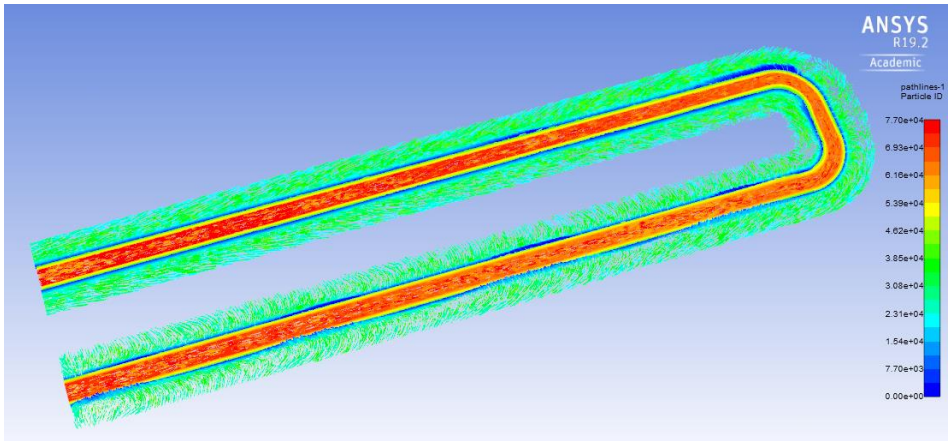

Path lines coloured by temperature for a heat exchanger

Length varied for solar water heater

Length (mm)	Temperature at cold outlet (K)
20	306.5231
30	306.78729
40	310.22539
50	310.68158

60	311.80363
70	312.17537
80	313.44974
90	313.96184
100	314.54075

The table above shows how the temperature of the fluid changes with an increase in length of pipe. It can be deduced however that the temperature does not change greatly with this fluid flow geometry setup.

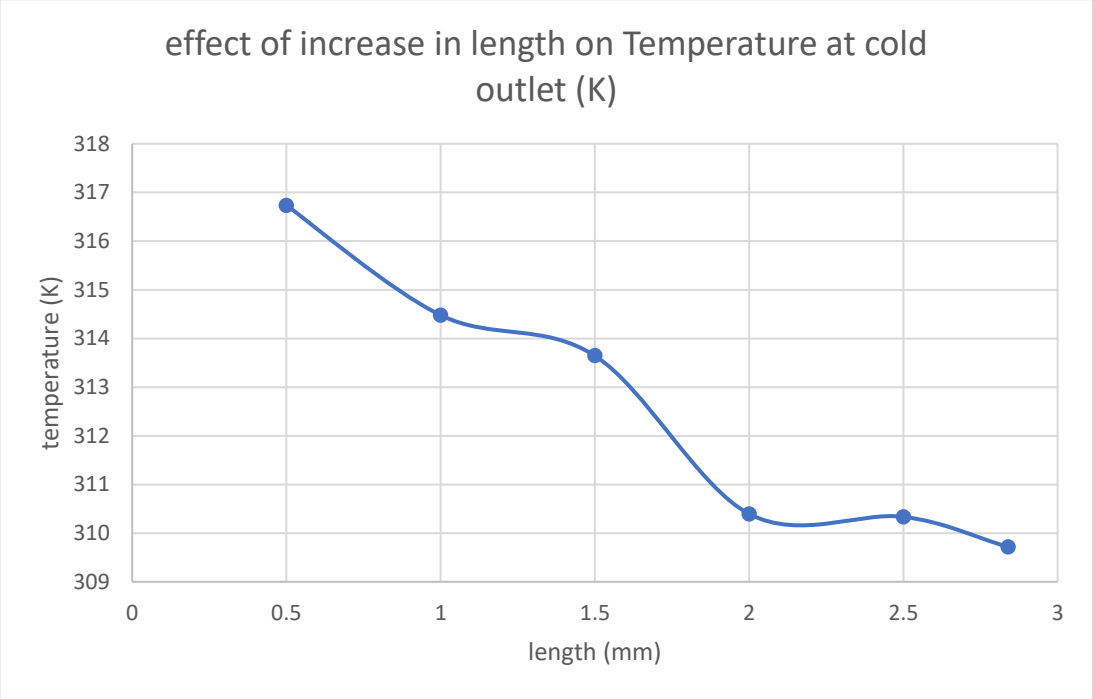

Graph showing the effect of change in length on the temperature at cold outlet

The square swirl geometry is applied to the heat exchanger to analyse its effects on heat transfer. Firstly, the size of the square geometry is checked to see how it affects the heat transfer as shown in the table below.

Square size varied for square swirl geometry solar water heater

Square size (mm)	Temperature at cold outlet (K)
2.84	309.71575
2.5	310.33614
2	310.39518
1.5	313.64536
1	314.47817
0.5	316.73628

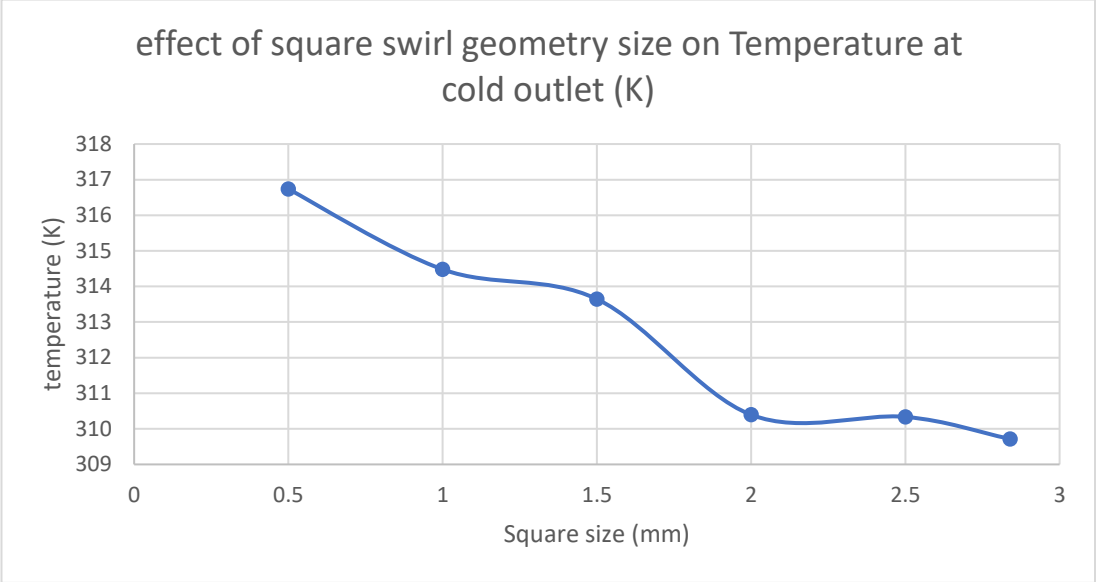

Graph showing the effect of square swirl geometry size on Temperature at cold outlet (K)

The results show that a reduction in geometry size of the cold fluid gives more area for the hot fluid to flow hence there is greater transfer of heat from the hot fluid to the cold fluid. The temperature at the cold outlet was seen to also increase when the swirl pitch is varied as shown in table.

Swirl pitch varied for square swirl geometry solar water heater

Square swirl pitch (mm)	Temperature at cold outlet (K)
50	316.79521
45	316.71907
40	316.77375
35	317.06653
30	317.0776
25	317.40087
20	317.90231
15	318.42876
10	321.07776
5	327.64625

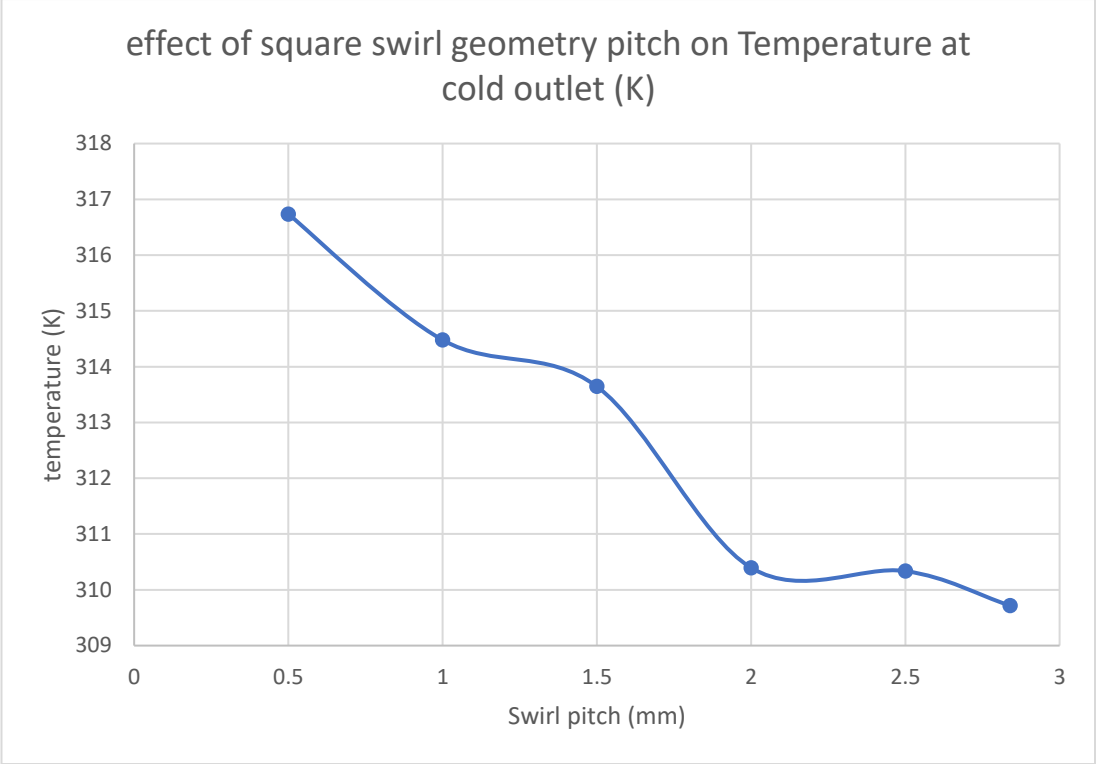

Graph showing the effect of square swirl geometry pitch on Temperature at cold outlet (K)

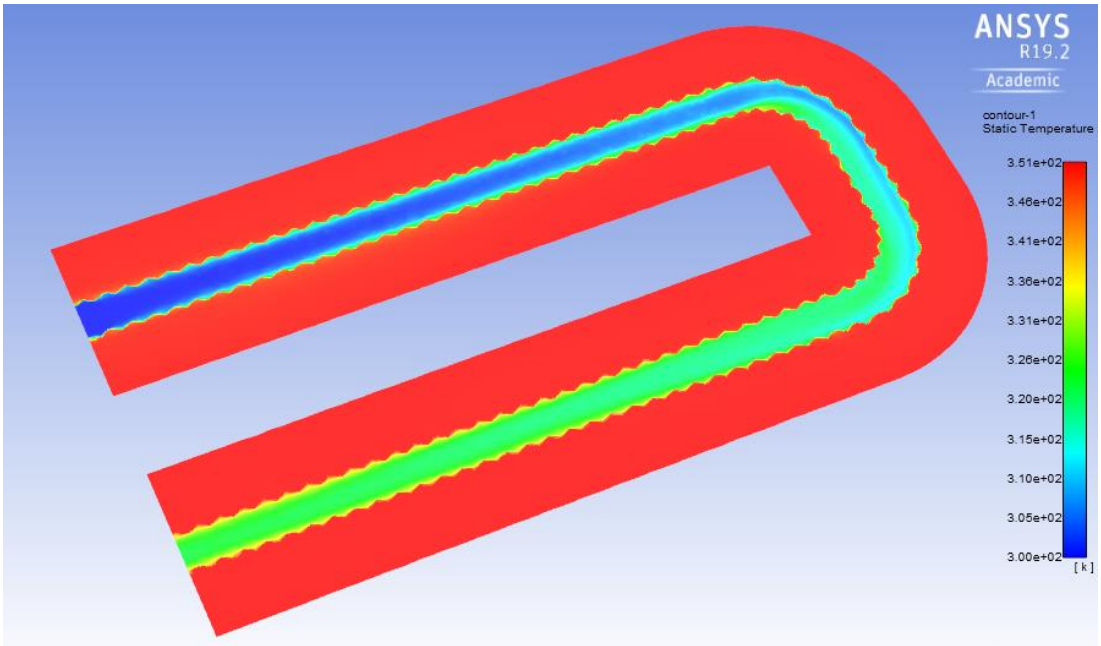

Contours of static temperature for a square swirl geometry solar water heater

The effect of the square swirl fluid flow geometry on the physics of flow in the heat exchanger is evident in figure.The re-circulation and turbulent effect created due to the square swirl fluid flow geometry leads to enhanced heat transfer.

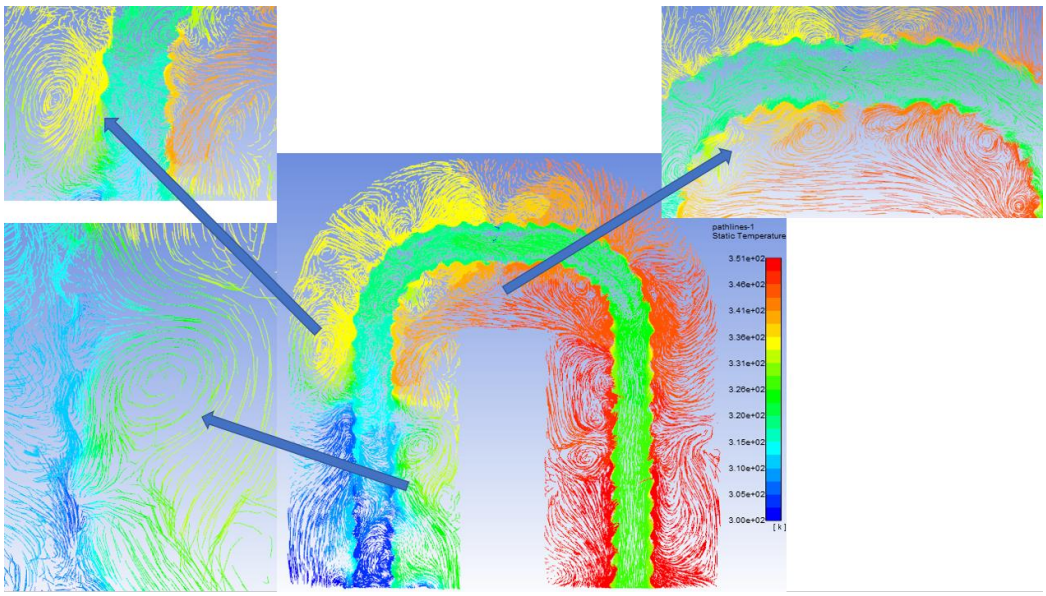

Path lines coloured by temperature showing the recirculation and turbulence for the square swirl solar water heater

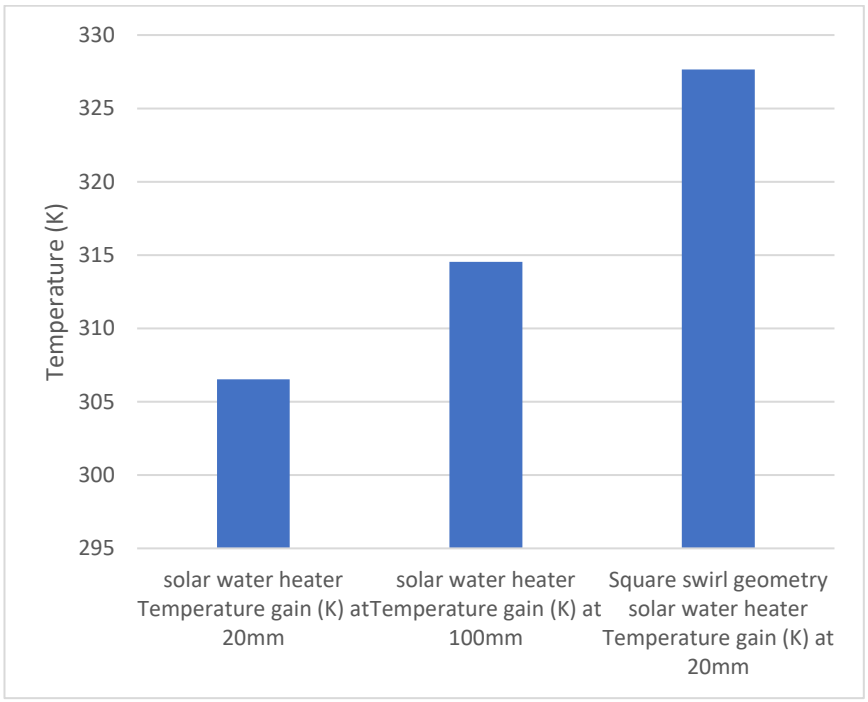

Graph comparing temperature gained using the square swirl fluid flow geometry

Appendix B

Effect of the square swirl fluid flow geometry on multiphase flow

Figure below shows the square swirl pipe geometry used to analyse the effect of fluid flow geometry on multiphase flow.

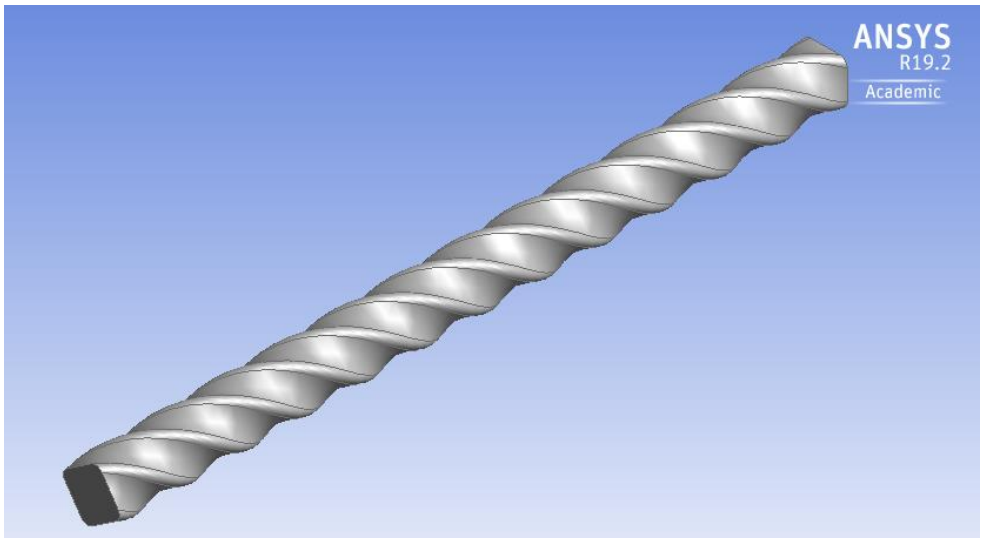

Square swirl pipe geometry

The multiphase Volume of Fluid method (VOF) is used to analyse the fluid flow of oil and water. The two Eulerian phases were set up as water and oil while the implicit formulation for volume fraction parameters was used to achieve larger time steps variations. In this scenario. The primary phase is set to water and the secondary phase is set to oil. The phase interactions are defined, surface tension of 0.005 and wall adhesion were used to specify how the two phases interact with each other, mass flow inlet 0.004 oil domain will be initialised with water and oil pumped into it. In figure the path lines coloured by velocity magnitude for the mixture at 500 steps is shown. It can be deduced from the image that the higher velocity occurs through the centre of the geometry while the slower fluid swirls around it forming a sort of lubricating layer permitting the fluid in the centre to flow much faster and smoother.

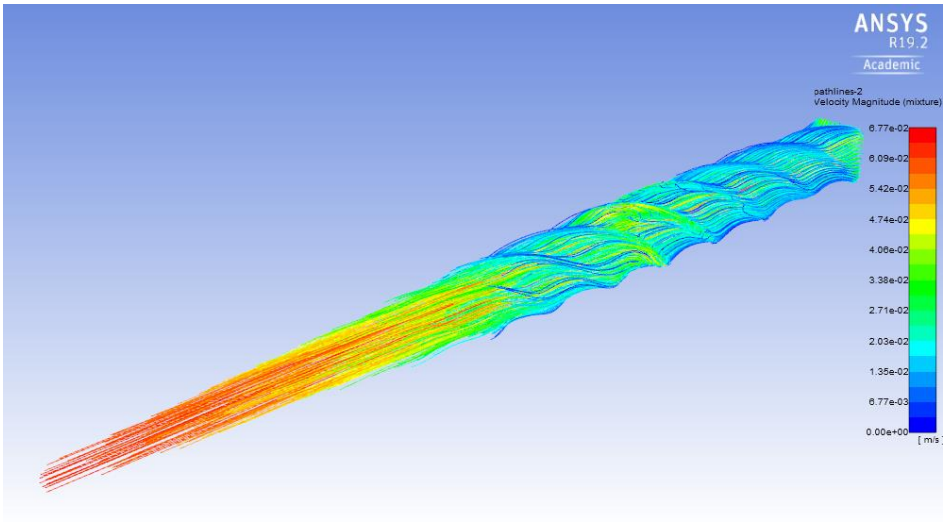

velocity magnitude Path lines for the mixture at 500 steps

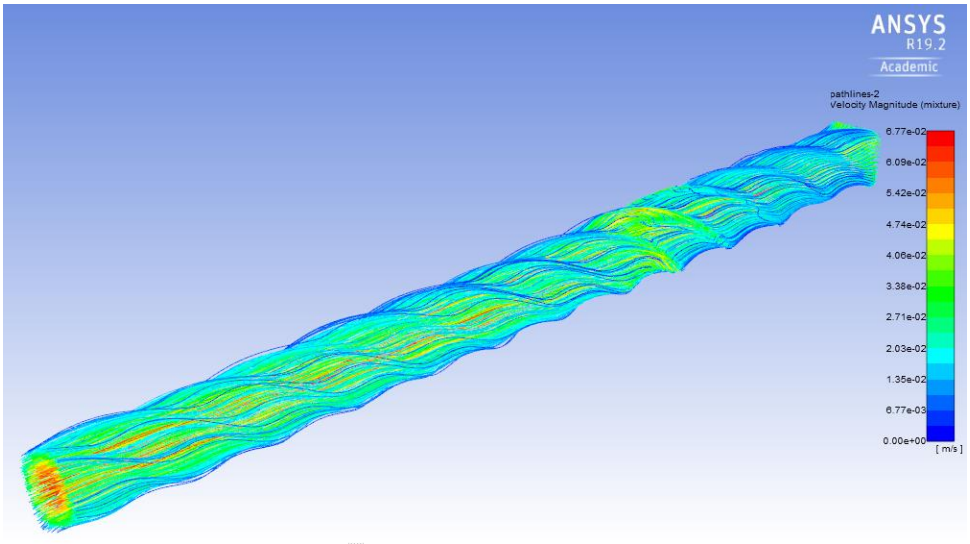

velocity magnitude Path lines for the mixture at 1000 steps

In figure, the path line for the mixture coloured by density is examined. It can be deduced for the figure that the oil phase of a lower density, 970kg/m^3 flows into the swirl pipe. When this happens as can be seen in the image, the water phase of density, 1000Kg/m^3 is moved to the outer region of the pipe. This causes a distinct separation of the two phases as the water acts as a lubricant layer for the oil to flow through. This phenomenon has application in oil transportation in pipelines.

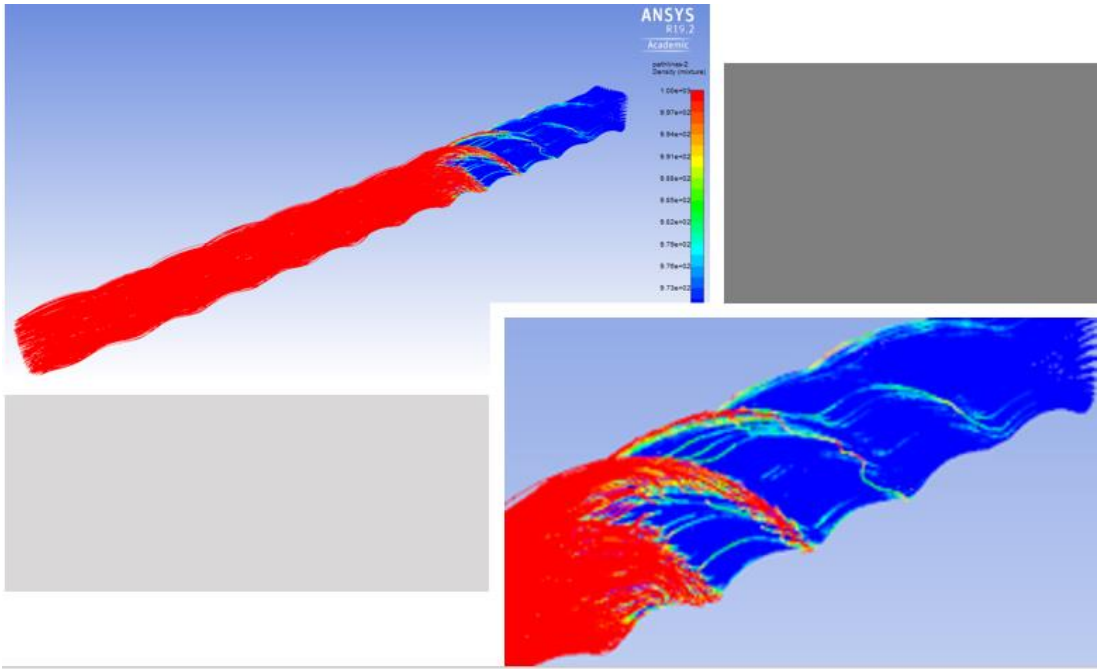

Density Path lines for the mixture at 500 steps